CRANFIELD UNIVERSITY

Kan Hong

Remote sensing of strong emotions using Electro-optical imaging technique

Department of Informatics and Systems Engineering
PhD by research

PhD
Academic Year: 2009-2012

Supervisor: Peter Yuen
September 2012

CRANFIELD UNIVERSITY

Department of Informatics and Systems Engineering
PhD by research

PhD

Academic Year - 2009-2012

Kan Hong

Remote sensing of strong emotions using Electro-optical imaging technique

Supervisor: Peter Yuen
September 2012

This thesis is submitted in partial fulfilment of the requirements for the degree of PhD

ABSTRACT

This thesis reports a summary of the PhD programme for the assessment of person's emotional anxiety using Electro-optical technology. The thesis focuses mainly on the understanding of fundamental properties of physiological responses to emotional anxiety and how they can be captured by using Electro-optical (EO) imaging methods such as hyperspectral imaging (HSI) and thermal imaging (TI) techniques.

The thesis summarises three main areas of work that have been undertaken by the author in the programme: (a) Experimental set up including HSI system and data acquisition software design and implementation, (b) fundamental understanding of physiological responses to emotional anxiety from the EO perspective and (c) the development of a novel remote sensing technique for the assessment of emotions without the requirement of base line information.

One of our main results is to provide evidence to prove that the mean temperature in the periorbital region remains the same within 0.2°C during emotional anxiety. Furthermore, we have shown that it is the high temperature pixels within the periorbital, which increases in numbers by a huge amount after 2 minutes of the onset of anxiety. We have also developed techniques to allow the assessment anxiety without the need of base line information. The method has been tested using a sample size of about 40 subjects, and achieved promising result. Technologies for the remote sensing of heart beat rate has been in great demand, this study also involves the development of heart beat detection using TI system. Moreover, we have also attempted for the first time to sense glucose concentration from the blood sample in-vivo using HSI technique remotely.

.

Keywords: Remote sensing, emotional status, thermal imaging

ACKNOWLEDGEMENTS

I would like to thank my supervisor Dr. Peter Yuen for giving me the opportunity to study and work in the Cranfield University and to lead me into the fields of thermal and hyperspectral imaging for all the guidance during the course of this exciting research.

I would like to thank my parents for the continuous support. I also would like to thank my friends Umair Soori, WenTao Chen, Izzati Ibrahim, James Jackman for their help. Finally, I would like to express my gratitude to the CTC and MOD UK, the Directed Research programme and the InnovTech Solutions Lab for their support of this research.

TABLE OF CONTENTS

LIST OF FIGURES

LIST OF TABLES

LIST OF EQUATIONS

LIST OF ABBREVIATIONS

AOTF	Acousto-optical tuneable filters
A/D	Analog-to-digital
AU	Action unit
bpm	Beats per minute
BDO	Behaviour detection officers
BL	Beer-Lambert Law
CRH	Corticotropin-releasing hormone
CTW	Continuous wavelet transform
COTS	Commercial-Off-The-Shelf
CO_2	carbon dioxide
CU	Cranfield University
DFMT	Differential Forehead Mouth Temperature
DFNSO	Differential Forehead Nose StO2
EO	Electrical optical
ES	Emotional anxiety
EA	Emotional Anxiety
EBL	Extended Beer-Lambert Law
ELM	Empirical Line Method
fMRI	Functional Magnetic Resonance Imaging
FPA	Focal plane array
FOV	Field of view
FMRI	Functional magnetic resonance imaging
FFT	Fast Fourier Transform
FACS	Facial Action Coding System
fps	Frames per second
Hb	Deoxy-Haemoglobin
HbO2	Oxy-haemoglobin
HSI	Hyperspectral Imaging
HPLC	High performance liquid chromatography
Hb	Deoxy-haemoglobin
HbO2	Oxy-haemoglobin
HPA	Hypothalamic–pituitary–adrenal
HBR	Heart beat rate
HSI	Hyperspectral imaging
IED	Improvised explosive devices
ICWT	Continuous wavelet transform
LBF	Limb blood flow
LCTF	Liquid crystal tuneable filters
LWIR	Long wave infrared wavelengths
MOD	Ministry of Defence
MSE	Mental strong emotions
MWIR	Mid wave infrared wavelengths
MGL	Measured glucose level

MHC	Metabolic heat conformation
MSI	Multispectral imaging
NEDT	Noise equivalent differential temperature
NIR	Near Infra-Red
PA	Physical Anxiety
PO_2	Partial pressure of Oxygen
ROI	Region of Interest
PS	Physical anxiety
PGP	Prism-Grating-Prism
PSE	Physical strong emotions
ROI	Region of interest
SDK	Software Development Kit
SiTF	Signal transfer function
SH	Stand horse
SDK	Software Development Kit
StO2	Tissue Oxygen Saturation
SWIR	Short Wave Infra-Red
TI	Thermal imaging
TSST	Triers Social Anxiety Test
TI	Thermal Imaging
VIS	Visible
VNIR	Visible Near Infra-Red
2D	Two-Dimensional
3D	Three-Dimensional

1 Introduction

1.1 Objective of Research

This PhD project formulates part of the research programme towards the understanding of how human's physiological features can be captured from stand-off distances. This is a basic research and the ultimate objective of the overall research programme is to understand how these remotely acquired physiological features can be deployed for assessing one's emotions. In this study two main kinds of basic emotions have been considered: (1) Clam emotion and (2) Strong emotions specifically anxiety due to (a) panic and anxiety resulting from psychological pressure and (b) pain or fatigue resulting from physical demands. These two different kinds of emotions in (a) and (b) are denoted as mental (MSE) and physical strong emotions (PSE) in this thesis.

This PhD project focuses on the remote sensing of physiological features in the facial region, together with heart beat rate (HBR) and a first attempt of glucose level assessment using Electro-Optical (EO) imaging technique. The research involves three main parts: (a) instrumentation design and experimental set up, (b) properties of physiological features in the facial region acquired by remote sensing technique and (c) how these physiological features can be used for the detection of strong emotions, such as anxiety, due to emotional or physical stimulations or stressors. The project was initially funded by the UK MOD and the Directed Research programme, and it was later partially supported by the InnovTech Solutions (ITS) Ltd particularly in the area of heart beat rate (HBR) detection development. Subsequently all publication related to this work needs the consents from both UK MOD and ITS.

1.2 Motive of Research

The research for the detection of human's emotional states from standoff distances without direct contact with the object, have been one of the greatest demands in biomedical, man-machine interfacing, and affective computing sectors. Conventional methods have largely been using facial expressions (Edwards, Jackson, & Pattison, 2002)(Fasel & Luettin, 2003) for the remote sensing of people's emotional state,

however, the facial expressions can be suppressed by will, which makes this approach not robust enough for the detection of malicious intent. Involuntary physiological responses under the command of the sympathetic nervous system such as body sweat, heart rate, breath rate, body temperature, blood perfusion and oxygenations, have been proposed (Chen, et al., 2009)(Yuen P. , et al., 2009) as a tool to monitor the emotional states of people (Pavlidis, Levine, & Baukol, 2001)(Pavlidis & Levin, 2002).

One novelty in this work is the use of EO imaging technique for the detection, and subsequently classification, of human's emotional state from a stand-off distance for the very first time (Yuen P, 2009). The basis of the present work is based on the fact that elevated level of adrenaline is secreted into the blood stream when a person is experiencing extreme emotional or physical conditions causing anxiety or excitement, which in turn triggers an elevated heart beat and breathing rates resulting in an increased level of blood perfusion and StO2 in the body. This work serves as the first study in the field thus to allow other researchers in the community to continue the approach for a deeper understanding of how physiological features can be used for the classification of human's emotional states.

1.3 Contribution and Achievements

One innovation in this study has been using multiple physiological features extracted from thermal and hyperspectral imaging (HSI) technologies to assess people's emotional state semi-quantitatively from a stand-off distance for the very first time. The detection includes the remote sensing of HBR and the assessment of blood transfusion in the forehead region.

The main contributions of this research have been:

i) To produce new evidences to invalidate the deeply believed concept of an increased skin temperature in the perorbital region when strong emotional states such as anxiety is taking place.

ii) The development of capability for the remote sensing of heart beat rate (HBR), facial physiological features and glucose level using imaging technique.

iii) The first attempt for using electrical optical (EO) technology for the remote sensing and classification of human's emotional state without the need of base line information.

1.4 Thesis layout

The layout of this thesis is arranged in the following manner: the motives and the objectives of the project are highlighted in chapter 1, which is then followed by a review of EO imaging techniques in chapter 2. The experimental set up and the methods for the data analysis employed in this work are described in chapter 3. This chapter includes a review of the principles and theories of thermal emission, diffuse scattering, Beer-Lambert law for the StO2 assessment and blood perfusion models adopted in this work. Subsequently a survey of remote sensing of emotions is given in chapter 4, followed by a description of the EO signatures found in this work in chapters 5. Chapter 6 outlines the main results for the clarification of the anomaly temperature induced by anxiety in the periorbital region, and chapter 7 describes the main technique developed in this study for the remote assessment of emotions without base line information. Chapter 8 address the issue for using EO data for emotion classification and finally the main conclusion of this work is summarised in chapter 9.

2 Introductions of Electro-Optical imaging techniques

When an object is illuminated by light it is quite common that not all the incident energy is absorbed: part of it will be transmitted, and part will be reflected and some of the absorbed energy will be re-radiated. The electromagnetic band in the visible to near infrared (VNIR) ranging from 400nm-2500nm wavelength region is commonly termed as the reflective band, as most of energies in this waveband is scattered back into the space from the illuminated object. Longer wavelengths beyond 3μm are known as radiative or emissive band due to the fact that they are the photon energies that are re-radiated from the body of the illuminated objects.

In this study we have utilised sensors in both the reflective and emissive bands to capture the physiological features of people with a view to understand their emotional states without direct contact with them. These two classes of sensors and their operation principles are briefly outline in the next two sections.

2.1 Sensing of emissive band by thermal imaging (TI)

Thermal imaging (TI) senses predominantly the emission bands in the mid and long wave infrared (MWIR/LWIR) wavelengths to deduce the ‘temperature’ of the emissive body. The amount of radiation emitted from various parts of an object keeps in pace with the temperature change across the surface of the object, thereby the thermal image presents an outlook of temperature variations over the object. With the advent of highly sensitive thermal camera off the shelf, temperature measurements can be made remotely during the day and at night. Thus TI has been deployed widely including geological mapping and military applications.

Bounded by the visible and the microwave spectral bands, the infrared light spans 3 orders of magnitude in wavelengths and it is normally divided into (a) the near infrared spans from 0.7 to 3 μm, (b) the middle wavelength infrared band 3-14 μm, and (c) the far infrared spans from 14 to 1000 μm, respectively. The near infrared is being used for telecommunications and remote sensing, e.g., to study land using and geological mapping. Long wavelength and middle wavelength infrared find its main use in thermal imaging. The wavelength range of interest in the present study has been the VNIR, MWIR and LWIR regions (figure 2-1).

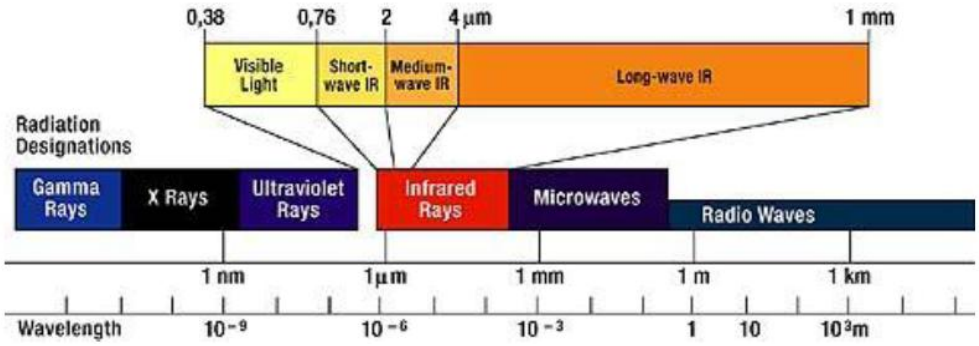

Figure 2-1 Wavelength of interest of the electromagnetic spectrum in the present study: VNIR and LWIR.

2.1.1 Overview of radiative theories

Emissivity is a term describing a material's ability to emit thermal radiation and it varies considerably from substance to substance spanning anything from zero to one. It is noted that the black body has been a theoretical object which does not exist in real life and thus the extent of radiations from all objects are in fact less than their true temperatures. Further complication of the issue is that radiative emission is a property not only stemming from the material's temperature characteristic, but also that it depends on the spectral wavelength, as well as the angular emission angle which is hardly isotropic. In most engineering applications it is however assumed that the surface's spectral emissivity behaves like a constant and in this case it is commonly termed as the grey body assumption.

Since many substances are capable to reflect or transmit a part of the incident radiation, the radiation energy that is absorbed and emitted will be less than that of blackbody. Non-blackbody emitter can only emit a fraction of radiation energy with respect to the blackbody at the same temperature. Therefore, the emissivity can also be defined as a measurement of the maximum amount of radiation that a substance is able to emit.

2.1.1.1 Emissivity and Kirchhoff's Law

The emissivity ε is defined as ratio of the radiant emittance W' of the source to the radiant emittance of a blackbody W at the same temperature:

$$\varepsilon = W'/W \qquad \text{Equation 2-1}$$

Emissivity is a function that dependent on the wavelength and the temperature of the material. A more general expression in terms of the spectral emissivity $\varepsilon(\lambda)$ is

$$\varepsilon = \frac{\int_0^\infty \varepsilon(\lambda) W_\lambda d_\lambda}{\int_0^\infty W_\lambda d_\lambda} = \frac{1}{\sigma T^4} \int_0^\infty \varepsilon(\lambda) W_\lambda d\lambda \qquad \text{Equation 2-2}$$

Where W_λ is the spectral emitted radiation, ε denotes the emissivity and T is the absolute temperature, σ is the stefan's constant. Note that the emissivity $\varepsilon(\lambda)$ can be ε =1, or ε = constant, or varies with wavelength.

Thermal radiation over a body is usually categorized into three portions: transmission, absorption, and reflection. When a given radiant energy is incident on a surface there are three situations that may happen: a fraction of the incident energy α may be absorbed by surface, a fraction p may be reflected to air and a fraction Γ may be transmitted through substance. Due to the fact that energy must be conserved, the sum of these terms must be equal to one:

$$\alpha + \rho + \Gamma = 1 \qquad \text{Equation 2-3}$$

The absorptivity α^λ is the ratio of the energy absorbed by the object to the incident energy for a particular wavelength. The absorbed energy will be proportional to $\alpha^\lambda E_{b\lambda}(\lambda, T)$ where $E_{b\lambda}(\lambda, T)$ is the intensity of black body radiation at wavelength λ and temperature T. The emissivity of the object is $\varepsilon_\lambda(\lambda, T)$ where ε_λ is the emissivity at wavelength λ. For a black body this yields:

$$\alpha^\lambda = \varepsilon_\lambda \qquad \text{Equation 2-4}$$

$$W'/\alpha = W \qquad \text{Equation 2-5}$$

This is also commonly known as "good absorbers are good emitters" and the Stefan–Boltzmann law describes the total energy radiated from per unit surface area of a black body in unit time (j^*) which has been shown to be proportional to the fourth power of the black body's absolute temperature T:

$$j^* = \sigma T^4 \qquad \text{Equation 2-6}$$

To combine the Kirchhoff's law with the Stefan-Boltzmann's law:

$$\varepsilon\sigma T^4 / \alpha = \sigma T^4 \qquad \text{Equation 2-7}$$

From this it follows that ε = α . Thus the emissivity of any material at a given temperature is numerically equal to its absorptions at that temperature. For an opaque material it does not transmit energy and thus ($\alpha + \rho$) = 1 and:

$$\varepsilon = (1 - \rho) \qquad \text{Equation 2-8}$$

2.1.1.2 Wien's law

The temperature-dependent spectrum of radiation emitted by a black body is termed as black-body radiation and at room temperature it emits nearly all wavelengths which are mostly in the infrared. The peak of the blackbody radiation tends to move towards longer wavelengths with lower intensities when the temperature reduces (see figure 2-2). The Wien's displacement law has shown that the spectral distributions of blackbody radiation at different temperatures are in a trend according to an inverse relationship between the black body temperature and its peak wavelength of emission:

$$\lambda_{\max} = \frac{b}{T} \qquad \text{Equation 2-9}$$

Where λ max is the peak wavelength in meters, T is the temperature of the blackbody in Kelvin's (K), and b, normally refers to Wien's displacement constant.

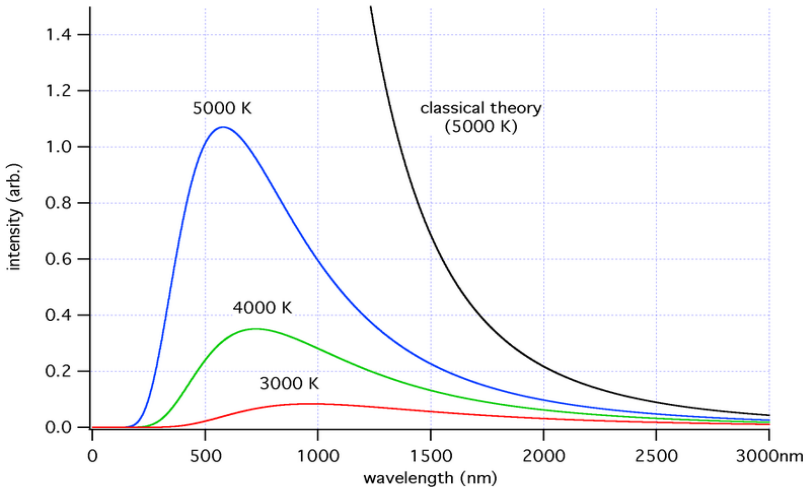

Figure 2-2 shows the Wien's law of black body radiations which exhibits a characteristic peak of radiation intensity moving towards to shorter wavelengths as the temperature of the black body increases.

It is noticed that both the Wien's and the Rayleigh-Jeans law has got problems which seem to work well only in the short and long wavelengths respectively. Subsequently Planck proposed a radiation function based on quantum mechanical principle:

$$E = h\nu \qquad \text{Equation 2-10}$$

$$I(\nu, T) = \frac{2h\nu^3}{c^2} \frac{1}{e^{\frac{h\nu}{kT}} - 1} \qquad \text{Equation 2-11}$$

where $I$is spectral radiance, or energy per unit time per unit surface area per unit solid angle per unit frequency or wavelength (as specified), ν is frequency, T is temperature of the black body, h is Planck constant, c is speed of light, k is Boltzmann constant. Planck function is only practically valid only when many photons are being measured.

2.1.1.3 Angular dependence of emissivity

Real objects are not perfect emitters and will therefore emit less radiance than a blackbody. The spectral emissivity$\varepsilon(\lambda)$, is a measure of the effectiveness of an object as a radiator. For Lambertian surfaces, the emitted radiance is distributed equally into the hemisphere above the surface. The self-emission for Lambertian surfaces is defined as

$$L(\lambda, T) = \varepsilon(\lambda) L_{\mathrm{B}}(\lambda, T) \qquad \text{Equation 2-12}$$

Most materials are not Lambertian and the emissivity term is modified to incorporate this dependence on viewing angle. The self-emission for non-Lambertian surfaces is then

$$L(\theta, \phi, \lambda, T) = \varepsilon(\theta, \phi, \lambda) L_{\mathbf{BB}}(\lambda, T) \qquad \text{Equation 2-13}$$

Where (θ, ϕ) indicate the direction of the sensor. The parameter $\varepsilon(\theta, \phi, \lambda)$ is known as the directional emissivity.

The emissivity of a material is a function of the angular emission, wavelength and temperature. For example the emissivity of water varies considerably from band to band, and at wavelength of 10 um it is a perfect blackbody while it becomes a mirror at 'low' angle of emission (ie ~90). Shown in figure 2-3 is the emissivity value simulated for human skin using a dielectric model (Shahram, 1992) at the wavelength of 10um using polarised (E & O) and unpolarised light as functions of

angle of emission. It is seen that the emissivity spans from zero to one for the emission angles of 0 to 90 degree with respected to the normal of the plane.

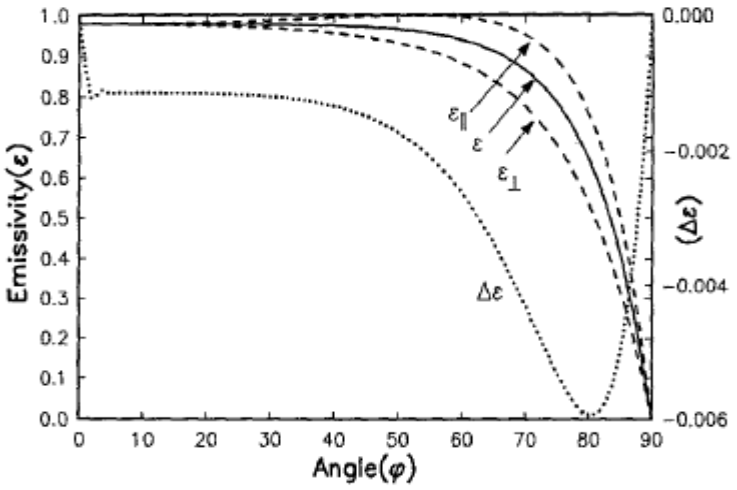

Figure 2-3 shows the angular dependence of emissivity in human skin simulated for 10um wavelength and note that the emissivity stays constant for the emission angles less than 60 degree with respected to the normal of the plane (Shahram, 1992).

2.1.2 Infrared Detects

There are two main different types of infrared detectors, namely the photon and thermal detectors.

2.1.2.1 Photon Detectors

Photon detectors directly convert incoming photons into photocurrents. In a photodiode, incoming photons are absorbed and generate electron-hole pairs that are given rise to a photocurrent. For the photons to be absorbed by the semiconductor, the band gap of the semiconductor must be higher than the photons' energy. For a given material, the achievable photodiode signal-to-noise ratio depends on the ratio α/G, where α is the absorption coefficient and G the rate of thermal generation of free charge carriers. In the LWIR range, i.e., the most suitable range for thermal imaging, it is required to cool down the semiconductor to cryogenic temperatures (≤ 77K) in order to obtain a good performance.

2.1.3 Thermal Detectors

Thermal detectors are one kind of photon detectors in which it firstly convert photons into heat before measuring the induced change in temperature. There are several physical mechanisms that can be used to measure this change in temperature.

2.1.3.1 Pyroelectric Detectors

Pyroelectric detectors use pyroelectric materials to measure the temperature change caused by infrared radiation. Pyroelectric materials are materials that change polarization upon change in temperature. Pyroelectric detectors can only operate in AC mode, as free charges will cancel the obtained polarization in DC. The current flowing into or out of a pyroelectric detector is made out of two electrode in between which is a pyroelectric material and the current is given by

$$I = Ap\frac{dT}{dt} \qquad \text{Equation 2-14}$$

Where A is the area of the electrodes, p the pyroelectric coefficient, and dT/dt the rate of temperature change.

2.1.3.2 Thermo-mechanical Detectors

Thermo-mechanical infrared detectors use deflection of composite cantilevers made of two materials having different coefficients of thermal expansion. The deflection at the tip of the cantilever is given by

$$\Delta Z = C * L^3 (a_1 - a_2)\Delta T \qquad \text{Equation 2-15}$$

Where C is a constant that depends on the materials' thicknesses and their Young's modulus, L is the length of the cantilever, and α1 and α2 are the coefficients of thermal expansion of the two layers. There are several ways this deflection can in turn be measured, e.g., optical reading (deflection of a light beam on the cantilever), capacitive sensing ,or piezoresistive sensing.

2.1.3.3 Bolometers

Bolometers are thermal sensors that use a thermistor to measure the temperature change induced by incident infrared radiation. The change in bolometer resistance due a change in temperature is given by

$$\Delta R = \alpha R \Delta T \qquad \text{Equation 2-16}$$

Where α is the temperature coefficient of resistance of the thermistor and $\triangle T$ the temperature change due to the incident radiation.

2.1.4 Thermal Camera

A thermal camera is a non-invasive device that detects IR energy and converts it to an electronic signal, which is then processed to produce a thermal image. Therefore, radiation energy from the object as sensed by camera can be accurately quantified. In order to operate thermal camera effectively without being affected by the noise arising from the dark current, most TI cameras normally employ a number of detector elements together with cooling system. There are also uncooled FPA-type (focal plane array) cameras which is more affordable but with a trade-off of having lower sensitivity.

In the areas of imaging system analysis, image quality specification and sensor trade-off studies are most commonly refer to spatial resolution and sensitivity. The sensitivity is normally defined as the noise equivalent parameter that would lead to the radiance difference of the target with respected to that of the background.

A thermal camera can be characterised by its signal transfer function, noise equivalent temperature difference, contrast transfer function and minimum resolvable temperature difference. Signal transfer function (SiTF) is the slope of the linear portion of the response function of a system. The responsivity function is defined as the output to input transformation in which the target size is fixed and the target intensity is varied. It is typically S-shaped as shown in Figure 2-4. For many systems, the electronics have a limited dynamic range compared to the detector and the output is therefore designed to centre at about some average value. Saturation in the positive and negative directions about this average value is typically limited electronically by the dynamic range of an amplifier or analog-to-digital (A/D) converter.

Noise is defined in the broadest sense as any unwanted signal components that arise from a variety of sources. The RMS noise voltage can be referred to the input that produces an SNR of unity. The noise equivalent differential temperature (NEDT) is a measure of system sensitivity. The system noise signal can be measured as the output signal when no useful input signal is applied. Once SiTF is obtained from the responsivity function, the NETD can be calculated as follows

$$NEDT = \frac{\Delta V_n}{SiTF} \qquad \text{Equation 2-17}$$

$$SiTF = \frac{\Delta V}{\Delta T} = slope\ of\ responsivity\ function$$

ΔV_n = output root mean square (rms) noise voltage

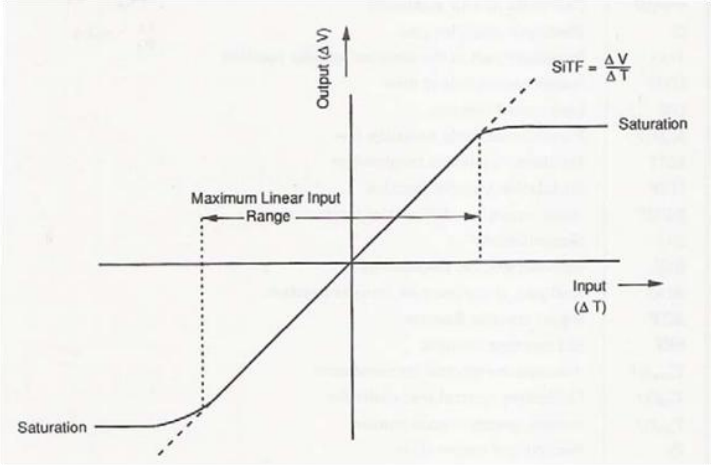

Figure 2-4 Typical responsivity function illustrating the SiTF.

2.2 Hyperspectral imaging (HSI)

Hyperspectral imaging (HSI) is a spectral sensing technique which takes hundreds of contiguous narrow waveband images in the visible and infrared regions of the electro-magnetic spectrum (figure 2-2) (Shaw & Burke, 2003) (Smith R, 2006). The image pixels form spectral vectors which represent the spectral characteristic of the objects in the scene and therefore HSI has been mostly applied for material identifications and discriminations purposes. Although HSI was originally developed for mining and geology applications, its usage has quickly spread into other civilian sectors and more recently into the military sector due its capability of material discrimination (Goldberg, 2003). In military and security applications the technique has been specifically adopted for the detection and recognition of targets which are normally well camouflaged with respect to the background and hence HSI is designed as a counter-countermeasure allowing 'look-alike' targets to be differentiated (Yuen, 2006). As illustrated in figure 2-5, which depicts the red/green/blue (RGB) image of an apparent green leafy plant (figure 2-6a) but in fact there is only one live leaf and the rest of them are fake leaves. This highlights the need of a technique like HSI which exploits information in high spectral resolutions

over a wide spectral range to allow the discriminative detection of targets even when they exhibit subtle spectral contrast with respect to the background.

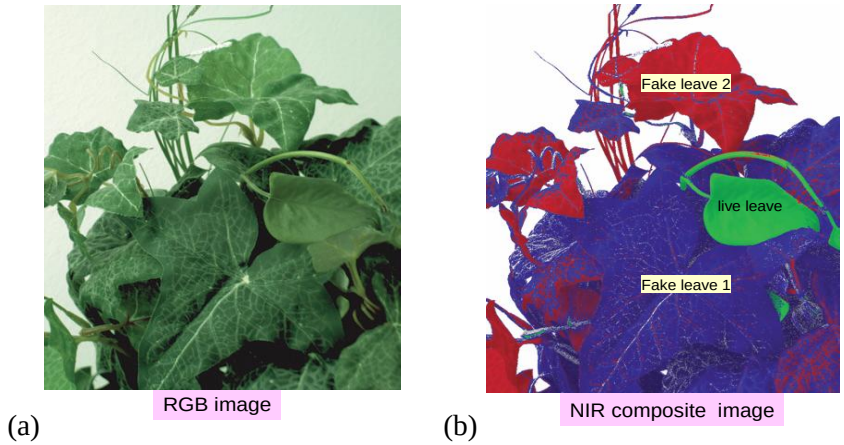

Figure 2-5. Highlights the common usage of HSI for material discrimination: in (a) it shows the 3-broad bands of RGB picture of a green plant and in (b) it shows the image of the same plant but using a composite of 3 narrow wavebands in the visible and near infrared region, which is shown capable to discriminate the live leaf (in green) from the fake (in blue and red).

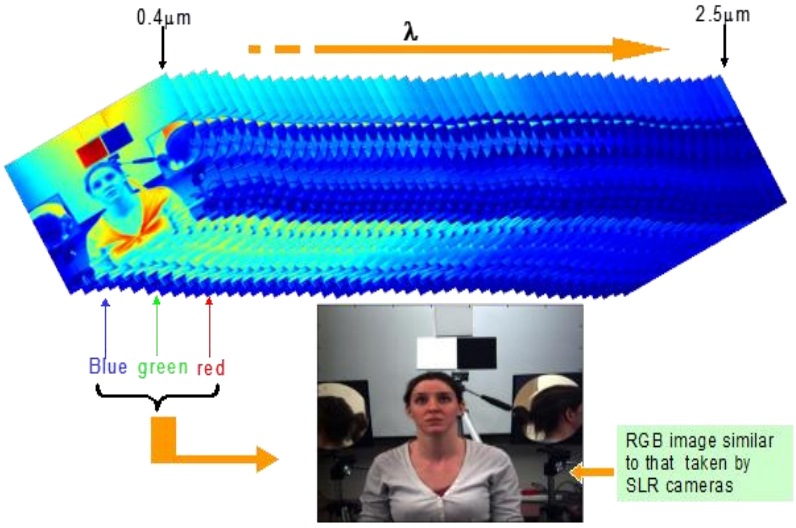

Figure 2-6 Introduces the concept of hyperspectral imaging (HSI) which is literally a technique that takes many contiguous narrow waveband images instead of just the 3 broad bands of red, green and blue colours as in the conventional digital photography.

2.2.1 HSI instrumentations: an overview

HSI collects large numbers of contiguous narrow spectral bands for a scene forming a hyperspectral cube (figure 2-6) which contains two dimensions of spatial and one dimension of spectral content (Shaw & Burke, 2003) (Smith, 2006). In the heart of the HSI instrumentation is the spectral dispersion mechanism which is known as spectrograph (figure 2-7), and it exists in various different forms of which the most

common three categories have been the dispersive spectrometer, the Fourier transform interferometer and the narrow band tuneable filter. Details of these spectrographs can be found in the literature by Vagni (Vagni, 2007).

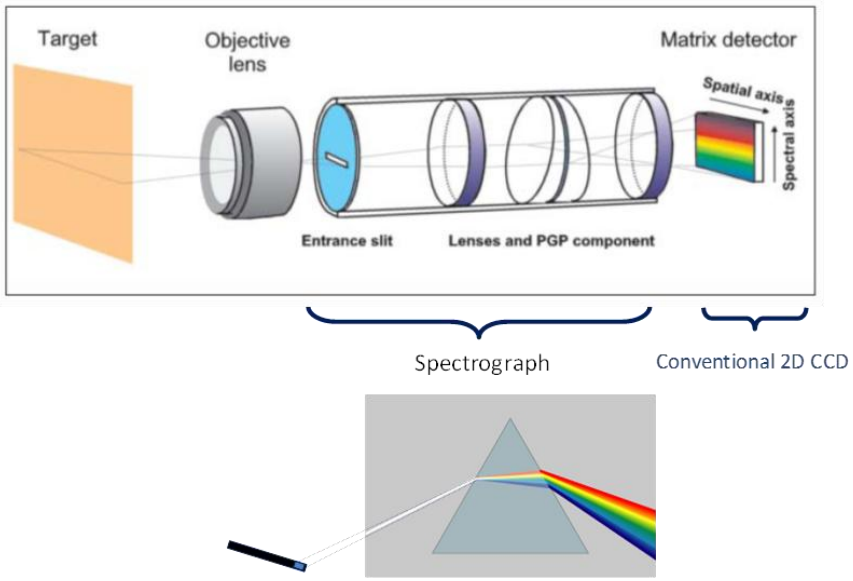

Figure 2-7. Outlines the components of a typical HSI system which consists of a spectrograph and a 2D CCD sensor as imaging device.

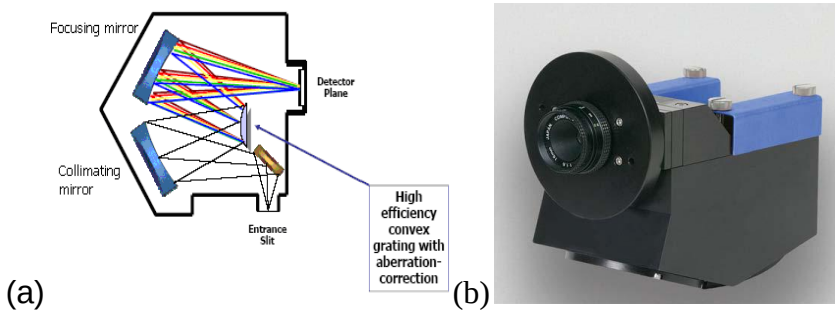

Figure 2-8. (a) Shows the schematic ray diagram of the Offner convex spectrograph. (b) the very compact housing for the Offner spectrograph manufactured by the Headwall Photonics.

2.2.2 Dispersive spectrograph

Dispersive imaging spectrometer employs either a grating or prism for light dispersion. The hyperspectral cube is formed by sensing one line of image such that the spatial and spectral information is stored in each dimension of the 2D sensor array. This means that the system can only image a line of the scene at a time and this is commonly realised through a small slit (~40□m width) situated at the back of the objective lens (see figure 2-8). A prism has advantages of having high efficiency and low scatter, but their optical design tend to be considerably more complex than their grating-based counterparts.

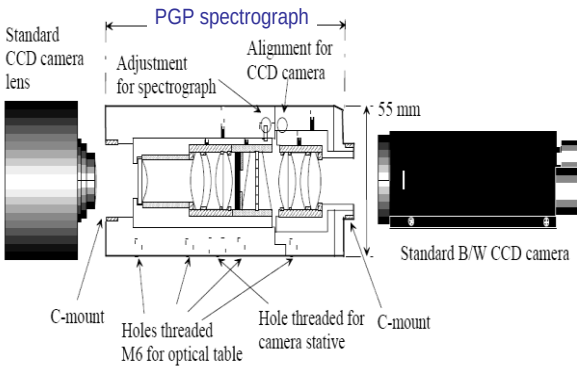

Figure 2-9. Shows the schematic drawing of the PGP based spectrograph

Gratings can be optimised to achieve high optical power for a certain order of interference within a specific wavelength region. The spectral resolution of a grating is proportional to the order and to the number of lines in the grating, and it is constant over the image plane for a constant incident angle of the radiation. In a grating spectrometer the prism is replaced by either a transmissive or reflective grating and in the all-reflective optical design the grating system can achieve high efficiencies of about 85%. There are two forms of gratings and the most common one has been the convex grating utilising the Offner spectrometer design as that illustrated in figure 2-9. The gratings of this type tend to be small, typically ~25mm diameter. The advantages of the Offner spectrometer are that it operates with a relatively low F-number (≥f/2) and it accepts a long slit while maintaining a compact size. The design can be very simple as it needs only three optical surfaces and it utilises only spherical and centred surfaces. Note the compact size of the spectrometer which makes it very suitable for some applications such as surveillance tasks.

The other design of the dispersive imaging spectrograph has been using both the dispersing elements prism and grating in a single package. This is generally achieved using a special designed volume transmission grating which is cemented between two almost identical prisms, and it is commonly known as Prism-Grating-Prism (PGP) (Aikio, 2001) as shown in figure 2-9. The PGP has the advantage of preserving the optical axis but with a penalty of losing transmittance due to the fact that materials with high dispersion also exhibit high absorption which results in a reduction of the overall throughput of the system. Due to the linear layout of the PGP the physical dimension of the PGP spectrometer is more extensive than that of the Offner design.

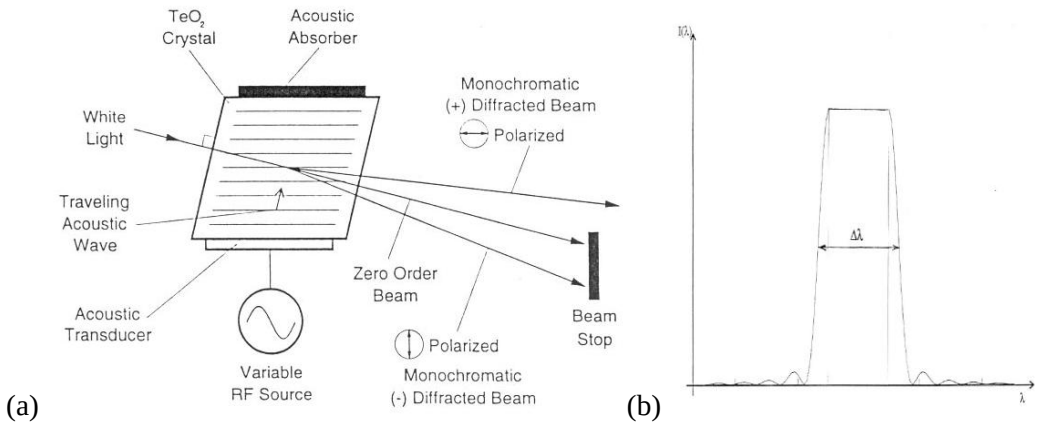

Figure 2-10. In (a) it shows the schematic working principle of AOTF for MSI illustrated by using the TeO_2 as the piezoelectric crystal and operated in a non-collinear configuration. One important characteristics of the AOTF MSI is the flexibility of tuning, which not only allowing the user randomly select the pass wavelengths in any spectral order, but also that it enables a variable band width of the passband as shown in (b), and all these features are not possible to be achieved by using the dispersive spectrograph system.

One of the greatest drawbacks for using dispersive spectrograph in HSI instrumentation have been the requirement to operate the system in a line scanning mode like a push broom. Hence this design will require the movement of the imaging system or alternatively the need of an optical scanning device in order to capture the full hyperspectral cube of the scene. One way to avoid this shortcoming is the use of narrow band tuneable filters which 'scans' along the spectral dimension. Filters like circular or linear variable filters, acousto-optical tuneable filters (AOTF) and liquid crystal tuneable filters (LCTF) (Gat N, 2000) (Rajwa B et al, 2005), (Vagni, 2007) have been implemented in step stare mode operations such that snap shots of the whole scene at the pass band wavelengths can be taken in a sequential manner. Amongst these filters, the AOTF and the LCTF have been the most popular (Fong et al, 2008) choices for multispectral imaging (MSI) implementation.

The acousto-optical tunable filter (AOTF) makes use of light diffraction within a piezoelectric crystal such as TeO_2, by passing an acoustic wave simultaneously with the light beam through the crystal. There are several different configurations and the acoustic wave can be propagated orthogonally or in parallel to the input light beam. When an acoustic wave is propagated through the piezoelectric crystal, the refraction index of the crystal is modulated by the alternating planes of compression and rarefaction of the travelling ultrasonic wave as it propagates through the crystal. As shown schematically in figure 2-10 the crystal behaves like a grating which diffracts light of specific wavelength into a beam stop or a polarizer, and the

diffracted beam is then sensed by the sensor. At a given wavelength of the acoustic wave λ_a, the diffracted light at the passband of λ_l can be given by:

$$\lambda_1 = \delta_n \alpha \lambda_n \qquad \text{Equation 2-18}$$

where δ_n is the birefringence of the crystal and α is a parameter dependent on the design of the AOTF system. The diffraction efficiency of AOTF is proportional to the strength of the acoustic beam and it can achieve a maximum of ~90% split between the two polarised diffracted beams with a net throughput of ~30-45% in each beam. The spectral range of the AOTF depends very much on the characteristics of the crystal as well as on the size of the angular aperture, which, tends to reduce the overall useable spectral range when a large angular aperture is used. In practise the crystal utilises small aperture sizes of ~12x12mm with FOV of ~4 degree capable to deliver a spectral range of ~500nm-850nm (Pannell , 2006) (Fong, 2008). In general the crystal is driven using a very small range of acoustic frequency δf_a centred at f and this effectively broadens up the transmission characteristic by $\lambda_l \pm \delta\lambda_l$ allowing a user selected bandpass width (figure 2-10b), which otherwise is fixed in the grating design (by the entrance slit). As in equation 2-18 the diffracted beam λ_l can be changed by alternating the frequency of the acoustic wave, thus giving a complete electronically tuneable optical filter without any moving parts. Furthermore, the λ_l can be tuned either sequentially or even randomly in any spectral order; something that the grating/prism based spectrometer could never attain. The tuning times are typically in the order of microseconds and consequently the AOTF system remains to be one of the most suitable candidates for catering applications which require high speed multispectral imaging (MSI), such as those in the surveillance applications where real time video recordings are required.

3 Experimental set up and data analysis

A significant portion of this research has been devoted to the experimental instrumentation which consists of building up two HSI systems and one AOTF MSI system during the first 18 months of the PhD study. These HSI and MSI systems have been used to capture the saturated tissue oxygenation (StO2) of the participants and to deduce their emotional states. The hardware construction of these systems and the models used for extracting StO2 are briefly outlined in this chapter while the software design is presented in the Appendix.

(a) 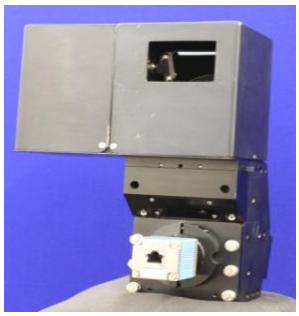 (b) 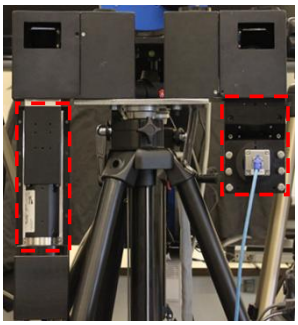

Figure 3-1 (a) the VNIR HSI camera constructed by our group at DA-CDS which consists of the Headwall's spectrograph and a PCO camera, together with a home built mirror scanner assembly situated at the top of the spectrograph. (b) The two line scanning hyperspectral cameras made by our group and on the left is the PGP based SWIR camera and on the right is the Offner VNIR system, the red rectangles depict the physical dimensions of the two spectrographs showing how compactness is the Offner design compare with the PGP one.

3.1 Home built HSI & MSI systems

Two different types of hyperspectral cameras with spectral sensitivities in the visible-near infrared (VNIR) and short wave infra-red (SWIR) have been extensively employed throughout this project. Commercially available hyperspectral imaging systems are extremely expensive to acquire and in many cases the performances of these off-the-shelf products are very limited. To tailor make for a fit-to-purpose instrumentation we opted to develop our own HSI systems by assembling Commercial-Off-The-Shelf (COTS) components together such as spectrographs, cameras, mirror scanners and device drivers. Unlike conventional push-broom type of hyperspectral cameras that have been frequently employed for the geographic information system and battlefield operation, all of our HSI cameras are designed in such a way that they are capable to acquire full hyperspectral cubes without the need to move the camera. One of the HSI cameras has been made using an Offner

convex gratings design (Bannon, 2007) as shown in figure 3-1, which depicts the spectrometer together with the home built mirror scanner (fig 3-1 a) for sweeping the image across the scene optically. This design has the advantages of being able to operate at a relatively low F-number (≥f/2) while maintaining a compact size. The other HSI camera has been using both the dispersing elements prism and grating in a single package known as Prism-Grating-Prism (PGP) (figure 3-1b).

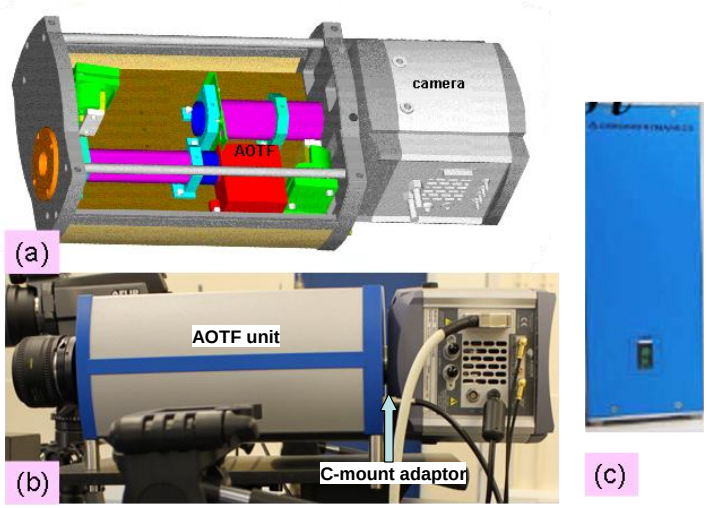

Figure 3-2. (a) Shows the AOTF system put together by our group for imaging in the VNIR spectral range using TeO_2 as the active crystal The figure shows the associate steering optics together with the AOTF spectrograph (in red) which is made by the Gooch & Housego Photonics with transmission characteristics of ~35%, and therefore a high end EMCCD camera (Andor Ixon 897) with a peaked QE of ~90% is employed. Due to the small FOV (~4) a 50mm objective lens is deployed as shown in (b). The unit is powered via a separate driver box through standard BNC interface (c).

Another camera which selects multiple narrow bands of wavelength using an acousto-optical tunable filter (AOTF) has also been deployed in this study. Shown in figure 3-2 is the AOTF multispectral imaging (MSI) system put together by our group and the system comprises of an AOTF filter (Gooch & Housego) together with an EMCCD camera (Andor Ixon 897). The system is capable to deliver ~50 frames per second at 512x512 pixel resolutions and it is sensitive for wavebands between 450nm and 850nm. The instrumentation work for the HSI and MSI systems includes the mirror scanner construction, optical alignment, and the image acquisition software design and implementation.

3.1.1 Mirror Scanner

The optical scanner is designed by my supervisor and the housing assembly is made by an engineering company in Bristol. The scanner consists of a motor and a mirror, which scans the scene through a step motor. The camera captures one frame of

spectral information for every motor step position and it is then stored in the memory of the computer. After a sequence of mirror rotation the spectral information of various parts of the scene are then stacked together to form a hyperspectral image cube. A servo driver board and a dual-axis controller board with independent power supply have been used for driving the motors. The driver electronics and controller boards are housed in a custom-made cooled housing.

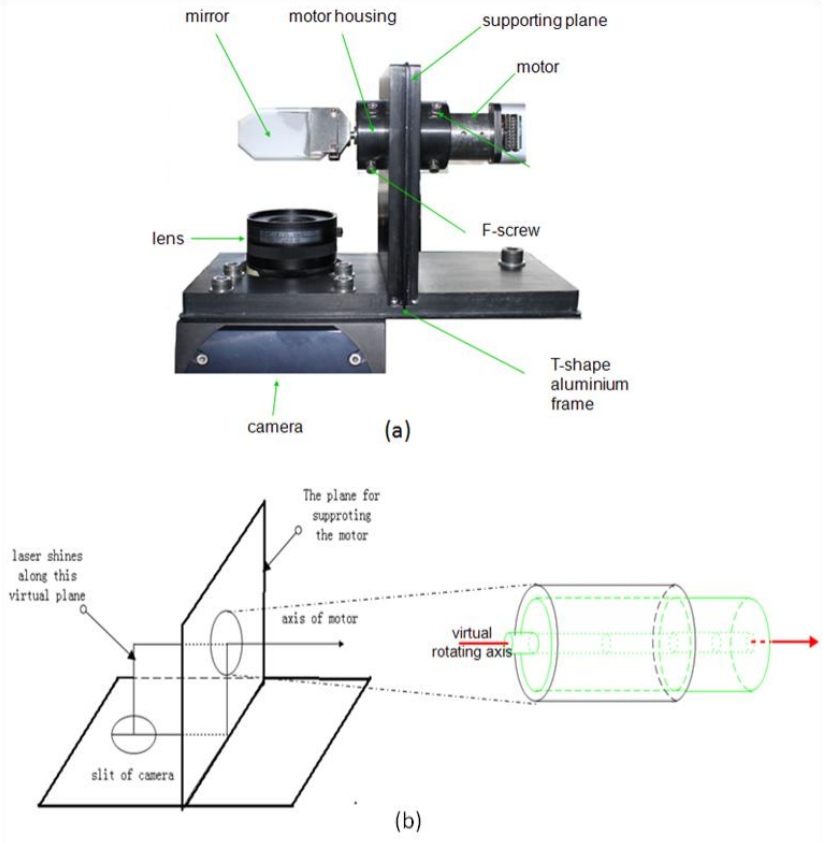

Figure 3-3 (a) Outlines the construction of the step motor assembly of the mirror scanner. (b) A schematic view of the motor housing and the optical axis of the spectrograph and the rotating axis of the step motor.

The step motor is located just above the objective lens of the camera through a T-shape aluminium frame as shown in Figure 3-3 (a), which is then in turn fixed on the top of the spectrograph. Eight adjustable scrub screws have been used for the alignment between the motor axis with respected to the optical path in the camera. The axis of the motor should be aligned perpendicular to the optical axis (Figure 3-3 (b)). The alignment is achieved using a perspex dummy motor which has a hollow cavity in the centre to allow a laser beam to pass through.

3.1.2 Thermal imager

This project requires a range of advanced equipment to maximise the probability of capturing the relatively ‘unknown’ signature. A great deal of the project resources has been utilised in the equipment acquisition, including an upgrade of an existing HSI camera into a fast multispectral system. This programme has employed two different types of thermal imagers with thermal sensitivities of NETD 17mK (SC7600) and 40mk (SC640) working in the usable spectral ranges of 3-5um and 8-12um respectively. The sensors of both imagers are of large format (640x480) MCT semiconductor FPA. Figure 3-4 shows the range of the equipment that has been employed during the course of this work.

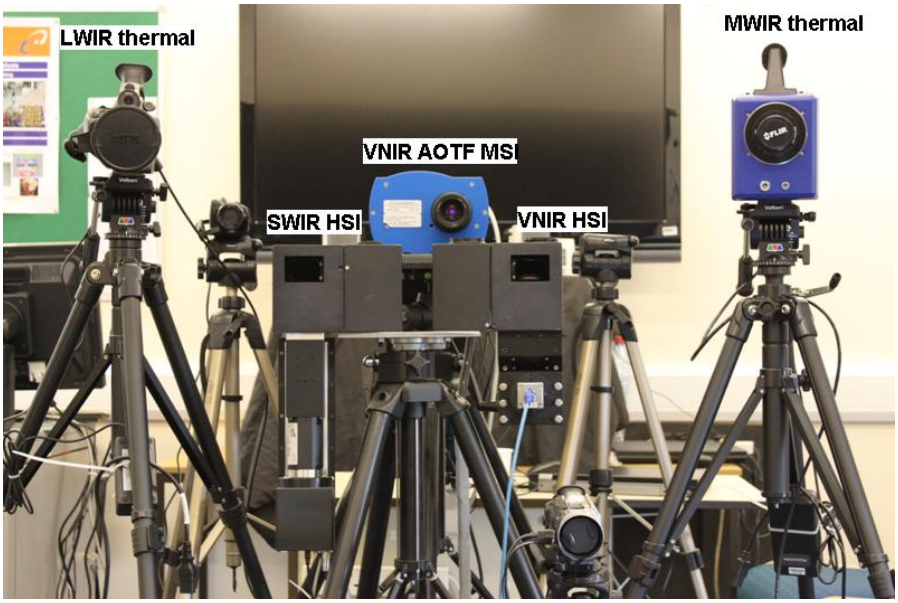

Figure 3-4 shows the equipment that has been employed in this study: (from left to right) the LWIR FLIR SC640, the home built SWIR HSI using a PGP spectrograph, the VNIR AOTF MSI using Gooch & Housego’s TeO2 AOTF unit, the home built VNIR HSI camera which utilises the Offner spectrograph, and the MWIR SC7600 FLIR thermal imager.

3.2 Experimental procedures

3.2.1 Stressor protocols & ethics approvals

All stressor protocols and the conduct of experimental trials involved in this study have been approved by the IRAS Ethics Committee under the REC reference 09/H0107/2. All participants in the study are required to comply with the conditions as stated in the health screening form and their consent is sought in terms of a written agreement as set out in the consent form. The experimental protocols are in

the order of i) mental stressor session (Triers Social Anxiety Test (TSST) (Yuen, 2009), pattern recognition test and physical anxiety test.

3.2.2 Outline of stressor sessions

All of the experiments that have been carried out in this study follow the protocols and procedures according to the approved REC forms and they are largely implemented in the following three main steps. Firstly, the participant is asked to wear a heart monitor (Garmin and Miroxi type) beforehand, and then the subject is led to a well-illuminated room for her/him to sit down comfortably. Throughout the experiment the subject is asked to avoid substantial body movement and to sit down calmly as much as possible. Then a rest time of about 5 minutes is given to allow the subject to settle in the new environment and subsequently base line information together with the saliva sample is taken. Shortly afterwards a series of stressors will be given to the participant, normally beginning with emotional stressor TSST which consists of a 3-5 minutes of mental maths and pattern recognitions, then follow by a 5 minutes rest during which another saliva sample together with a set of image is taken at this point.

The second procedure involves a physical stressor which involves an endurance test by asking the participant to sit down but without chairs, this is known as ‘stand horse’ (SH). The participant is encouraged to keep in the position as long as possible. In the final test it involves another physical exercise stressor which simply requests the participant to run upstairs a couple of times and then return to the room as quickly as possible. The participant is expected to be heavily loaded physically but not exhausted, and typically it takes only a minute or two to complete the test. Sets of images together with their saliva samples are subsequently taken prior to and after the stressor is applied.

3.2.3 Experimental setups & calibrations

A typical setup for the experiment is shown in figure 3-5 which consists of standard reflectance panels for spectral calibration in the 0.4-2.5um range, black bodies which are kept at constant temperatures of 30-40 C to serve as temperature calibrations, and mirrors for reflecting light within 0.4-20um wavelengths designed for viewing the side faces of the target from the front. A chair and a table have been provided for the

participants to rest and all cameras are set out at a range of about 3-5 meters from the target. The room is well illuminated by broad band halogen lamps diffusively scattered onto the target, and the participants are requested to wear a chest strap heart monitor (Garmin) as well as a finger probe (Miroxi) for measuring the StO2 and the heart rate (HBR).

During the trial we have collected over ~6 Terabyte of data and all the TI and HSI data has been processed using third party software and also our own algorithms on Matlab platform respectively.

Figure 3-5. (Left): shows the layout of the experimental setup for the anxiety assessment exhibiting a range of calibration panels and black bodies in the background. The room is well illuminated (~750 lux) by diffused halogen lamps as shown in the picture on the right.

3.2.4 Participants

Participants in this programme have been recruited mainly from within the Defence Academy and Cranfield University. There are a total of 85 volunteers to participate in the experimental trials and amongst them there are mixtures of different skin colours (Caucasians, Indians, Chinese, Malaysian, South Africans) in both genders and they are in the age group of 22-55 with a median age of 25. Over two third of the participants come from military background and the remaining are research students and academic staffs. Figure 3-6 shows representative pictures of participants in this study highlighting their various skin types, gender and professions.

The trial has been taken place both in the morning and afternoon during the Feb/March month and it is noted that the facial colours of the volunteers have exhibited substantial variations: ranging from brightly blush to rather pale. This wide range of facial flushness variations across this relatively small sample size has yet

again emphasised the significance of the large variability in individual's health/physiological conditions which emphasis the real difficulty for defining the exact 'base line' level.

Figure 3-6. shows the representative pictures of the participants involved in this study. Over 2/3 of the participants are from the military background and some participants have repeated the test several times in attempt to study the effects of diurnal variations and food/drink/smoking effects. Note the large variations of the facial flushness over these participants.

3.3 HSI Data processing for StO2 assessment

A small portion of this work involves the assessment of saturated tissue oxygenation (StO2) which is defined as the percentage ratio between the oxy-haemoglobin (HbO2) and the total haemoglobin (sum of deoxy-haemoglobin (Hb) and oxy-haemoglobin (HbO2)). Throughout this study we have utilised the Beer-Lambert model for the extraction of Hb and HbO2 and the methodology and algorithm are briefly outline in this section.

It can be seen in the following chapters that emotional anxiety induces predominantly an increase of heart beat and breathing rates, which in turn increase the tissue saturated oxygenation (StO2). In this study we have employed HSI technique for assessing StO2 through the optical absorption characteristics of the haemoglobin within the dermis layer. There are some reports on the remote sensing of StO2 using HSI technique (Cancio, 2006). However, there is an absence of work ever reported for assessing emotional anxiety using HSI.

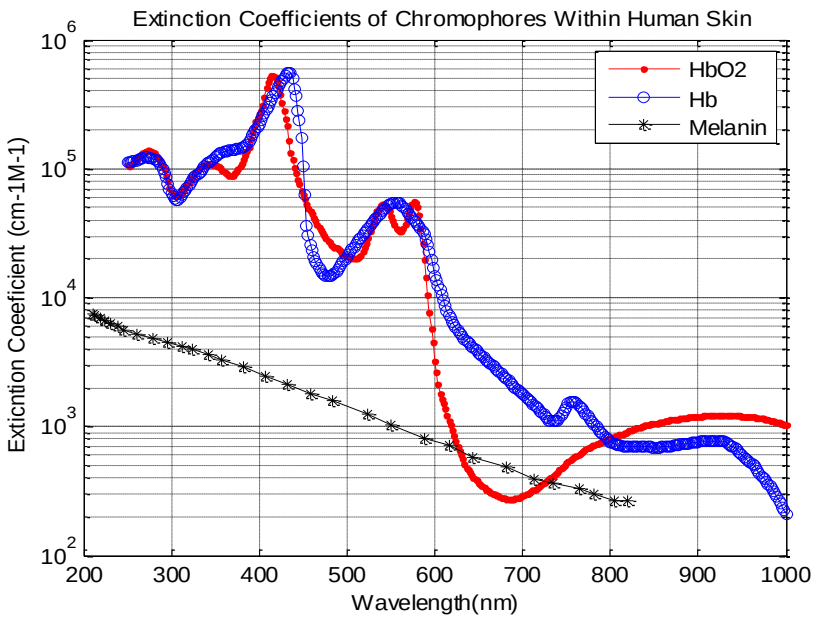

Figure 3-7 Molar extinction coefficients of melanin, oxy-haemoglobin (HbO2), and deoxy-haemoglobin (Hb) (Prahl, 1999) chromophore in human tissue.

3.3.1 Tissue chromophores absorptivity

The main chromophores in skin tissues are melanin, oxy-haemoglobin (HbO2), and deoxy-haemoglobin (Hb). The molar extinction coefficients of these three chromophores, in the unit of $cm^{-1}M^{-1}$, as function of wavelengths are shown in Figure 3-7 (Prahl, 1999). It is seen that melanin absorbs more photons in the shorter wavelengths region than that in the longer wavelengths, and the extinction coefficient of the melanin drops rather linearly from 200nm to 800nm wavelength. The Hb & HbO2 have nearly 40 times larger absorptivity in the ultra-violet than that in the near Infrared region. The absorption properties of HbO2 and Hb are quite close to each other but still discernible. In the region of 500nm to 600nm, Hb has one prominent absorption peak at about 556nm, while HbO2 has two absorption peaks at around 542nm and 576nm. In the region of 610nm to 900nm, an absorption dip is observed at around 686nm for HbO2, while one peak is seen at around 756nm for Hb. Both Hb and HbO2 show the strongest absorption properties in the region of 400nm to 450nm with peaks found in 412nm and 434nm for HbO2 and Hb respectively. The Hb and HbO2 has the same extinction coefficient at the wavelengths (isosbestic point) of 390nm, 442nm, 452nm, 550nm, 530nm, 545nm, 570nm, 584nm, and 797nm.

3.3.2 Beer Lambert (BL) models for StO2 assessment

3.3.2.1 Basic BL model

A great deal of work in the field of StO2 assessment has been based upon the Beer-Lambert Law (BL) which relates the absorption of light to the properties of the material through which the light is travelling:

$$A = \varepsilon l c = \alpha l \qquad \text{Equation 3-1}$$

where A is the absorbance, ε is the molar extinction coefficient ($cm^{-1}(mol/L)^{-1}$)(or molar absorptivity) of the material, c is the molar concentration (mol/L) of the absorber, l is the distance (cm) where the light travels through the material, α is the absorption coefficient (cm-1) of the chromophores. Equation 3-1 implies that the absorbance is linear with the concentration of chromophores. If the path length l and the molar abosorptivity ε are known and the absorbance A is measured, the concentration c of the substance can be deduced (K. J. Zuzak, 2001).

However, in the HSI reflectance model, the path length l can hardly be measured. The product $l\ c$ in equation 3-1 is thus normally reduced to C_{eff}, commonly known as effective concentration ($10^{-3}mol/cm^2$), which represents molar concentration of absorbers per unit area.

If only HbO2 and Hb are taken as two main chromophores for the HSI data recorded in the range of visible to near infrared region, the BL formulation can be written as

$$A = \varepsilon_{HbO2} C_{effHbO2} + \varepsilon_{Hb} C_{effHb} \qquad \text{Equation 3-2}$$

where ε_{HbO2}, ε_{Hb} and $C_{effHbO2}$, C_{effHb} are the molar absorptivity and the effective concentrations of HbO2 and Hb respectively. Equation 3-2 is commonly referred as basic Beer Lambert Law formulation (K. J. Zuzak, 2002).

If HbO2, Hb, and melanin are taken as the main chromophores for the StO2 assessment, then the basic BL model will be in the form of:

$$A = \varepsilon_{HbO2} C_{effHbO2} + \varepsilon_{Hb} C_{effHb} + \varepsilon_{melanin} C_{effmelanin} \qquad \text{Equation 3-3}$$

where $\varepsilon_{melanin}$ and $C_{effmelanin}$ are the molar absorptivity and the effective concentration of the melanin in the skin.

3.3.2.2 Extended Beer Lambert (EBL) Law

In the basic BL model it is assumed that the photon passes through the material without being scattered. In practise photons are scattered into different paths inside inhomogeneous turbid material like the body tissue, and some of them are simply lost after multiple scattering leaving only a small fraction of photons following the pathways and they are then collected by the detector. The path lengths of these photons travelled is much longer than the inter-optical distance l of the detector probes, and it is typically 4-6 times of l in live body tissue (Delpy, 1988). Thus the basic BL law in equation 3-2 is commonly modified into (Delpy, 1988) (Sassaroli, 2004):

$$A = \varepsilon lc \times DPF + G \qquad \text{Equation 3-4}$$

where DPF is the 'differential path length factor' to reflect the effective optical path length, G is the portion of photons that is lost due to the scatters. Equation 3-4 is commonly known as the modified Beer Lambert (MBL) law (D. T. Delpy, 1988) (A. Sassaroli, 2004). Note that the DPF is not a constant and it exhibits wavelength dependence behaviour (Kohl, 1998).

In many cases the effective photon mean free path $l \times DPF$ is unknown and many authors in the field (Zuzak, 2009) (Shaw, 2000) (Wolff, 1996) have approximated the DPF as a wavelength independent constant and to replace the $l \times DPF \times c$ into effective concentration C_{eff} turning equation 3-4 into (D. Yudovsky, 2011) (G. M.Palmer, 2012):

$$A = \varepsilon C_{eff} + G \qquad \text{Equation 3-5}$$

Equation 3-5 is commonly known as the extended Beer Lambert (EBL) formulation. And for two chromophores of Hb and HbO2 as the main absorbers in dermis tissue within the visible to near infrared (NIR) region (Zuzak K. J, 2002) then equation 3-5 becomes (D. Yudovsky, 2011) (K. J. Zuzak, 2007) (K. J. Zuzak, 2009):

$$A = \varepsilon_{HbO2} C_{effHbO2} + \varepsilon_{Hb} C_{effHb} + G \qquad \text{Equation 3-6}$$

Where ε_{HbO2}, ε_{Hb} and $C_{effHbO2}$, C_{effHb} are the molar absorptivity and the effective concentrations of HbO2 and Hb respectively. The parameter G has been treated as i) the collection of photons that have been scattered out of the angle of view of the

sensors (Yudovsky D, 2011), ii) those specularly reflected by the epidermis (Zuzak, 2007) and iii) the regression offset residues (Zuzak, 2009) (Cancio, 2006).

Due to the wavelength-dependent nature of the reflection from the melanin within the epidermis (Huang & Jacques, 1998), the G term in equation 3-6 (D. Hattery, 2002) (D. Yudovsky, 2011) (K. J. Zuzak, 2007) is often further split into two components (Yudovsky D , 2011) (Palmer, 2010) (Hattery, 2002):

$$A = \varepsilon_{HbO2} C_{effHbO2} + \varepsilon_{Hb} C_{effHb} + \varepsilon_{melanin} C_{effmelanin} + G' \quad \text{Equation 3-7}$$

where $\varepsilon_{melanin}$ and $C_{effmelanin}$ are the molar absorptivity and the effective concentration of the melanin in the skin, and the term G' represents all other factors not related to the tissue absorption such as specular reflection of the skin and the regression errors.

All the StO2 analysis has adopted the EBL in equation 3-7 throughout this study. The effective concentrations of Hb and HbO2 are obtained through the absorptions at three wavelengths of 563nm, 577nm and 796.8nm, together with the extinction coefficients of these chromophores adopted from the literature. This methodology is found simpler and sometimes more robust than that of the regression approach using a range of wavelengths (Yuen, 2012).

3.4 TI processing: Blood perfusion model

The other means for remote sensing of physiological features has been the use of thermal imaging (TI) technique. TI senses the skin temperature and it is necessary to translate the sensed temperature into physiological quantity, such as the blood perfusion. Blood perfusion is defined as the blood volume flow through a given volume or mass of tissue (in units of ml/ml/s or ml/100 g/min), and it represents local blood flow through the capillary network and extracellular spaces in the tissue. This section outlines the model that we adopted for translating the skin temperature into the blood perfusion rate.

There are quite a few blood perfusion models and one of them is based on the Heat-Conduction formulation (Iwao Fujimasa, 2000). This model has been adopted by Ioannis Pavlidis for his Polygraph Testing research (Ioannis Pavlidis, 2002).

Specifically, at thermal equilibrium the heat balance equation for human skin tissue is modelled as:

$$Qr + Qe + Qf = Qc + Qm + Qb \qquad \text{Equation 3-8}$$

Where Qr is the heat radiated from the subject to the air in units of calories; Qe is the basic evaporated heat; Qf gives the heat loss via convection into the air neighbouring the skin surface; Qc is the heat conducted by subcutaneous tissue; Qm gives the heat corresponding to the metabolic rate of cutaneous tissue; and Qb is the heat gain/loss via convection attributable to blood flow of subcutaneous blood vessels. After differentiating, the blood perfusion model is obtained in the following form:

$$\frac{dV_S}{d_t} = \frac{T_B\left(C_S + \frac{K_C}{3d}\right) - C}{(T_B - T_S\ )^2}\frac{dT_S}{dt} \qquad \text{Equation 3-9}$$

where α = 0.8 (counter current heat exchange in a warm condition); p_c = 0.92 cal/mL/K (heat capacity of blood); T_B =310K(blood temperature in the core); TS = the skin temperature; S = the thickness of the skin; Kc = 0.168 kcal/m/h/K (thermal conductivity of skin); and d = the depth of core temperature point from skin surface. C is constant. Cs = the heat capacity of skin. Figure 3-8 presents the sample images of blood perfusions from the thermal image (Ioannis Pavlidis, 2002).

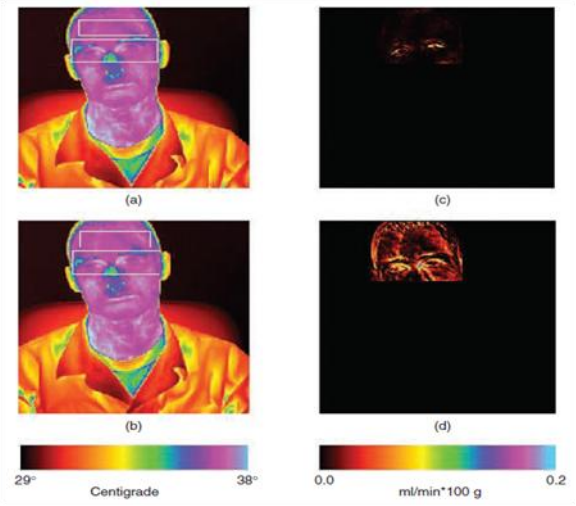

Figure 3-8 shows (a) Raw thermal image of subject when he starts to answer the question. (b) Raw thermal snapshot of subject when he almost finishes the question session. (c) The blood flow rate in subject's face as he start to answer the question. (d) Blood flow rate in subject's face as he almost finish the question session (Ioannis Pavlidis, 2002).

In order to avoid the situation that thermal pattern of face is highly affected by many factors, Wu simplified the blood perfusion model (Wu, 2006) as follows:

$$\omega = \frac{\varepsilon\sigma(T^4 - T_e^4)}{\alpha c_b (T_a - T)} \qquad \text{Equation 3-10}$$

Where ω represents the blood perfusion in the unit of ml/S per unit weight of tissue, σ is Stefan-Boltzmann constant, ε is the Tissue/skin thermal emissivity 0.98, T defines the Skin temperature, T_e is Ambient temperature, α defines the tissue/skin countercurrent exchange ratio (0.8) and Ta represents the artery temperature of 312.15K.

In this study we have adopt equation 3-10 for obtaining the blood perfusion from the thermal data throughout this work.

4 A survey of remote sensing of emotional states

4.1 Emotions and physiological response

4.1.1 Relevant emotional states in this study

Emotion is a complicated psycho-physiological experience that potentially offer a status of mind that can interact with biochemical (internal) and environmental (external) influences. Since human emotion is highly affected by physiological arousal, expressive behaviours, conscious experience, and associated with mood, temperament and motivation, reliable assessment of the affective component is important.

A classification of basic emotions was developed by Paul Ekman in 1972 and its model is categorized by: anger, disgust, anxiety, happiness, sadness and surprise. To focus on the difference of different emotions, Robert Plutchik proposed the “wheel of emotions”, suggested eight primary bipolar emotions: trust versus disgust, joy versus sadness, and surprise versus anticipation and anger versus fear.

In this study we focus exclusively on strong emotions such as anxiety, happiness and sadness that are stimulated by both mental and physical stressors (see section 3.2 for more information).

4.1.2 Hormones and emotional states

Two hormones, adrenaline and cortisol, are predominantly released by adrenal medulla and cortex respectively during the anxiety state. When the psychological stressors are identified as threat, the Hypothalamic–pituitary–adrenal (HPA) axis is activated and the cortisol is released from the adrenal cortex into the blood stream. Around 90% of cortisol in the plasma becomes bound by other tissues and membranes, and only the rest 5%-10% unbound cortisol travels in the blood stream to the target tissue and affect the metabolism there. Due to its light molecular weight and lipid-solubility, the unbound cortisol is capable to diffuse through the acini and the salivary gland. Thus it is widely accepted that the salivary cortisol concentration is a good biomarker of activation of HPA axis.

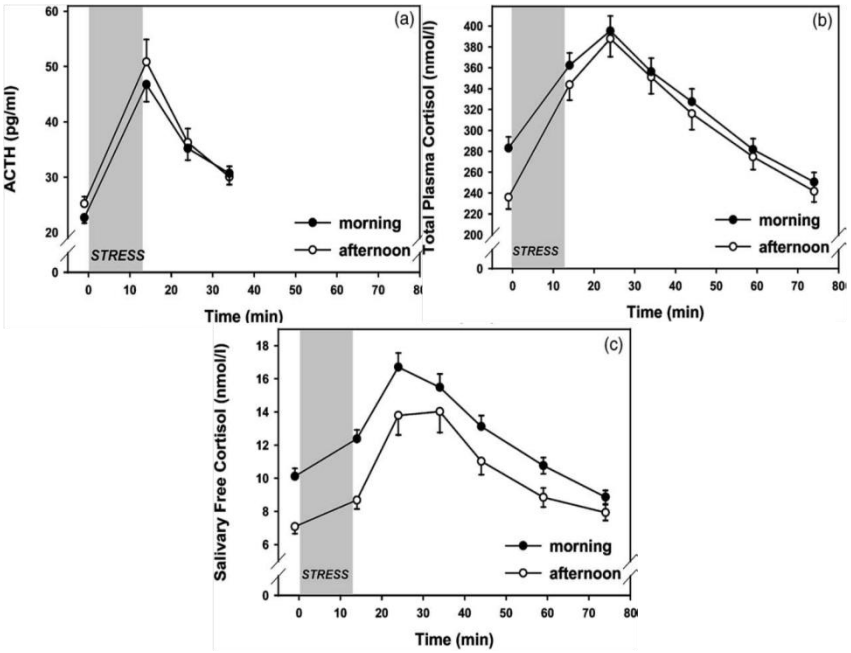

Figure 4-1Shows the time delay of hormone secretion upon anxiety (a) ACTH concentration (b) Total plasma cortisol concentration (c) Salivary free cortisol concentration (Kudielka, C, & Hellhammer, 2004)

However, there is a time lag between the increase of cortisol in the plasma and the increase of cortisol in the saliva. It has been reported that the concentration of salivary cortisol is observed to rise in the first minute of injecting 5 mg cortisol into the blood (Read, 1982), and the maximum salivary cortisol concentration appears after 1-2 minutes of injection. However, the release of the cortisol from the adrenal cortex is modulated by the adrenocorticotropic hormone (ACTH) from pituitary gland. There is about 10-15 minutes lag between the maximum secretions of these two hormones, despite of age, gender, and individual difference according to various reports (Federenko, 2004) (Kudielka, 2004). It is shown in Figure 4-1 that the ACTH exhibits a time lag of about 5 minutes after the stressor is applied, while the free cortisol in the saliva can have time lag of as long as 20-30 minutes after the stressor is applied (Federenko, 2004) (Kudielka, 2004) . It is also seen from Figure 4-1 that it will take a long time, and in some cases as long as 50 minutes, for the plasma cortisol and salivary cortisol to return to the normal state after the stressor is applied.

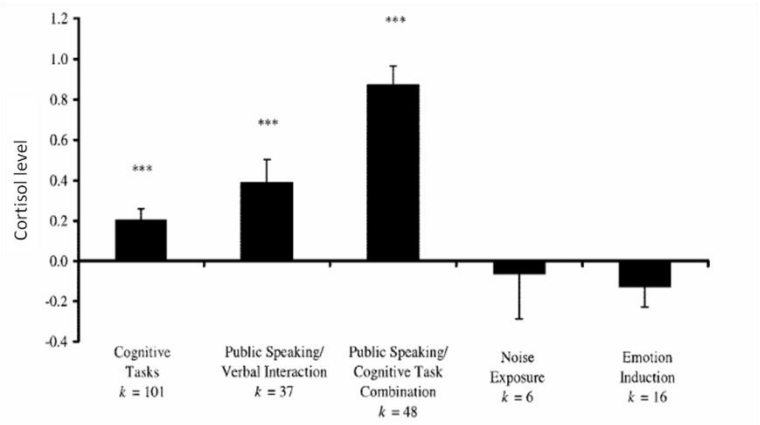

Figure 4-2 shows the use of a combined public speaking and cognitive task which can impose a more effective anxiety to the participants. (Dickerson, 2004)

Some studies have attempted to identify the effective stressor through the cortisol response, and various psychological stressors including public speaking (Sauro, 2002), cognitive task, (Condren, 2002) emotion induction (Berry, 2001) have been tried. Dickerson et al (Dickerson, 2004) conducted ~200 laboratory studies of acute psychological stressors and concluded that not all the stressors exhibited the same cortisol response. It was however indicated that the combination of public speaking and cognitive task might be more stressful to most people as evidenced by the higher concentration of cortisol as shown in Figure 4-2.

4.1.3 Physiological response to emotional anxiety

Emotional anxiety imposes direct effects over to the heart, lungs, and also in the circulation system which reacts by an accelerated heart rate and blood pressure. The lung tends to work overdrive by taking in more oxygen through an increased breathing rate, and at the same time the spleen releases more red and white blood cells allowing more oxygen to be carried to various parts of the body. A substantial leap increase in the blood flow particularly in the vessels to the muscles, lungs, and brain has been the forefront reaction upon the onset of emotional anxiety.

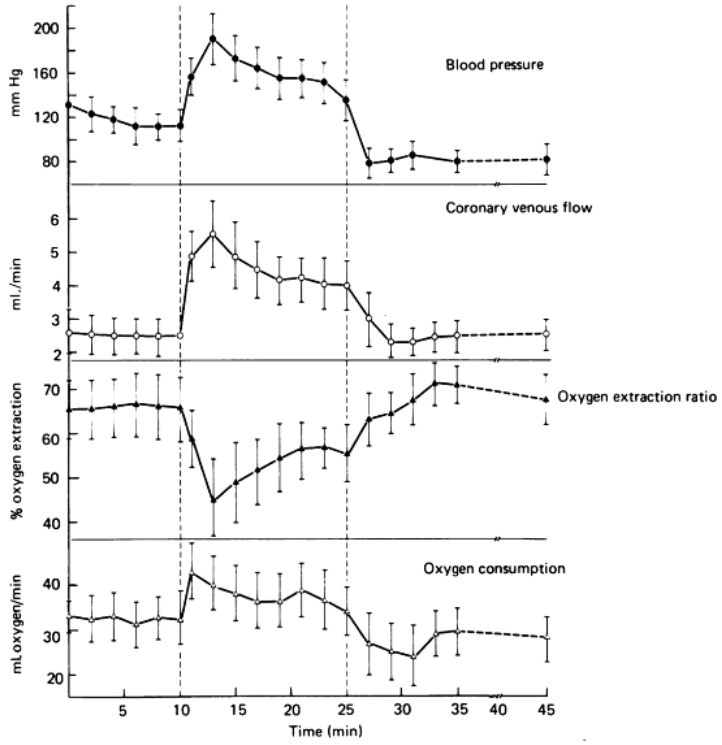

Figure 4-3 shows the variations of blood pressure, coronary venous flow, and oxygen extraction ratio and oxygen consumption of a dog under controlled injections of adrenaline (2ug/kg per min at the arrowed point) in an intravenous infusion experiment (Creates, 1980).

In summary the following physiological reactions have been identified during emotional anxiety characteristics of a fight-or-flight symptom:

- heart and lung action will increase
- glucose and oxygenation will be released for muscular action
- blood pressure increase
- Redirection of blood to provide the highest perfusion and fuel to the aroused brain, heart and muscles
- Constriction of blood vessels in many parts of the body, such as skin, stomach & intestine
- Acceleration of instantaneous reflexes
- Dilation of pupil
- Increase of sweat
- Suppression of concentration, short term memory, rational thought and navigation ability
- Auditory exclusion (loss of hearing), and general effect on the sphincters of the body and tunnel vision
- Inhibition of lacrimal gland (responsible for tear production) and salivation (mouth dryness)
- Inhibition of stomach and upper-intestinal action (digestion slows down or stops)
- Relaxation of bladder, evacuation of colon, inhibition of erection

4.1.3.1 Increase of tissue saturated oxygenation during anxiety

The combined first four physiological responses in the above list results in a remarkable elevation of blood oxygenation during anxiety: some ~100-200% increase according to previous clinical research [Creates et al, 1980]. The study has shown that the StO2 of the heart muscle of a dog increases substantially when 2μg/kg per minute of adrenaline infusion is applied (Figure 4-3). It is observed that an increase of blood pressure by almost 2-fold, together with ~90% increase of oxygen content in the blood while the oxygen consumptions by tissues are seen to remain more or less constant after the adrenaline injection, resulting in an abrupt drop of overall oxygen extraction ratio to almost a half causing a net increase of blood oxygenation ~100 - 200% after the adrenaline injections.

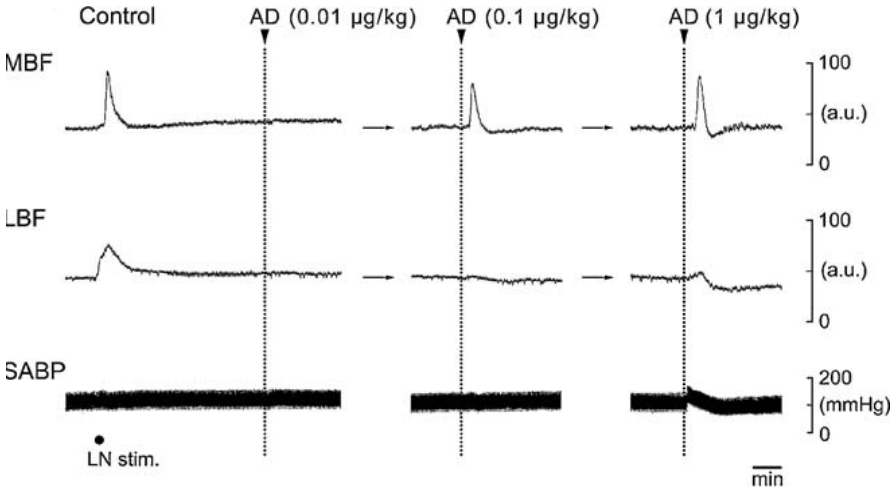

Figure 4-4(a) MBF is the blood flow of masseter muscle. AD represents adrenaline infusion. The transient increase of masseter blood flow caused by adrenaline is clear in both in 0.1ug/kg and 1ug/kg dose. The larger dose decreases the blood flow lower than baseline after the initial rise. (Ishii, 2009)

Another study on the blood flow of the rat's masseter muscle after intravenous infusion of adrenaline has been reported (Ishii, Niioka, & Izumi, 2009). It is shown that the masseter blood flow (MBF) exhibits a transient increase when 0.1ug/kg of adrenaline is injected (Figure 4-4), while the limb blood flow (LBF) and the blood pressure also exhibit a small increase upon the adrenaline infusion.

The increase of superficial blood flow 1-2mm below the skin surface on human facial region upon the onset of emotional stressor has been reported recently (Drummond, , 1997). The mean blood flow in the forehead (Drummond, 1997) (Drummond, 1994) (Drummond, 1987), and in the cheek (Drummond, 1994) (Drummond, 1987) are

seen to increase during the anxiety state. This result may imply an increase of tissue oxygen content in the facial regions during the anxiety state, although there is no direct evidence given in these reports. However, it is seen in next chapter that our HSI results have shown that it is indeed a substantial increase of StO2 especially in the facial region when one is in anxiety.

4.1.3.2 Change of blood perfusions during anxiety

4.1.3.2.1 Blood perfusions in the periorbital regions

Distinctive heat pattern in the facial region has been found associated with specific emotion state. Thermal signature of anxiety was firstly observed by Pavlidis et al (Pavlidis, 2000) (Pavlidis, 2002)(Pavlidis, 2001) (Pavlidis, 2003) in 2003 who reported that a person's anxiety, alertness, and fear, can be disclosed by an increase of temperature at around periorbital region. Figure 4-5 shows the original work published by the Honey Well team which portraits a seemingly unambiguous hot spot feature in the periorbital region due to a startle anxiety. Subsequently the team went further and reported how this anxiety-induced signature in the periorbital can be differentiated from other stressors, such as that due to physical exercise. Figure 4-5 shows the thermal images of a subject after a sequence of light and vigorous running exercise. The work claimed that there was almost negligible increase of blood perfusion at around the periorbital region after the running exercise.

However, other workers in the field have attempted the test on animals like the cow, and they found that their temperatures in the periorbital regions are fairly constant during the stressor experiment (Stewart, 2007).

It can be seen from our work that the mean temperature in the periorbital region is in fact quite constant when the subject is under anxiety (see chapter 9 for more information).

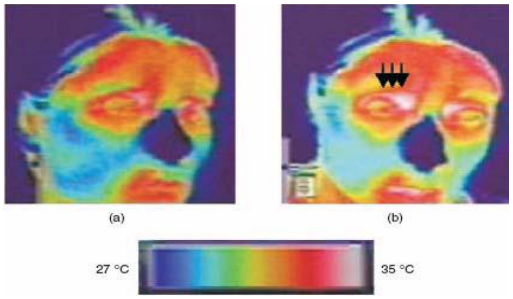

Figure 4-5: shows the false colour image of a subject before (a) and after (b) a startle. Note that the temperature at around the periorbital region of the subject which is seen to increase by almost 1C after the startle (Levine, 2002).

Figure 4-6: Highlights the Texas/Honeywell work which intended to demonstrate the 'uniqueness' of the anxiety signature found in the periorbital region. Shown in the figure is thermal pictures of a subject after (a) Base line b) walk for 1 minute c) walk for 5 minutes d) run for 5 minutes, Note that there is seemingly no increase of temperatures in the periorbital after physical exercising (Murthy, 2006).

4.1.3.2.2 Blood perfusions in the forehead

It has been reported that an elevation of forehead temperature is observed when a subject is under anxiety (Levine, 2009). The experiment was performed using two types of emotional stressors, namely the Stroop test and mental arithmetic. The Stroop test involved the reading of a number of words such as 'blue' or 'green' etc but they were in different coloured fonts. The temperatures of the subject in the forehead under these two tests were found to be highly correlated, with correlation coefficient of 0.96 (Levine, 2009). Figure 4-7 shows the experimental data of the temperature change in the forehead region using TI, and the blood perfusion of the region of interest (ROI) in the forehead using equation 3-10. It is shown that the mean temperature of the forehead was seen increased substantially when in comparison with that of the base line.

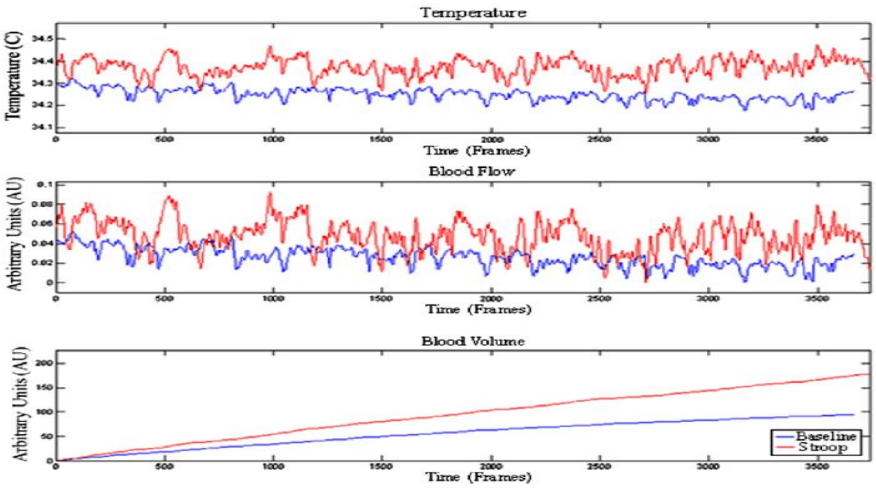

Figure 4-7 Shows the result of the strooping test performed by the Texas group: (Top) The forehead temperatures measured by TI technique showing an elevated temperature in the region throughout the test (red) comparing to the base line (blue). (Middle) The 'interpreted' blood flow and (Bottom) the 'interpreted' blood volume calculated by using a computational transfusion model using the temperature as the input.

4.1.3.2.3 Blood perfusions in the face

Blushing face has been one of the most common features for the indication of having an elevated anxiety. Many studies, have reported work on using high resolution TI system for monitoring one's anxiety through the temperature changes in one's facial region (Pavlidis I, 2003) (Puri, 2005) (TSIAMYRTZIS, 2007). Furthermore, recent work in the field has attempted to classify different types of emotions from the temperatures in the facial region. Jarlier et al (Jarlier, 2011) reported for the first time that distinctive heat pattern in the face can be associated with the activation of specific facial action unit (AU). The experiment was performed to monitor the change of face temperature with respected to that of the base line. The difference of these two sets of images for each activated AU is shown in Figure 4-8. It is seen quite clear that, the activation of these AU can be detected from the TI data, provided that the participants remain stationary or when a sophisticated image registration algorithm is available. Nevertheless, this result may open up new avenues for the detection of human emotions using thermal imaging techniques.

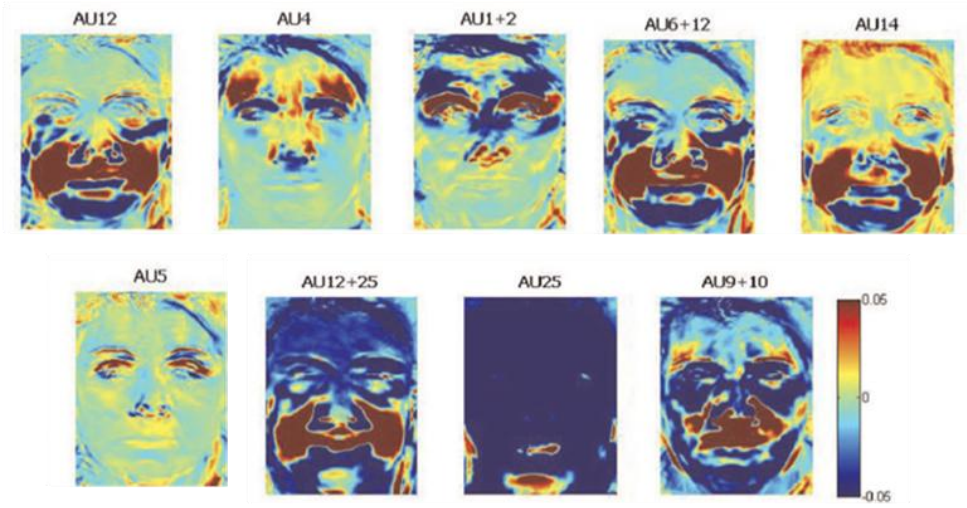

Figure 4-8 shows the heat patterns differences of a subject for the activation of different AU in the face with respected to the base line (Jarlier, 2011)

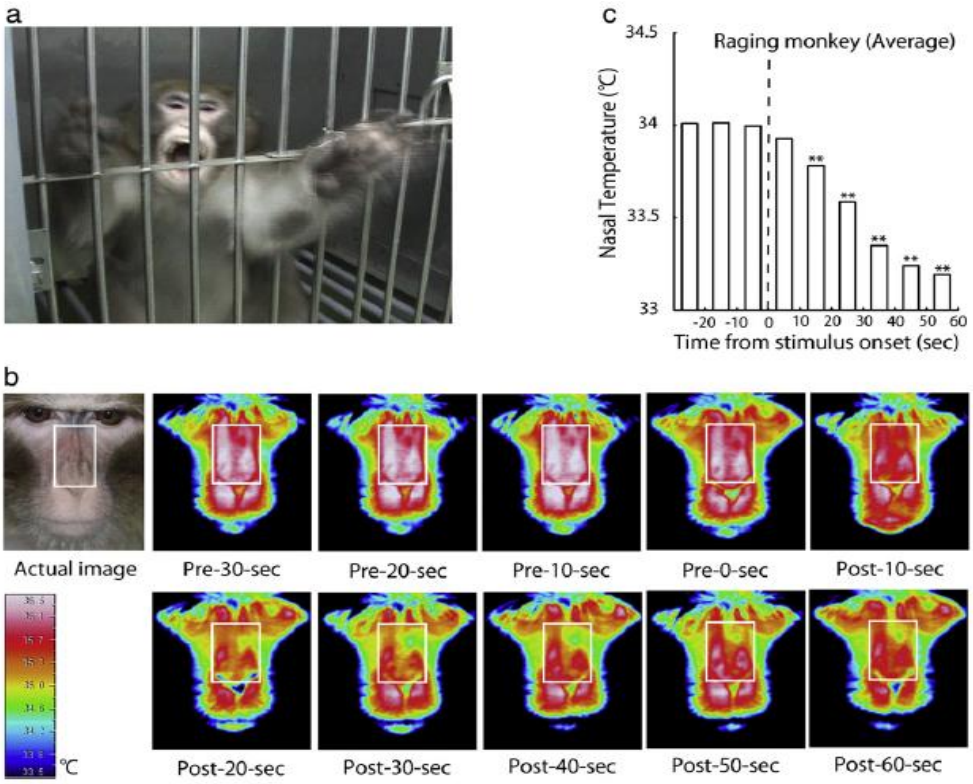

Figure 4-9 (a) illustrates the RGB image of a raging monkey. (b) shows the change of nasal temperature of the monkey (in step of 10s), before and after he was presented a video clip of a raging monkey. White rectangles within the thermal data represent the ROI for temperature measurement. (c) shows the ROI averaged temperature change in response to raging monkey video. It appears apparently that the nose temperature drop down significantly from the baseline after the raging video was presented to the monkey (Akio Nozawa, 2011).

4.1.3.2.4 Blood perfusions in the nose

It is found that the nose temperature of mammals like monkeys, is sensitive to anxiety (Kuraoka, 2011)(Nakayama, 2005). Koji Kuraoka (2010) and other workers

have observed a remarkable decrease of nose temperature in monkeys when they are in negative emotional state (anxiety). Figure 4-9 has shown that the nasal skin temperature of monkey can be reduced by ~2% (~0.8C) when it is under anxiety after a raging video is shown to it.

We have also obtained similar result when a human subject is under anxiety: the nose temperature is found reduced by ~1.5% (0.4-0.6C) (see chapter 10 for more information).

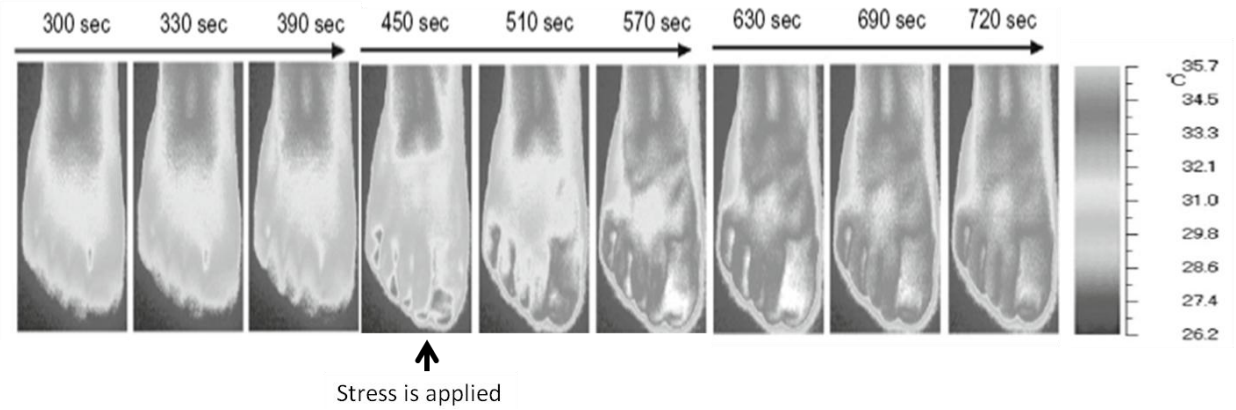

Figure 4-10.Thermal image of the dorsal side of the right foot during the stressor experiment

4.1.3.2.5 Blood perfusions in hand and foot

It has been reported that the dorsum of the foot is sensitive to the psychological status of individuals. It has been observed a rise in the peripheral skin temperature at the tips of the toes when one is under anxiety. Fig.4-9 shows the TI images of a subject after he is exposed to anxiety. It is seen that the temperatures at the tips of the toes exhibit a small drops as soon as the stressor is applied, and after a time lag of about 2 minutes the temperature at the toe is seen to rise by about 15% (~5C). (Akio Nozawa, 2011).

There are other parts of the body which have been seen also sensitive to the psychological state. Vianna et al has investigated the temperature of the rat's body, back, tail, and paw when the rat is exposed to a stressor (Vianna, 2005). It is observed that remarkable drop of the temperatures in the tail and paw of the rat are observed when the rat is under anxiety, while the temperatures in the eyes, head, and back have seen a slightly increase after the onset of the anxiety.

Note that the physiological features given by the hands and feet are not particularly useful to some applications such as the homeland security.

4.1.3.3 Glucose level during anxiety

Glucose measurement has conventionally been carried out using absorption spectroscopy technique, mostly in the visible and near infrared (NIR) range of around 590–950 nm, 1212–1850 nm and 2120–2380 nm due to the low water absorptions in these wavebands. In 2004, Cho et al has developed a method called the metabolic heat conformation (MHC) for the non-invasive measurement of blood glucose (Cho, 2004). The method employs a thermal and together with an optical sensor for fingertip measurement. It measures the thermal characteristics, the blood flow rate, haemoglobin (Hb) concentration, and oxy-haemoglobin concentration (HbO2), and through a multivariate statistical analysis to convert all these signals into a final glucose concentrations. Another approach in the area has been the use of thermal emission spectroscopy for probing serum glucose concentration (Carl, 2002). Olesberg performed an in vivo measurements of near-infrared rat skin absorption in the 2.0-2.5 um wavelength range during a glucose clamp experiment in order to identify the presence of glucose specific spectral information. His experiment demonstrates a significant similarity between orthogonal variations and the signal of glucose (Olesberg, 2006).

A rather interesting technique using temperature-modulated reflectance has been attempted (Shu-jen Yeh, 2003). The experiment consists of modulating the skin temperature between 22 and 38 °C to generate a periodic set of cutaneous vasoconstricting and vasodilating events and to induce a periodic change of light scattering in skin. This gives a period change of light absorption through the tissue and to give a more accurate glucose concentration.

Direct measurement of glucose level for healthy and diabetes patients upon anxiety hormone infusion have been conducted by Werner et al (Werner, 1992). It was found that the measured glucose level (MGL) is increased by almost 1.5 times of the base line level when small amount of anxiety hormone is infused into a healthy subject (Figure 4-11). However, there is again a time lag of 1-2 minutes for the glucose level increases to its peak after the anxiety hormone is infused. The amount of the time

lag seems to be very dependent on individuals: another study by Wing et al has shown that the glucose level is maintained to high level for another 30 minutes after the stressor is applied (Wing, 1985)[Figure 4-12].

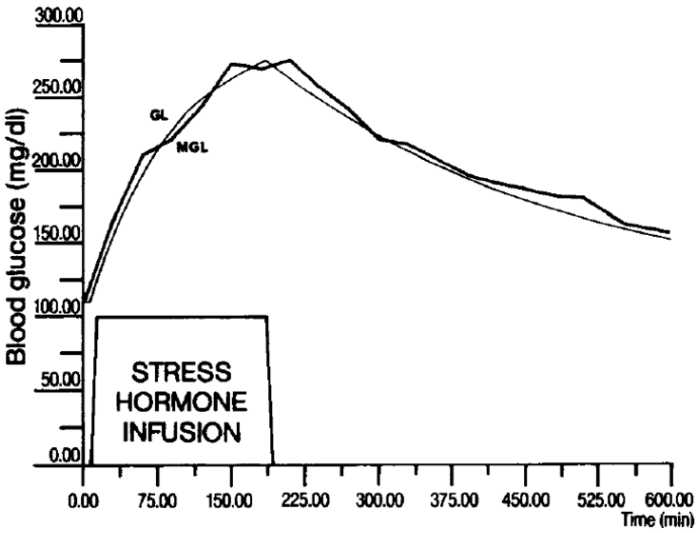

Figure 4-11. shows the measured blood glucose (MGL) response and the computer simulation (GL) during and after anxiety hormone infusion (SHI) in a healthy subject on intravenous somatostatin [250 pglhr. SHI: 3 h] (Werner 1992).

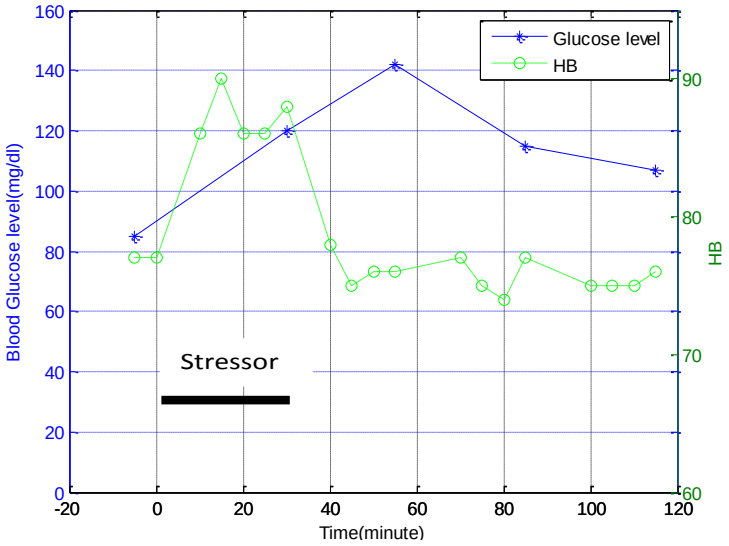

Figure 4-12: shows the long time lag (~30mins) of the blood glucose levels increase after the stressor is applied. The stressor is applied between 0 to 30 minutes (Wing, 1985).

There is a difference between the upsurge of the StO2 and the glucose level upon the onset of anxiety: the change of the StO2 has a shorter time lag of 1-2 minutes while the glucose level can keep increasing for 20-30 minutes!

4.2 Review of anxiety detection using physiological features

Anti-terrorism has been one of the greatest demands in the homeland security of the 21st century. Novel ideas such as direct detections of improvised explosive devices (IED) using electromagnetic wave, and indirectly through one's behaviour, activity, contextual and body language (gestures and facial expressions), have been proposed for the extrapolation of one's motive via human factor computational models within the last decade. However, it would be a technical challenge to detect explosives directly especially when they are packed in a light and air tight manner. Indirect methods using 'affective computing' approach relies a great deal on the concreteness of cognitive theories which itself remains to be a matter of intensive research.

Other direct methods, such as to assess one's intent through physiological or neurological states are viable, but it has been a technical challenge to make it practical. Conventional means for the detection of physiological states have been the direct contacting methods such as polygraph and functional magnetic resonance imaging (FMRI), and unfortunately both cannot be deployed in busy public places. This section reviews previous work in the field for the remote sensing of strong emotions such as anxiety.

4.2.1 Anxiety detection through HBR & blood perfusion assessment

4.2.1.1 Texas/Honey Well laboratory [2003-present]

Researchers in the Honey Well laboratory has been the first team to report the feasibility of sensing people's anxiety from a stand-off distance using thermal imaging method back in 2002 (Pavlidis, 2002) (Murthy, 2006). The exact signature discovered was a substantial increased amount of blood volume in the periorbital region as the result of adrenalins secreted into the blood stream upon the onset of anxiety (see section 4.1.3.2.).

Due to the high maturity in thermal imaging (TI) technology, the Texas team has studied how physiological features such as the change of blood flow, cardiac pulse, and breath rate signals can be probed using TI technique. His group has concluded that emotional anxiety brings about an instantaneous increase in the periorbital blood

flow and sustained emotional anxiety normally keeps pace with elevated blood flow in the forehead (Pavlidis et al 2007).

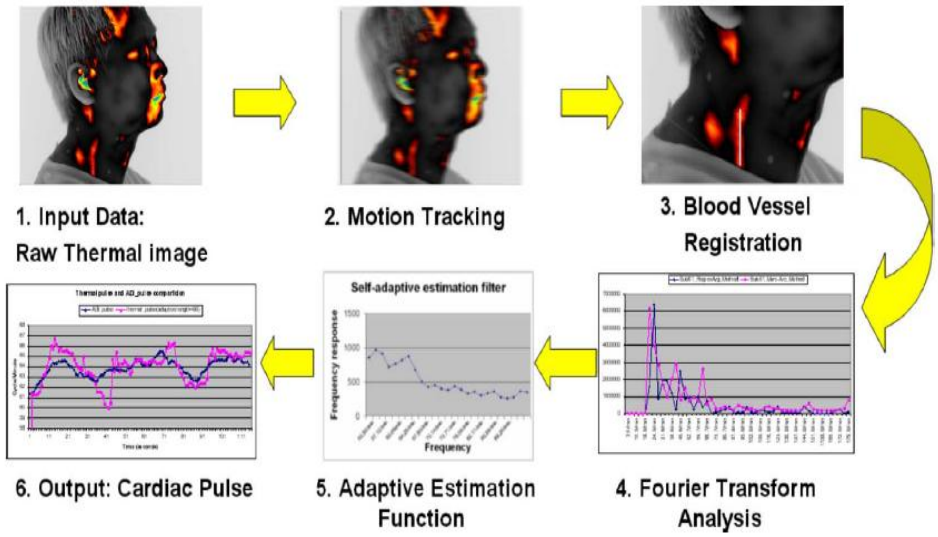

Figure 4-13.HBR measurement using TI: Steps 1-3 show the ROI tracking from the raw TI data. The FFT and the HBR and pulse estimation method are shown in step 4 to 6 (Pavlidis, 2007).

The Texas team has published a series of papers during the 2005-2010 period to demonstrate how the human's cardiac pulse can be extracted from the TI video of superficial vessels. The procedure consists of tracking the superficial vessel in the neck and then to apply Fast Fourier Transform (FFT) of the temperature data to obtain the frequency of the pulse (HBR). It is claimed that about 90% accuracy for the estimation of the HBR can be achieved. Figure 4-13 shows the procedure of the HBR detection by the Texas team (Pavlidis, 2007).

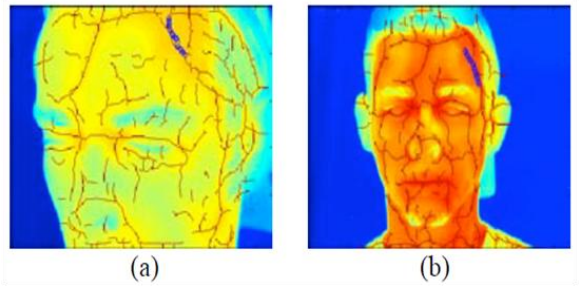

Figure 4-14Sample thermal images and overlays by the vascular maps in (a) near and (b) distant poses. The feature labelled by blue point is the ROI for further pulse extraction analysis (Gault, T.R, 2010).

Slightly different from the Texas team's HBR measurement approach, Gault et al has developed a wavelet based non-invasive assessment of human's facial vascular structure and arterial pulse rate using TI data [Figure 4-14] (Gault, T.R, et al, 2010). The vascular maps are firstly produced and the pulse information is then obtained

through a denoised continuous wavelet transform (CTW) and multi-resolution analysis. The pulse information is then filtered and subsequently the final HBR is reconstructed by using inverse continuous wavelet transform (ICWT). Typical HBR data obtained from this method is shown in Figure 4-15 and the accuracy of the HBR is claimed to be 89-99% accurate.

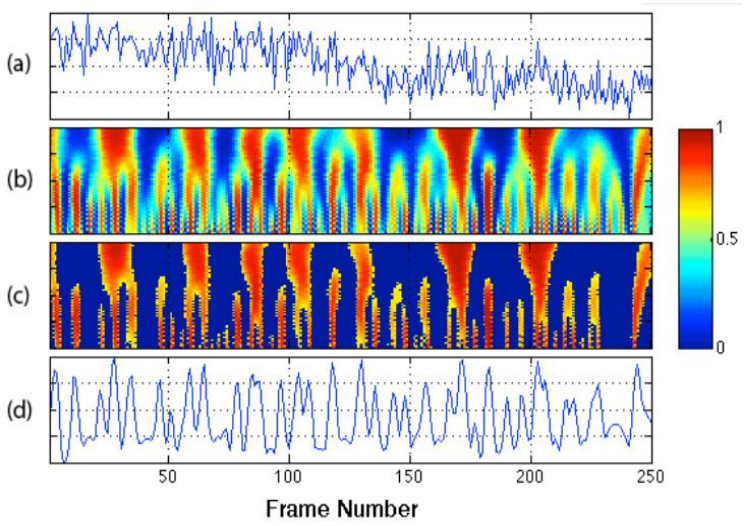

Figure 4-15.shows the quality of the HBR estimation using CTW technique: (a) 250 frames of raw TI data (b) wavelet coefficients (c). Filtered coefficients, (d) HBR obtained by ICTW (Gault, T.R, 2010).

4.2.1.2 US Army Research [2009-present]

The other physiological based research for the remote sensing of intent in the USA involves the Physiological Computing department of the Texas University Houston, the Electro-Optical (EO) companies OKSI Inc and the Draper laboratory. The core programme utilises thermal imaging expertises of the Texas University (Shastri et al 2009) which attempts to detect anomaly temperatures from the periorbital region, and to couple with HBR detections of moving targets in short ranges of several meters (Figure 4-16). This programme also utilises a 'new' concept similar to ours for detecting the intent through the blood oxygenation in the facial region. This part of the work is being carried out by the OKSI team, who had a brief discussion with us for possible research collaboration back in 2011. Unfortunately due to the complication of classification issues in both sides and eventually the research collaboration did not materialise.

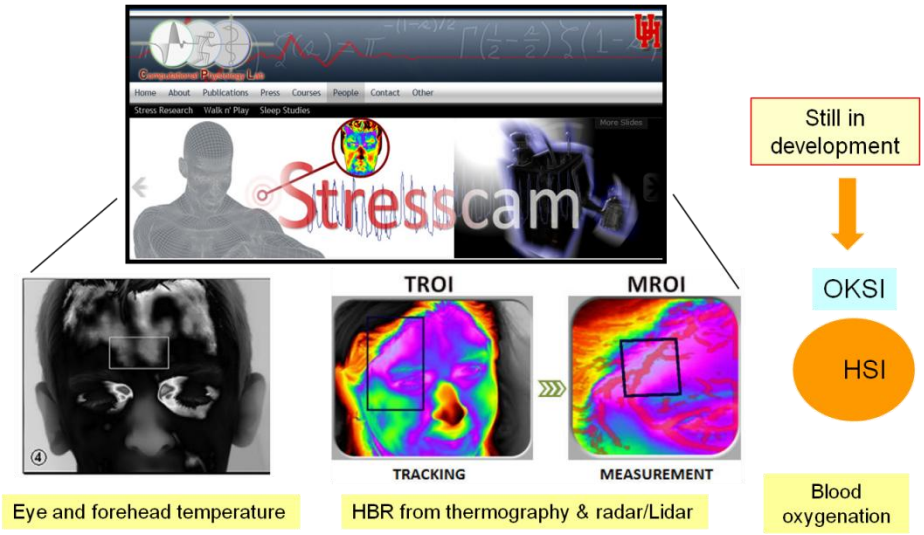

Figure 4-16: Shows the physiological based anti-terrorism consortium in the USA that includes the Texas University, OKSI and the Draper laboratory. We have been contacted by the OKSI for research collaboration in the area of remote sensing of blood oxygenation back in 2011.

4.2.1.3 UK Lincoln University [2009-2010]

Within the UK there have been a handful of research programmes about the remote sensing of intent initiated in the past five years. One of them is led by Dr Shigang Yue of the Lincoln University (Yue et al 2011) who has employed radar and thermal imaging for the detection of anxiety through facial blush and HBR. The research was funded by the Home Office in 2009. One great drawback in Dr Yue's work is the requirement of the prior baseline information for assessing the anxiety of individuals from standoff distances (Figure 4-17). Base line information is not always available in practical real situations.

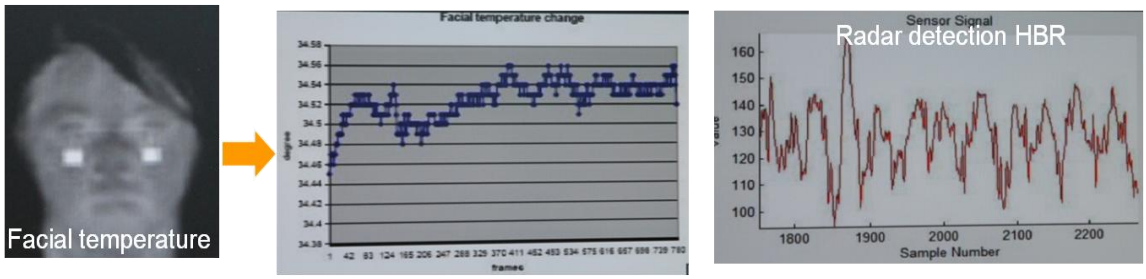

Figure 4-17: Highlights the Lincoln University work for the detection of anxiety from the face blush and the heart bit rate (HBR). Note that both techniques require the base line information in-prior for the anxiety interpretation. (Yue, 2011).

4.2.2 Facial expression & gesture classification

4.2.2.1 Conventional facial expression detection research

Many studies in this area have been using physical computing to extract the facial expression and/or gesture for emotions detection (Valstar, 2004) (Zhang, 2008)(Tong, 2007). This approach relies on the identification of the local facial Action Units (AUs) and to identify the anxiety through the Facial Action Coding System (FACS) (Ekman, 2002). There are a total of 44 AU identified and some of them are shown in Figure 4-18. Each AU is characterised by the activation of a set of muscle network in the facial region.

Note that facial expression and gesture can be suppressed by will and hence there are debates about the usefulness of this approach in real environment.

Figure 4-18 Outlines some examples of facial Action Units for coding and identification of facial expression (Ekman, 2002).

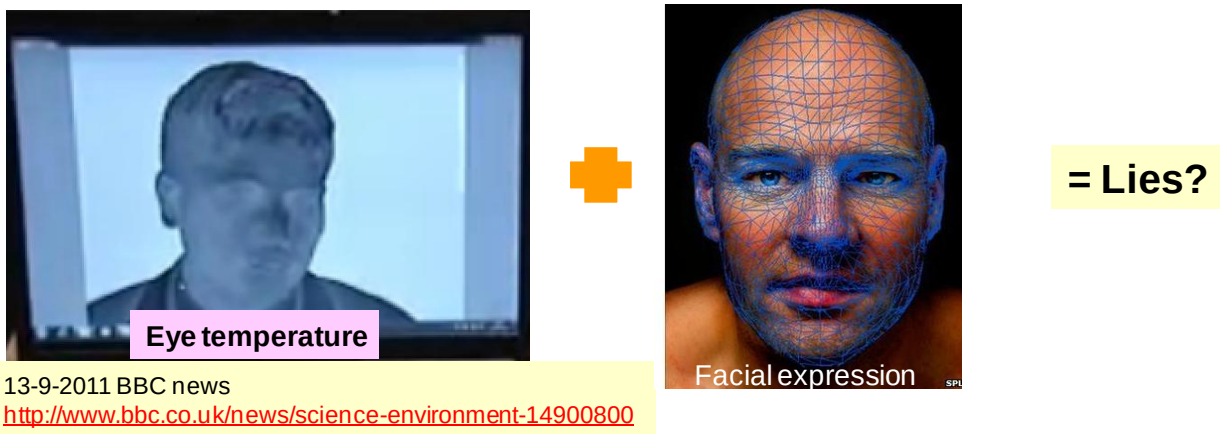

Figure 4-19: Highlights the Bradford University work for the lies detection using thermal imaging and physical computing of facial expression (Ugail, 2011).

4.2.2.2 Bradford University: [2009-present]

Prof Hassen Ugail of the Bradford university adopted the facial expression detection approach and couple with thermal imaging to formulate another means of polygraph assessment in 2009 (see Figure 4-19) (Ugail, 2011). Again, the thermography

attempts to detect the onset of anxiety through the anomaly hot spots in the periorbital region which then prompts the computer vision algorithm to focus on the facial expression analysis. However, the effectiveness of this approach for intent detection has not been confirmed yet.

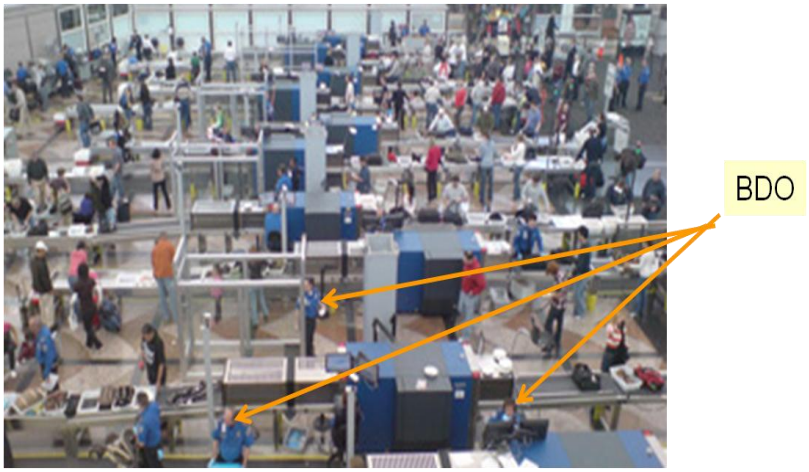

Figure 4-20: Shows the behaviour detection by trained behaviour detection officers (BDO) in blue uniforms currently deployed in the USA airports. The methodology is under review due to the extreme in-effective of the approach for anti-terrorism.

4.2.2.3 Human experts: SPOT & BDO in the USA [2006-present]

The research efforts in the USA within the areas of remote sensing of intent have been a lot more intense than any other countries in the world. There are two main streams of research in this area in the USA: one approach relies on the cognitive power of human experts to spot abnormal behaviour of people (Figure 4-20). The programme SPOT (Screening Passengers by Observational Training) deploys huge number of human Behaviour Detection Officer (BDO) post at around key checkpoints such as check-in desks at airports. The current budget for this programme costs the US taxpayers ~$200M p.a., and during 2006-2009 period the BDO has referred ~230,000 people for secondary screening and resulted in ~1700 arrests but none of them has been prosecuted for terrorism. The effectiveness of this approach for anti-terrorism has been heavily criticised and the US government is looking for alternative more cost effective approach particularly for passenger screening.

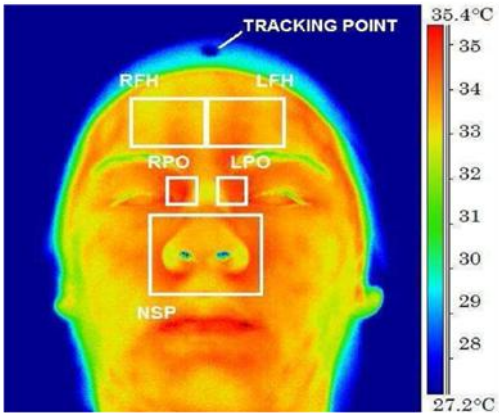

Figure 4-21 Features extracted from multiple ROI for arousal classification: left supraorbital (LFH), right supraorbital (RFH), left periorbital (LPO), right periorbital (RPO), and nasal (NSP) (Nhan BR,, 2009).

Feature subset dimensionality	Classification accuracy (mean±std)		
	BASE−HA	BASE−LA	HA−LA
12	80.6±6.6	74.5±17.0	58.8±9.3
11	81.1±7.2	74.1±15.9	58.2±11.2
10	80.3±6.8	72.7±15.7	54.6±10.3
9	80.1±7.2	73.5±14.8	56.8±11.5
8	79.2±7.9	71.2±13.9	54.5±9.5
7	79.2±6.8	69.4±14.8	54.3±10.6
6	78.0±7.1	67.8±17.1	56.9±9.6
5	75.2±8.5	67.1±16.8	58.0±9.4
4	73.4±7.3	65.8±17.2	54.5±10.3
3	72.7±7.6	65.5±17.0	56.2±12.0
2	70.9±8.7	65.3±18.1	56.9±11.7
Best Performance	**81.1±7.2**	**74.5±17.0**	**58.8±9.3**
Subset Dimension	11	12	12

Table 4-1 Shows the classification accuracies for the arousal states: high arousal(HA) versus base line(BASE), low arousal (LA) versus BASE, HA versus LA (Nhan BR,, 2009).

4.2.3 Multiple physiological features

4.2.3.1 Multiple features extracted from the facial region

It have been reported that the detections of emotions such as the arousal (A. Nozawa, 2009), fear (J. A. Levine, 2001) and happiness (R. Nakanishi, 2008) are not good enough by using single feature such as facial muscles contractions (Sophie Jarlier, 2011). Thus it is emerged that the requirement of multiple features is essentially important for the remote assessment of emotional states robustly. Recent work (Brian R. Nhan, 2010) has utilised multiple features extracted from the face, such as left and right sides of the supraorbital and periorbital regions and nasal, blood volume, pulse and respiration data, to identify the high arousal anxiety state

(Figure 4-21). By using a genetic algorithm and a Fisher LDA classifier to analyse the time and time-frequency data of these physiological features, the author has obtained about 80% accuracy for the detection of anxiety with respected to the base line when 11 features are used (see Table 4-1). The detection accuracy is about 12% better when in comparison with that using only 2 features for the classification.

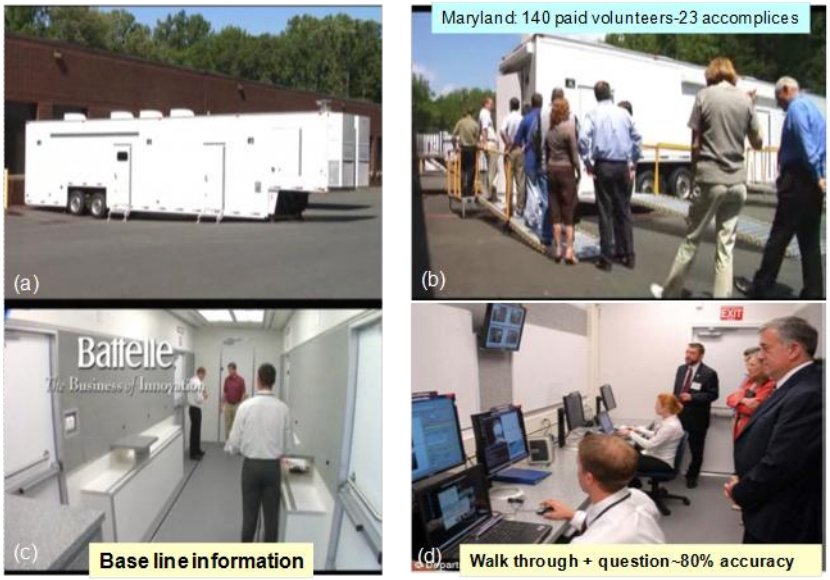

Figure 4-22: Shows the mobile screening laboratory under the FAST programme: (a) mobile trailer lab (b) a trial in Maryland consisting of 140 paid volunteers, (c) the acquisition of base line information when participants enters into the trailer (d) participants are monitored by a group of experts who analyse various physiological features during the trial.

4.2.3.2 Future Attribute Screening Technology (FAST) & Malicious intent screening (MALINTENT) [2008-2012]

This is a 4 year $2M programme which was awarded by the US government to the Draper Lab back in 2008. The objective is to monitor HBR, breathing rate, face temperature, eye tracking, voice pitch and facial expression using EO imaging equipment from stand-off distances. The purpose is to detect 'Mal Intent' by screening people for physiological indicators through a mobile screening laboratory, such as a trailer as shown in Figure 4-22 (Malintent, 2008). The budget of the FAST and the MALINTENT programme is about $10M p.a. It is claimed that the accuracy for the detection of mal-intent and deception is about 80% although the validity of the claim has been questioned by the Federation of American Scientist. The system attempts to capture seven pre-defined emotions through various physiological features such as facial expression, speech tone and HBR [Figure 4-23].

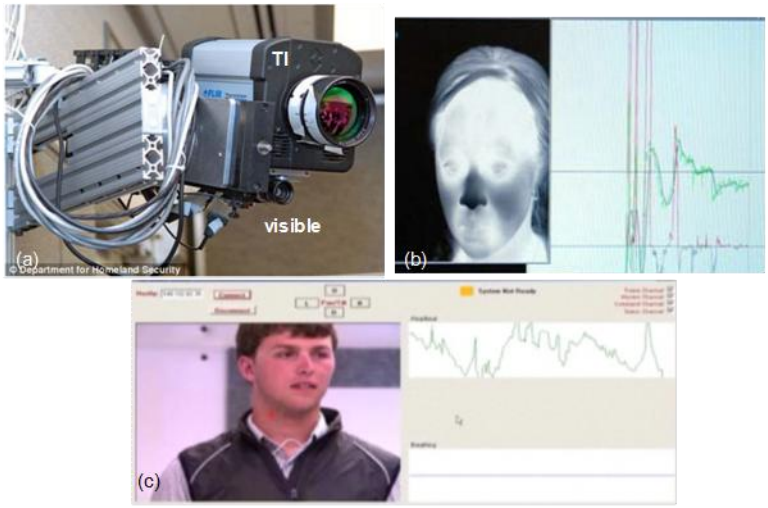

Figure 4-23: Shows the Malintent programme (a) the EO equipment which consists of a thermal camera, a visible camera and a LIDAR. (b) typical thermogram of a participant who is being interrogated (c) typical voice pitch analysis.

4.2.3.3 UK MOD projects: Cranfield University

4.2.3.3.1 Counter Terrorism Centre CTC DSTLX-1000013688: [2009-10]

This is a feasibility study awarded to our team in Cranfield University during 2009-2010 period. The aim was to testify whether people's anxiety could really be detected using Electro-optics (EO) remote sensing technique. The study utilised hyperspectral (HSI) EO equipment in addition to the thermal imaging (TI) for capturing physiological features in the facial region that triggered by anxiety. It was found that four out of seven subjects involved in this short study had reacted positively to the applied stressor methods, and that their responses to the anxiety had been in the form of elevated temperature spots particularly in their forehead regions (Yuen, 2009) which had been detected successfully. It was also noted that the thermalgram patterns caused by emotional anxiety were seen quite different from that triggered by the physical one (Yuen, 2009) (Hong, 2009). This result appeared to be quite different from that previously reported by the Texas group (Murthy, 2006), and we have shown that the activities in the forehead region had been increased significantly when the anxiety began to set in, rather than just an increase of hot spots in the periorbital region according to their work (Pavlidis, 2002) (Murthy, 2006).

In 2009 we have exploited hyperspectral imaging (HSI) technology to sense the haemoglobin tissue oxygenation (StO2) from the facial region and to use it to deduce

the mental states of people for the very first time in the homeland security research. The developed technique was immature at that time and a number of issues, such as illumination and shadowing factors, remained to be the most demanding issues to be solved.

4.2.3.3.2 CTC DSTLX-1000030030 and DR RACR/025/09 RACR/001/10 [2010-12]

These programmes were awarded to Cranfield University following the initial success in the feasibility project DSTLX-1000013688. The objectives of this programme are to extend previous findings particularly to focus more into the following two key areas:

1. To investigate how the anxiety can be detected without base line information.
2. To improve the robustness of anxiety detections for example the development of near real time heart beat rate (HBR) assessment.

Several work packages have been implemented during the course of the study to meet the objectives:

a. To expand sample sizes to over 50 subjects to improve the statistics of the result.
b. To correlate the EO characteristics with physiological data such as heart beat rate (HBR) and the cortisol levels.
c. To develop HSI detection algorithms with performances independent of illumination issues such as shadowing and viewing angle artefacts.
d. To develop near real time heart bit rate (HBR) detection capability.

This programme was carried out through two PhD projects and also subcontracting to third parties:

i) Hyperspectral imaging for the remote sensing of blood oxygenation and emotions: PhD student Mr Tong Chen.
ii) Remote sensing of strong emotions using Electro-optical imaging technique: PhD student Mr Kan Hong.
iii) Subcontracts and collaborations with engineering companies: Advanced Equipment Solutions (AES) and InnovTech Solutions UK LTD (ITS).

One characteristic of this programme is the use of multidisciplinary of physics, bio-medical & engineering expertises through a joint programme amongst the neuroscience & endocrinology researchers at the Bristol Royal Infirmary (BRI), the discriminative imaging experts at DSTL, the Advanced Equipment & Solutions (AES) as well as the Innovtech Solutions Ltd (ITS) companies, to understand how the emotional state can be assessed in a quantitative or semi-quantitative fashion.

A great deal of the present work is associated with the above programmes and one of key achievement in this MOD contract work is the development of the capability for the detection of people's anxiety without the need of base line information. Furthermore, the detected anxiety can be classified into high and low categories with ~90% accuracy. The features for the anxiety assessment include the blood oxygenation obtained from HSI technique, near real time detection of heart beat rate through RGB and TI video data, and the blood perfusions in the facial region as probed by TI. The detection range is about 5-10 meters and the anxiety assessment is not in real time as the data is processed after the event.

Part of this research programme such as the remote sensing of HBR using video images and the exact methodology for the quantitative assessment of anxiety level has been classified to RESTRICTED. However the materials that have been presented in this thesis are unclassified.

4.2.4 Direct contacted approach

4.2.4.1 Direct brain activity probe: FMRI

Functional magnetic resonance imaging (FMRI) has been one of the most important non-invasive technologies reported so far for the detection of brain activities due to emotional anxiety. The oxygen consumptions in some areas of the brain could be monitored readily as function of its activities such as that triggered by emotion, experience or any other stimulants. It has been postulated that the active area in the brain is proportional to the emotional stimulant. The FMRI detection method has been firstly reported by Kozel who has claimed a 90% accuracy of emotional anxiety detection. It is also reported that FMRI is capable to detect specific regions with reproducible activation when subjects attempt to deceive (Kozel ,2005). However, the detection result so far cannot be quantified and extensive research in this area is needed.

4.2.4.2 Emotional anxiety hormones approach

The detection of the emotional anxiety hormones adrenaline and cortisol which are released by adrenal medulla and adrenal cortex respectively can be used for emotional anxiety assessments. The level of hormones is claimed to be proportional to the emotional anxiety level and that they can be measured through the adrenalin

content in the blood using high performance liquid chromatography (HPLC) method. Alternatively, the measurement of cortisol content from saliva samples can be used as another means for emotional anxiety level assessment too.

4.3 Summary

A survey of remote sensing of emotions is given in this chapter. The survey includes what are the physiological responses to the emotional anxiety that has been reported in the field of research. Specific topics that are more relevant to this study such as the detection of the change of tissue of oxygenation and blood perfusion have been presented in more details.

5 Anxiety induced EO signatures found in this work

5.1 Physiological features as detected by EO technique

As outlined previously in Chapter 4 that EO imaging techniques such as HSI and TI have the capability to probe physiological features such as the saturated oxygenation as well as the blood perfusion in the dermis layer. This capability is illustrated in Figure 5-1showing the images of a subject when he was relax and also when he was under emotional anxiety. In the figure, it is seen that there is little differences between his base line and under anxiety state when it is revealed by the board band RGB images (Figure 5-1(a)). However, both the StO2 (Figure 5-1(b)) and the skin temperature images (Figure 5-1(c)&(d)) as revealed by the HSI and TI techniques respectively, the excited state is quite distinct and can easily be recognised. Note that the StO2 is deduced using the extended Beer Lambert law as outlined in section 3.3.2.2.

The blood perfusion of the tissue in the facial region can be estimated using the models as depicted in section 3.3.2. According to the adopted model, it is noted that the perfusion rate is proportional to the skin temperature T^4 and effectively the predicted perfusion image, as depicted in Figure 5-2, is a rescale of the skin temperature which emphasises the high temperature pixels while at the same time to suppress the low temperature ones. Typical perfusion rate for the liver is about 0.02 ml/s per ml of tissue volume (Mudaliar, 2008), and rates of ~0.02-0.03ml/s per 100g of facial tissue in men and women under heated conditions have been reported (Mayrovitz, 1993). The model gave the perfusion in the order of 0.01ml/s which is almost half of Mayrovitz's work. The discrepancy may be due to the different measurement environment as we have performed our experiment under air-conditioning and the room temperature is kept at ~19C all the time.

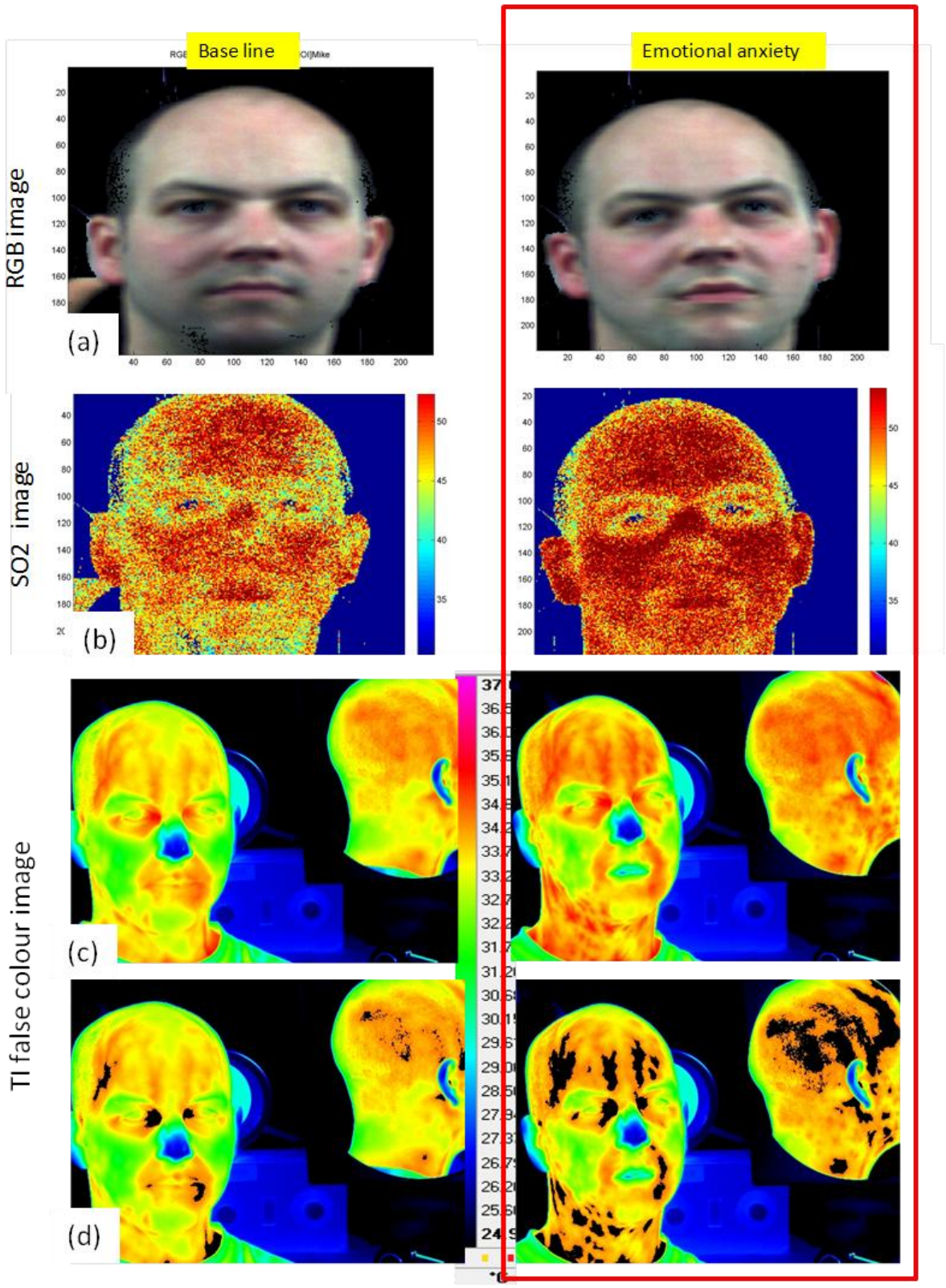

Figure 5-1. Highlight how EO imaging technique detects anxiety from a range of 5 meters. Left panel: Base line, Right panel: after applied emotional stressor. (a) RGB image, (b) StO2 image obtained by HSI, (c) TI false colour images, (d) threshold TI image at 34.4C with black pixel showing temperatures above the threshold.

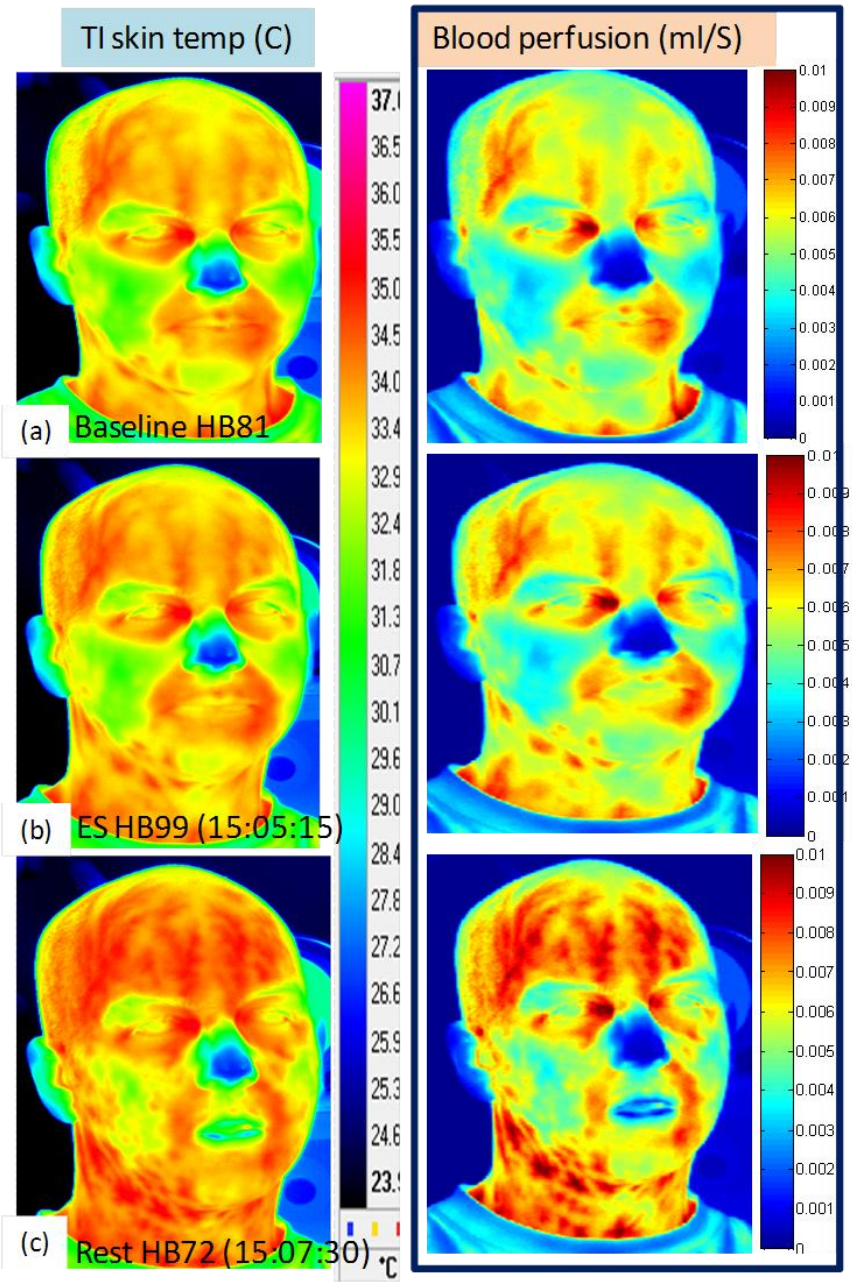

Figure 5-2. shows the blood perfusions of a subject when he was in various emotional states (a) base line, (b) at maximum anxiety, (c) after 2 minutes of anxiety. The perfusion is estimated according to the model illustrated in section 3.3.2.

5.2 Heart beat rate (HBR) and its detections

Figure 5-3 shows typical heart beat rates (HBR) of two participants who have gone through a series of stressor sessions, highlighting the almost instantaneous increase of the HBR to the anxiety to cope with the situation. As mentioned before different subjects may response differently to the same stimulant, and it is very common to see very different physiological responses from various persons even for the same type of stressor is applied to them. For example, in the top and bottom traces of

Figure 5-3 the HBR exhibit a two and three peaked features from two different individuals during the same emotional stressor (ES) session. Note that the amount change of the HBR is not a straightforward function of the cortisol level as mentioned in section 4.1.2.

5.2.1 HBR detection using thermal imaging (TI) data

One contribution of this work has been the development of the HBR detection using TI data.

Due to the relatively low frequency of the HBR which typically ranges from ~1-2Hz, it is possible to capture this slow frequency data through the thermalgram, HSI or even RGB viewcam video. Shown in Figure 5-4 is the HBR that deduced from the thermalgram for a subject who was exercising with a dumbbell. The feature is extracted from the temperature of pixels inside the periorbital region, and the algorithm has been developed on the Matlab platform. It is seen from Figure 5-4 that a very good agreement between the TI deduced HBR with respected to the measured data has been obtained.

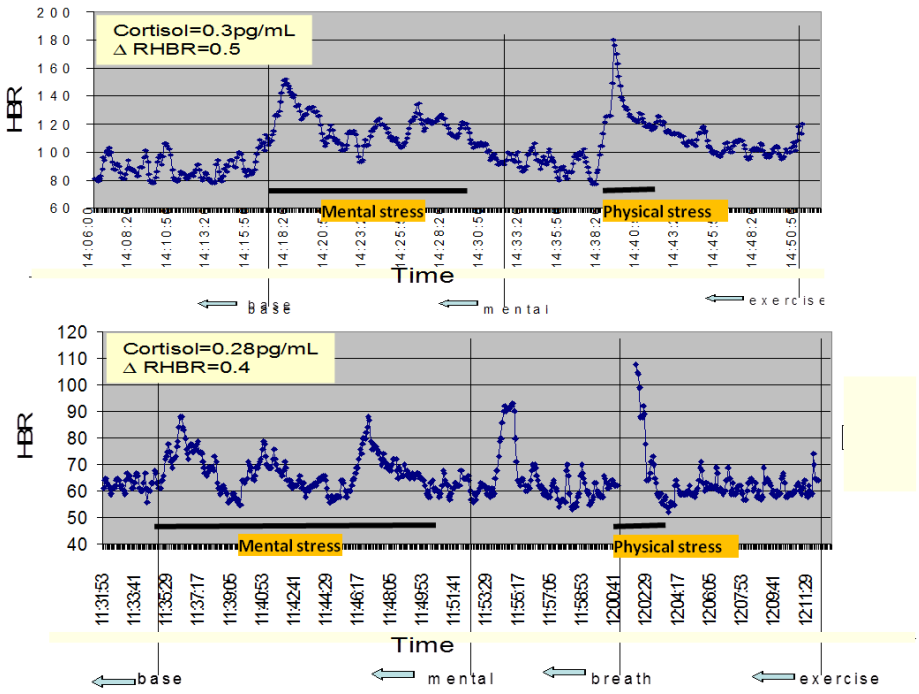

Figure 5-3. highlights the physiological response to anxiety through the raising of HBR when the anxiety begins to set in. Shown in the figure are the HBR of two persons responding to the same stressors (emotional and physical) but the HBR responses from these two persons are seen to be very different.

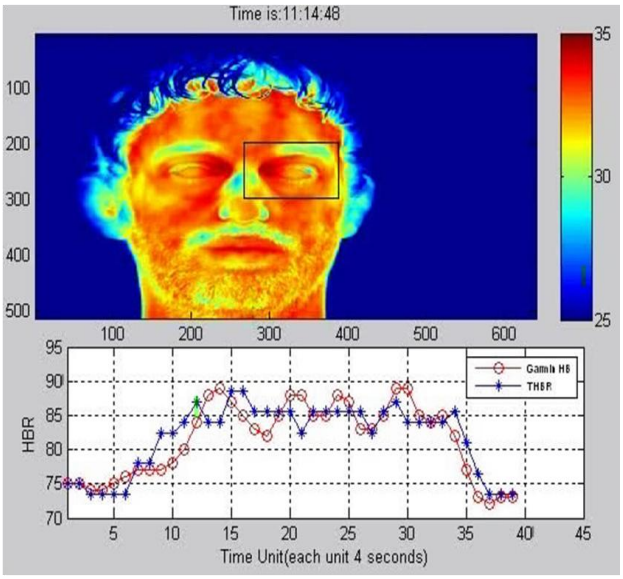

Figure 5-4. Shows the heart beat rate detection using thermal imaging (TI) technique: upper panel- false colour thermalgram of the subject who was sitting in front of the TI with a dumbbell in his hand. Lower panel: the measured HBR (red) and the HBR deduced from the periorbital ROI of the thermalgram (blue) when the subject is exercising the dumbbell.

5.2.2 HBR detection using thermal Multispectral Imaging (MSI)

The MSI system in our laboratory is capable to take 30 frames/sec of image and hence it is feasible to use it for capturing the slow changing HBR of human at ~1-2Hz frequency. Figure 5-5 shows the typical result of the HBR that deduced from the MSI for a subject who was exercising with a dumbbell. The feature is extracted from the intensity of the MSI video taken at λ~600nm and the algorithm has been developed exclusively by the AES/ITS company. It is seen from Figure 5-5 that a very good agreement between the MSI deduced HBR with respected to the measured data has been obtained. Unfortunately this program has been maliciously removed from our computers by an ex-PhD student who left Cranfield University at the end of July 2012.

5.2.3 HBR detection using RGB video

The video frame rate for commercial off the shelf view cam is typically 20-30 frames per second (fps) and therefore it is feasible to detect the slow HBR of human. The feature is extracted from the intensity of the RGB-band video and the algorithm has been developed exclusively by the AES/ITS Company. We have obtained very good agreements between the view cam deduced HBR with respected to the measured data. The program is implemented in C++ and it is capable to detect the HBR in very near real time. Unfortunately this program has been maliciously removed from our

computers by an ex-PhD student who left Cranfield University at the end of July 2012.

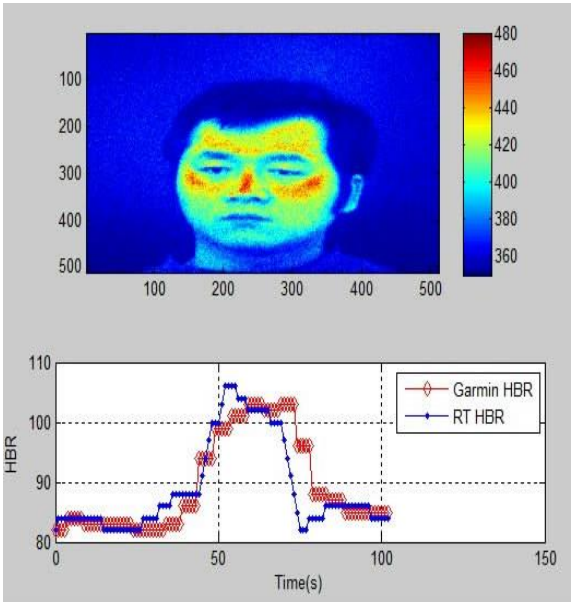

Figure 5-5. Shows the heart beat rate detection using MSI technique: upper panel- false colour MSI image (λ=600nm) of the subject who was sitting in front of the MSI with a dumbbell in his hand. Lower panel: the measured HBR (red) and the HBR deduced from the face of the subject (blue) when the subject is exercising the dumbbell. This program was developed by AES/ITS and unfortunately it was maliciously removed from our computers by an ex-PhD student who left us at the end of July 2012.

5.3 Blushing faces

As outlined in the previous sections that blushing in the face has been considered as one of the most common physiological responses to anxiety. However, we have observed a time delay of the blushing to occur when one is under anxiety. This delay time is found variable from person to person, ranging from seconds to a few minutes. Typical time delays of this kind can be seen from Figure 5-6, which presents example false colour thermalgrams of four subjects who were at their peak HBR during the ES (Figure 5-6 (a)), and then the moment when a maximum flushness in their face is observed (Figure 5-6 (b)). The thermalgrams in (b) have been threshold and all pixels with temperatures exceeding the threshold temperature have been presented in black colour. Note that the blushing in the face has been almost unnoticeable to the naked eyes in most of the cases.

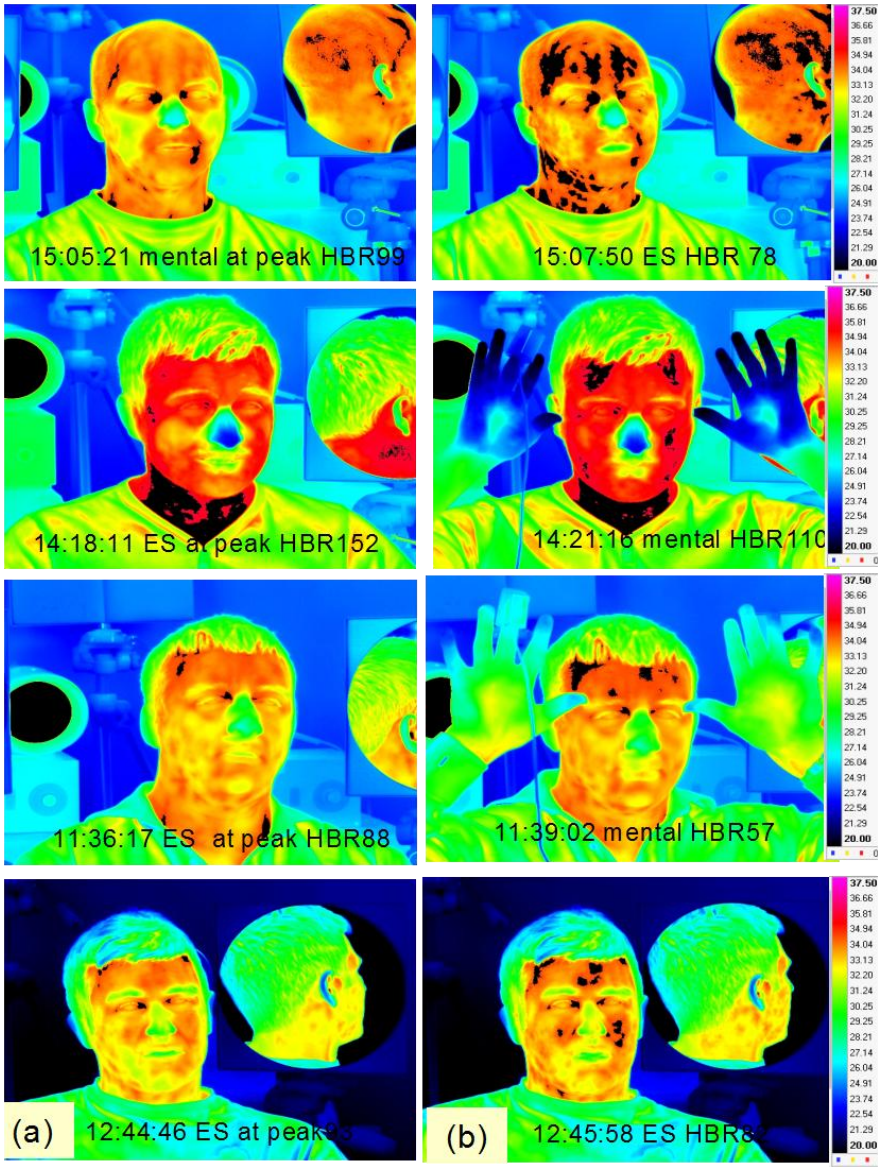

Figure 5-6. Shows the delay of facial blushing after the peak of the HBR during the ES session: (a) the thermalgram of 4 subjects when they were at their peak HBR during the ES, (b) the time when they exhibit a maximum flush in their faces. The thermalgrams are in false colours of temperatures, and the pixels exceeding the threshold temperature are presented in black. Note that the threshold temperatures for these subjects are different in each case.

5.4 Paling in the hands

The other signature of anxiety is the reduction of blood flow into the hands and skins inducing the commonly experienced ‘cold hands’ when one is in anxiety. Cold or sweaty hands are not easy to be detected by conventional imaging technique, however, it is seen that both the TI and HSI can detect the paling and blushing in the face and hand extremely efficient, as demonstrated in Figure 5-7. The figure presents the RGB, false colour thermalgram and the false colour StO2 images in three rows for a subjects when he was (a) relaxed (base line), (b) after emotional

anxiety (ES) and (c) after physical anxiety (PS) by performing an endurance exercise (stand-horse).

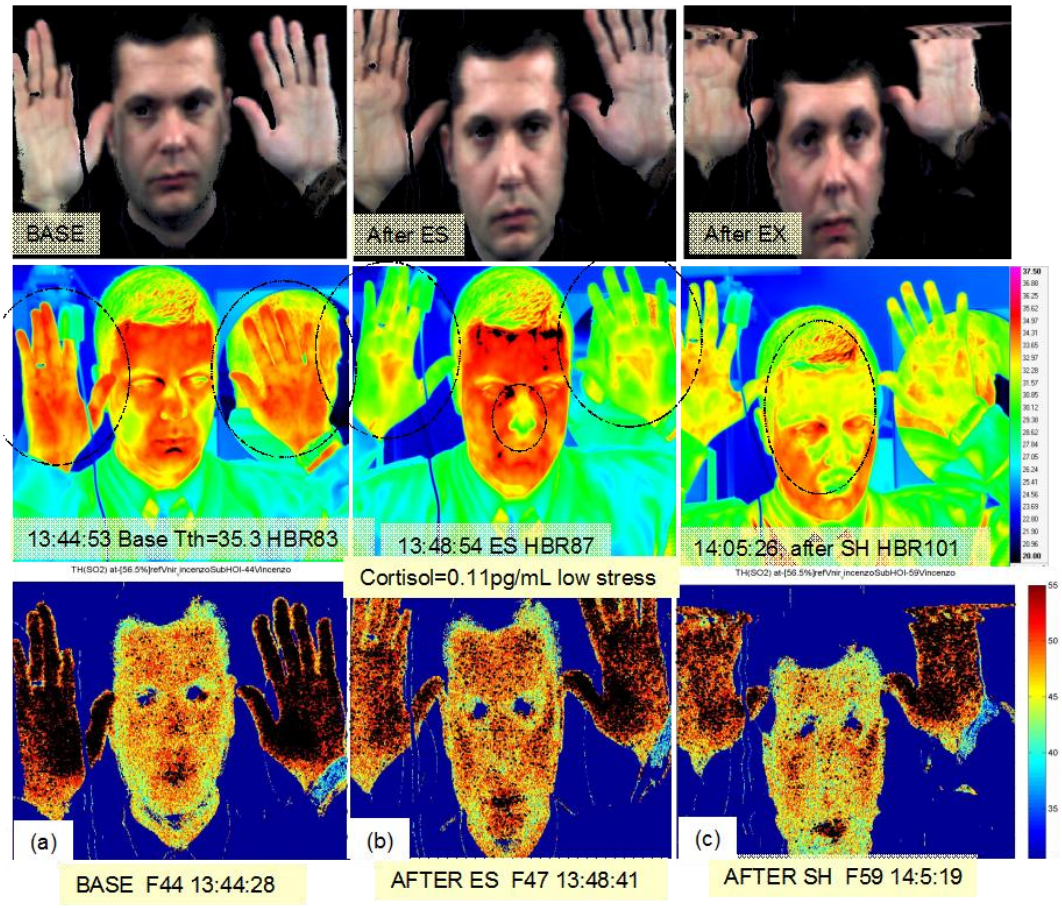

Figure 5-7. shows the RGB images, the thermalgram and the StO2 of subject A in the top, middle and bottom panels respectively. a) subject at rest, (b) after ES and (c) after PS. Note the change of temperatures and the StO2 in the forehead, hands and nose during the ES and PS. Both the thermalgram and the StO2 map have been threshold (in black colour) to aid visual observation of the change after the anxiety sets in.

The most striking features that stand out from these figures are the observation of the cold hands during and after the ES session, and in many cases it accompanies with a colder nose and at the same time, a flush in the face. It is noted that the hand temperatures can drop by as much as 4-5°C during anxiety, and when in extreme anxiety the nose temperatures can be reduced by 1-2°C. However, the picture is seen very different when the subject is under physical anxiety (PS) for example after performing bodily exercise such as stand-horse (SH): frequently there is a substantial paling in the face particularly in the forehead, and in some cases the subject's nose will also get colder too.

The reduction of oxygenation in the hands during the ES is seen quite clearly from the StO2 map as depicted in the bottom panel of Figure 5-7. Note that all the presented StO2 maps in Figure 5-7 have been threshold at 56.8% to aid visualising the change of the oxygenation after the anxiety sets in. It is also seen that oxygenation levels in the mid-forehead areas has increased substantially, with negligible change of StO2 in the nose despite of the ~1° C drop as suggested by thermalgram when the subject is under ES. Note that both the thermalgram and the HSI images were taken at the same time and it is not certain why the two sets of data are not consistent here. One likely explanation is the increased respiration rate during ES may cool down the skin temperature at the nostril due to the increased convection in the area inducing a temporarily thermal in-equilibrium. In chapter 7 it is evidenced that external environmental effects, such as ambient temperatures, have imposed enormous impacts on the skin temperatures, which, seems not to be a detrimental factor for the oxygenation assessment using HSI technique (see chapter 7 for more information).

It can be seen later in chapter 7 that we have derived a simple method for assessing the level of anxiety using local differences of skin temperatures and blood oxygenations extracted from various ROIs in the facial region. The chosen ROIs are the forehead, nose and mouth. The differential of the forehead and mouth temperature, acronym as DFMT, and together with the differential of forehead and nose saturated oxygenation, acronym as DFNSO, have been shown sensitive to the emotional state of human subject (see chapter 7 for more information). The DFMT and DFNSO values of this data set is found to be 0.97 and 2.05 respectively, implying that subject A was in fact under very mild anxiety during the ES session. In chapter 7 it is found that strong anxiety will give index values of DFMT and DFNSO higher than 1.8 and 2.75 respectively. This classification of anxiety level is supported by the presence of relative low level of cortisol in the subject's blood stream (0.11pg/mL) after the ES session, together with the subject's own view that he was not nervous during the test, indicative of a correct assessment of the anxiety level in this case.

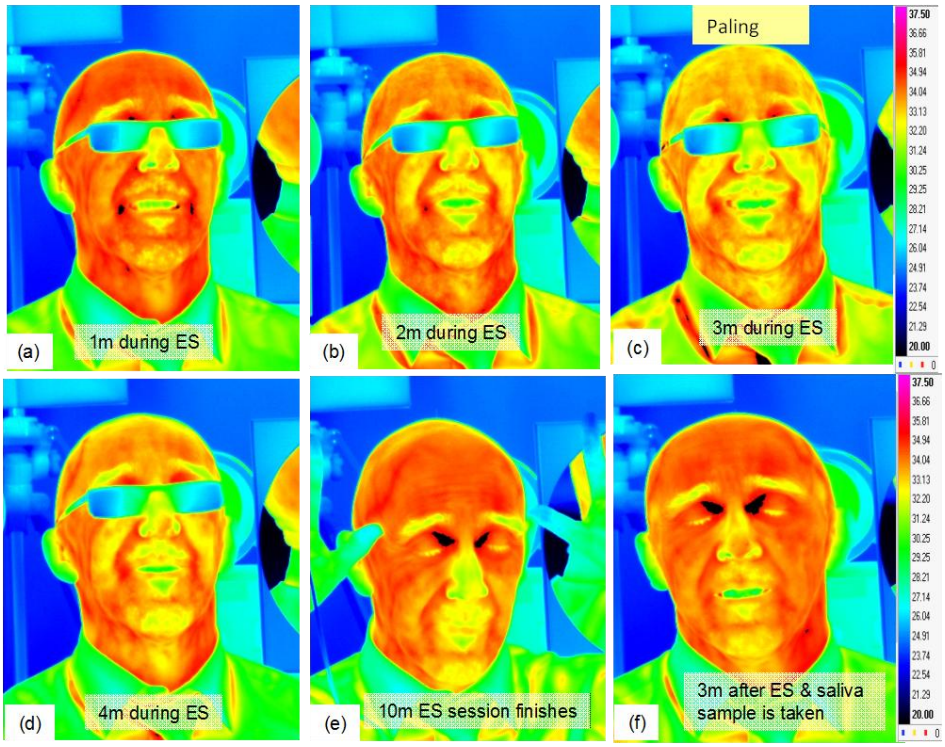

Figure 5-8. Shows the paling and flushing in the facial region during an ES session: (a)-(d) the thermalgram of the subject taken at a minute interval during the ES session, and note the acute paling in the face after 3 minutes into the ES session. (e-f) Flushing in the face.

5.5 Paling & sweating

We have observed one participant who has exhibited strong paling and perhaps perspiration during the ES in this trial. The subject is a Caucasian with strong academic background, and he has shown acute paling in the whole face together with cold fingers in both hands (see Figure 5-8) during the ES sessions. The StO2 data however indicates an increase of StO2 in both of the hands and in the face, thus suggesting that the subject might have undergone strong perspiration during the test. The ES anxiety according to the DFNSO is found to be 3.2 suggesting that the subject might have been in high anxiety.

It can be seen later that a very high level of flushness or paleness in the face do not necessary implies high level of anxiety.

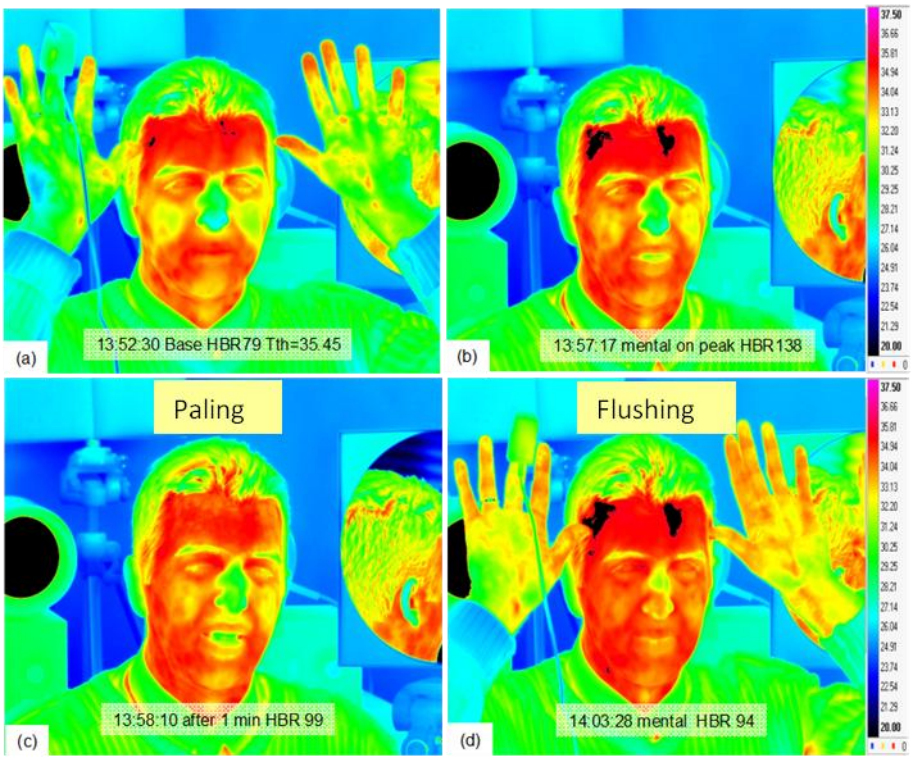

Figure 5-9. Shows one incident of alternative paling and blushing during the ES session amongst the data that we analysed so far. Shown in the figures are the threshold (Tth=35.45°C) thermalgram of (a) base line of a subject (Caucasian), (b) the moment at the peak of the HBR during the ES, (c) one minute after (b) showing paling in the face, (d) finishes the ES session.

5.6 Alternation of paling and blushing

Amongst the analysed data we have found one incident of alternative paling and blushing during the anxiety session. Shown in Figure 5-9 is the threshold thermalgram of a Caucasian subject who is currently a military officer serving in the Force and the data is recorded during the ES session. The subject is in good health despite of being a heavy smoker, and it is seen a blush in the face as soon as the ES begins to step in (Figure 5-9 (b)). Within one minute after his heart beat rate is peaked at 138 beats per minute (bpm), his face is seen getting pale rather remarkably (Figure 5-9 (c)). It is not sure for certain whether it is due to the secretion of enormous amount of cortisol by the adrenal cortex to inhibit the corticotropin-releasing hormone (CRH) at the peak of his HBR during the ES session. There was no HSI data recording during this period of time and therefore further experiment is needed for a better understanding of the phenomenon.

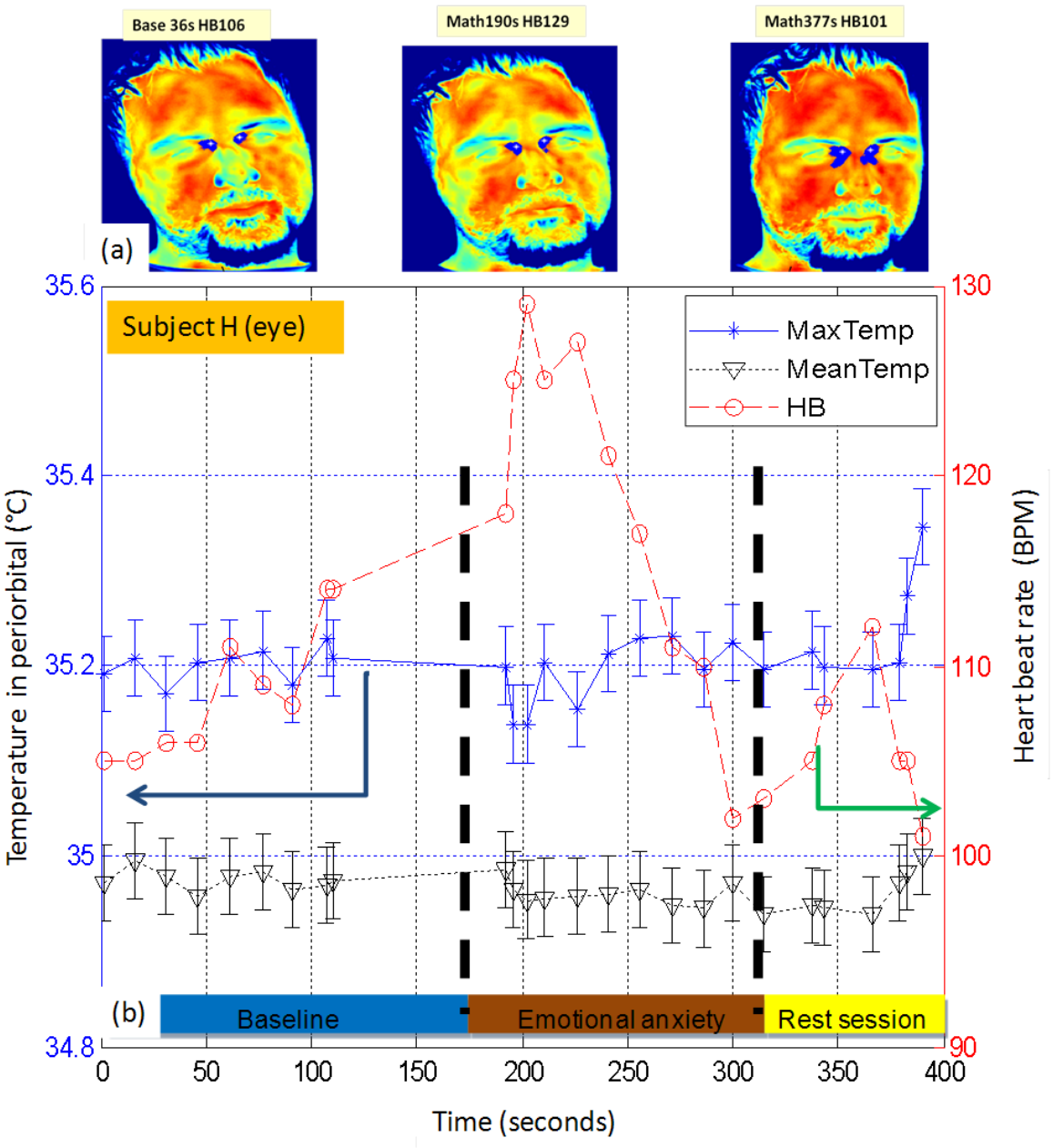

Figure 5-10. Shows the temperature change in the periorbital region during and after the ES session: (a) thermalgram of a subject: before (left), during (middle) and after (right) the ES session. The maximum temperature and hot pixels (threshold to 35.4°C) in the periorbital region have been depicted as white and blue colours respectively. (b) the heart beat rate (red), the maximum and mean temperatures in the periorbital region before, during and after the ES session. Note that neither the maximum nor the mean temperature in the periorbital region has increased during and within 2 minutes after the anxiety sets in. Note that this subject is under mild anxiety condition.

5.7 Anxiety induced anomaly temperature in the periorbital region

Greatly influenced by the Texas/Honey Well work (Pavlidis, 2002), most researchers in the remote sensing of intent field have commonly adopted the anomaly temperature in the periorbital region as the signature and indication of having anxiety. We have performed more detailed analysis for a number of participants but

unfortunately we cannot repeat their result. Shown in Figure 5-10(a) is a subject who has taken part in the ES session and the hot pixels in his periorbital region threshold to 35.4°C are depicted in blue while the maximum temperature is located by the white pixel. It is seen from Figure 5-10(b) that neither the maximum nor the mean temperatures in the periorbital region are seen to increase during and after the anxiety sets in.

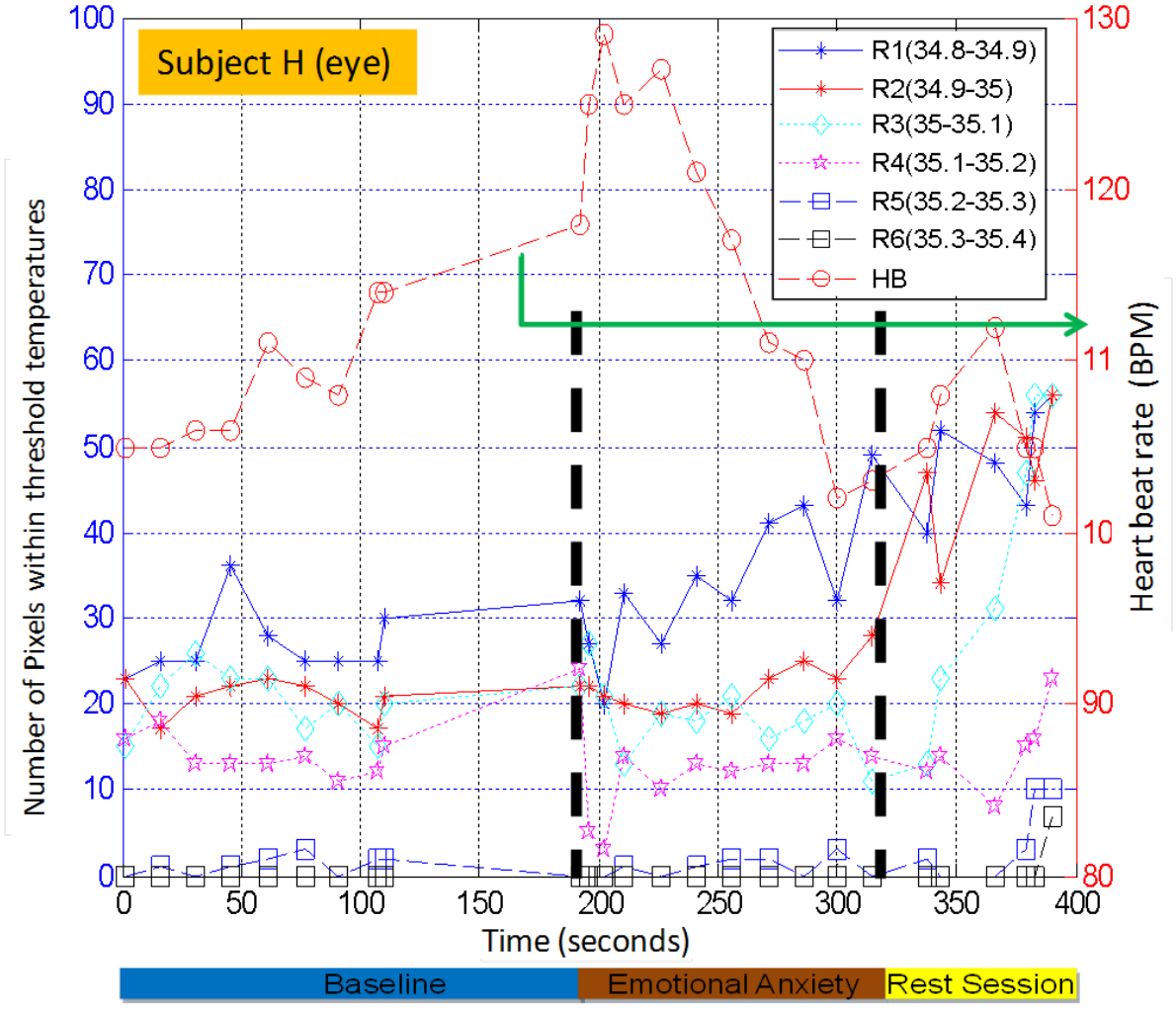

Figure 5-11. Shows the temperature profiles of the periorbital region of the same subject during and after the ES session: it is cleared from previous figure that the maximum temperature in the ROI has not been increased but the number of hot pixels in the perorbital region, is seen to increase in numbers after a few minutes of the peaked HBR. Note that this subject is under mild anxiety only.

However, it is seen that the number of the hot pixels, which are labelled in blue in Figure 5-10(a), is seen to increase in number. Figure 5-11 shows the temperature profiles of the periorbital region of the same subject during and after the ES session: it is quite clear that the maximum temperature in the periorbital ROI has not been

increased but the number of hot pixels, is seen to rise in numbers after a few minutes of the peaked HBR.

More detailed analysis of this anxiety induced anomaly temperature in the periorbital region will be presented in chapter 6.

5.8 Preliminary Study of glucose detection during anxiety

5.8.1 Glucose signature

Due to the 'transparent' nature of glucose when it is in solution such as water, the spectroscopic characteristic of the solution has been obtained through the reflection of a spectralon as shown in Figure 5-12. This means that the reflected light double passes the sample and then it is collected by the sensor, thereby effectively this set up measures the absorption characteristics of the sample.

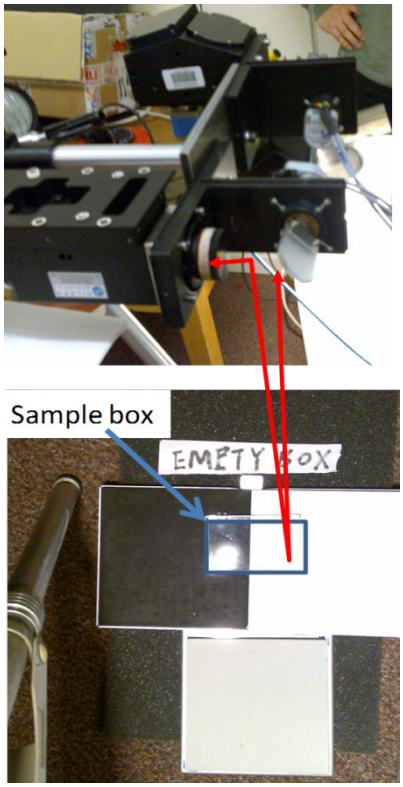

Figure 5-12 shows the setup of glucose spectroscopic experiment. The sample is placed directly onto a spectralon which exhibits a flat reflectance of 0.98 over the 300-2500nm wavelength region.

The spectral characteristic of the solid samples as measured in our laboratory is shown in Figure 5-13, and it is seen that solid glucose powder exhibits rather flat and almost negligible absorption in the visible spectrum (Figure 5-13(a)). In the SWIR

region there are 3 rather strong absorption peaks at about 1.25μm, 1.5μm and 2-2.5μm wavelengths (Figure 5-13(b)). Hence the useable waveband that may allow us to detect glucose by using our equipment in the laboratory is restricted to the SWIR band only.

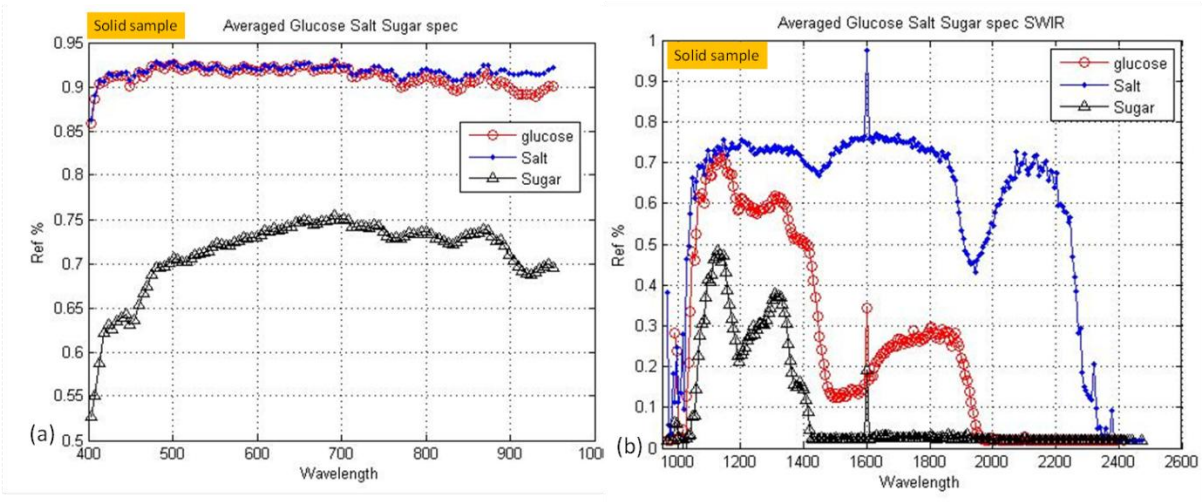

Figure 5-13 depicts the reflectance spectra of solid samples of glucose, salt and white sugar that measured in our laboratory using the HSI.

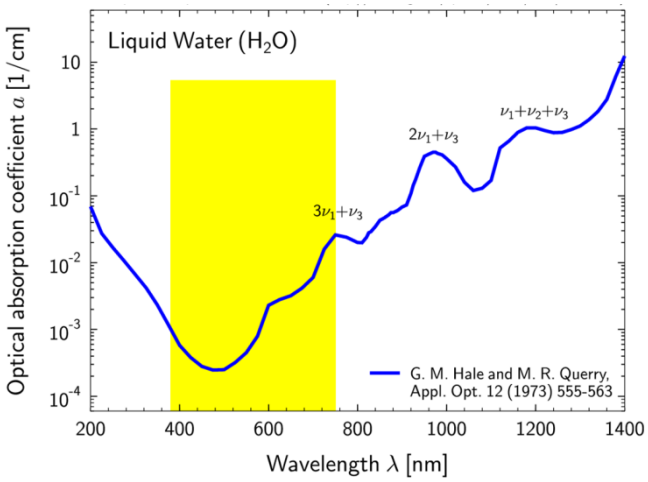

Figure 5-14 shows the typical water absorption in the visible and swir region (G. M. Hale, 1973).

Since we are concerning with the detection of glucose in blood, which contains predominantly water, it is necessary to understand the signature of glucose in water. As it is seen in Figure 5-14 the water absorptions in the SWIR region [1-2.5um] is about 4 orders of magnitude higher than that in the visible region (G. M. Hale, 1973). As such it is expected that the EO characteristics of water will be significant in the SWIR waveband. Figure 5-15 shows the reflectance spectra in the SWIR region for various concentrations of glucose in water. The solution is contained in a Perspex

box (12cm^3 in volume) and the control spectra of the container and the pure water is also presented in Figure 5-15 to help the analysis. One spoonful of glucose in the Perspex container is equivalent to 0.075g/cm^3 concentration. It can be seen in Figure 5-15 that the presented spectra all showing a common 3 valley structure, characteristic to the absorption peaks of water at about 1200nm, 1400 and 1900nm (see Figure 5-14). All wavelengths above 1400nm are observed strongly absorbed by water, and in the longer wavelength region the spectra appear to dip below zero which is caused by dark current subtraction and calibration accuracy artefacts. Figure 5-14 also shows that the SWIR HSI system is capable to sense the presence of 0.075g/cm^3 of glucose in water (red triangle trace). The glucose in the blood of human is about 5-10mmol/l which is equivalent to 0.001-0.002g/cm^3, and hence it may be a technological challenge for a direct detection of such small amount of glucose from the blood sample using HSI technique.

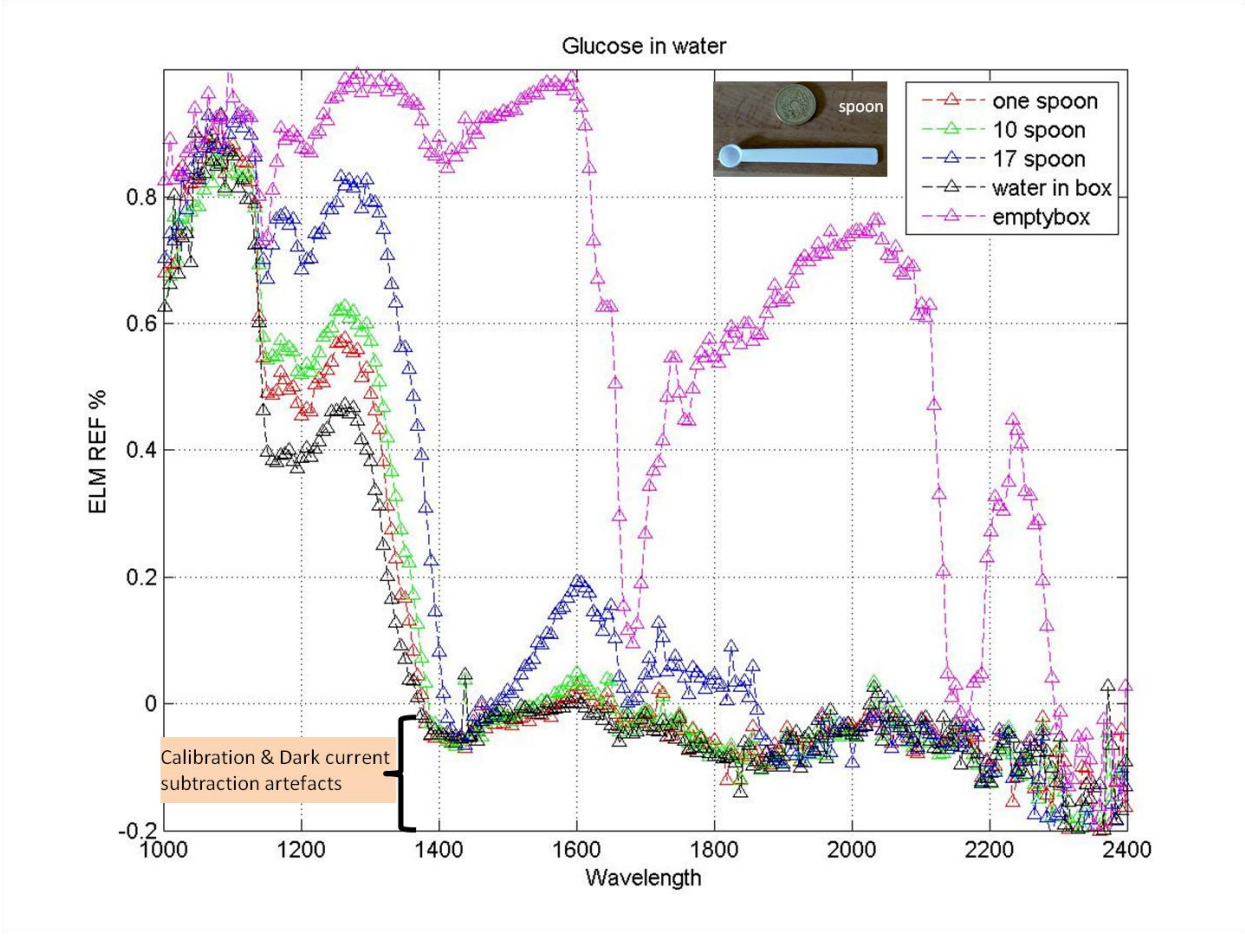

Figure 5-15 shows the reflectance of various concentrations of glucose in water solution in the SWIR region. The solution is contained in a Perspex box, and note that all the features in the spectra shown are in fact dominated by the water absorption peaks.

5.8.2 Physiological features in the SWIR band

This is the first attempt, as far as the author aware, to probe physiological feature of human subject using HSI in the SWIR waveband. Figure 5-16 shows the typical SWIR band spectra for various ROI within the facial region of a human subject. All spectra are seen to be dominated by a three-valley structure located at the characteristic water absorption peaks as mentioned in the last section. One important observation from Figure 5-16 is the significant absorptions at around the periorbital and lip regions (ROI 4, 5 & 8) in comparing with that of other ROIs in the face. Whether this is caused by the differences of the blood perfusions and water content underlying in these ROIs, is something to be confirmed in the future research.

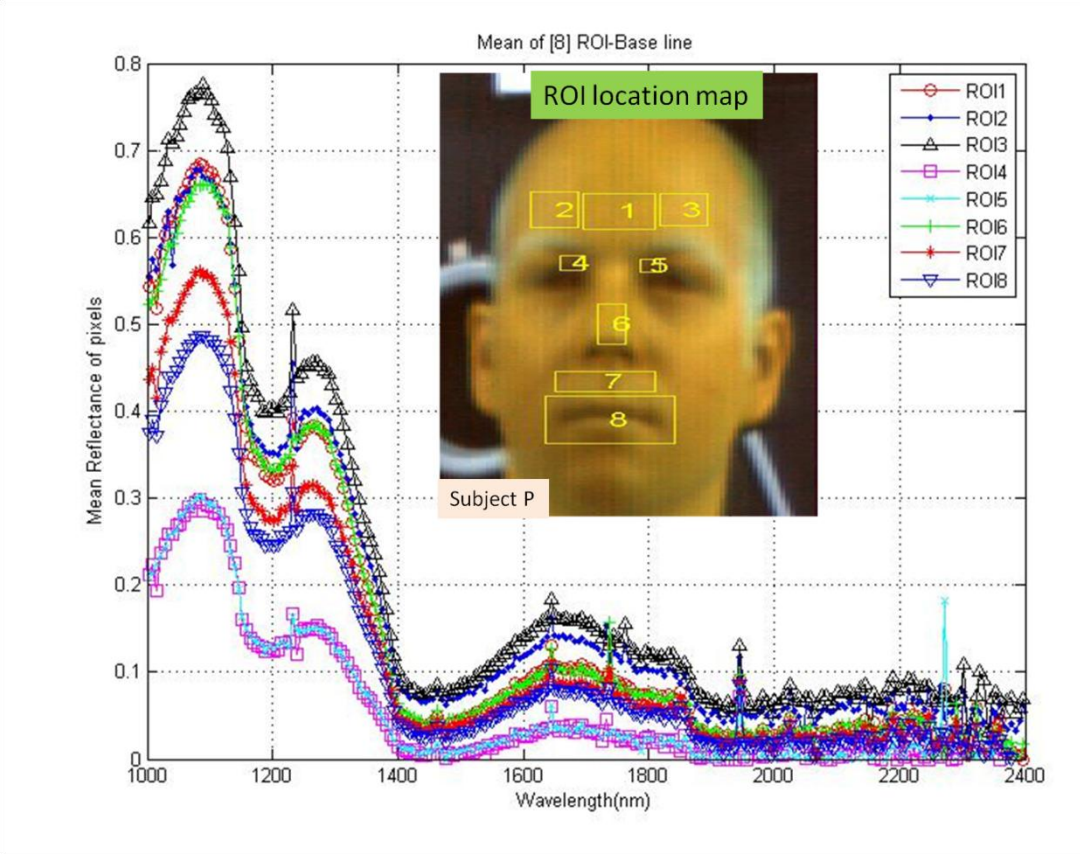

Figure 5-16 Shows the typical reflectance spectra in the SWIR waveband extracted from various ROI in the facial region of a human subject. The inset shows the false colour image of the subject. The spike point is the noise of the camera.

It is of interest to see if there is any spectral difference that can be observed from these ROIs when a person is in his base line and to compare with that when he is

under anxiety. It is found that there is some spectral changes for the ROIs in the periorbital regions (ROI 4&5), in the lip (ROI 8), and relatively small amount of difference in the nose (ROI 6), when the subject is under anxiety. This is illustrated in Figure 5-17(a), and otherwise there is almost negligible change of reflectance for all other ROIs (Figure 5-17(b)) between the excited and base level states. The HBR of the subject was 76, 92 and 72 for the three events of base line ('base' in the figure), ES ('math') and after ES during rest ('rest'), respectively. The spectral differences of the periorbital and mouth regions after emotional excitation are seen to be very small in comparison to the base level, and thus intuitively a differential between the excited state and the base line is made and the result is shown in Figure 5-18.

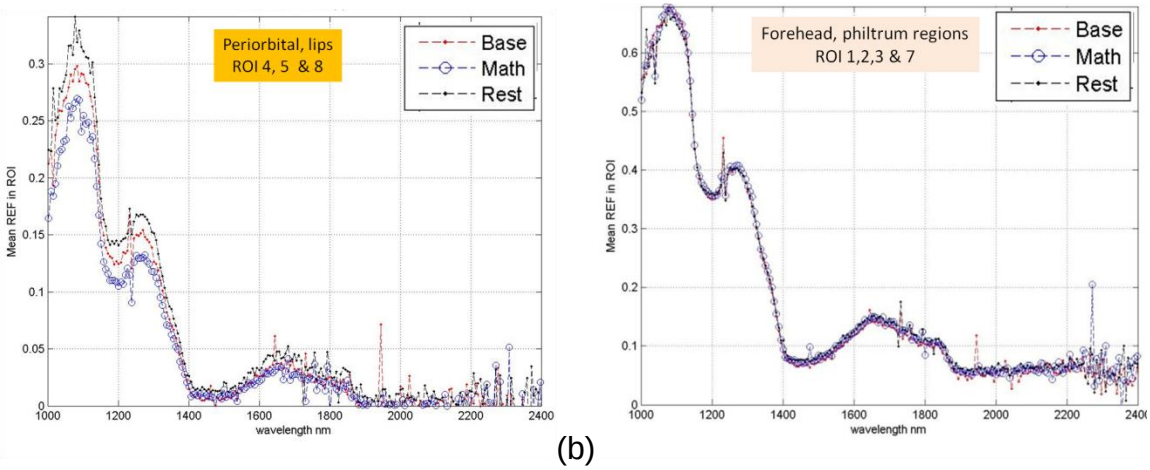

(a) (b)

Figure 5-17 highlight the spectral difference from the ROI in the face when a subject is under anxiety (math session) and to compare it with his base line level (base). (a) typical spectra for ROIs in the periorbital and lip regions (b) typical spectra of the forehead and mouth.

One common feature of the differential spectra shown in Figure 5-18 is the negligible differences in wavelengths longer than 1400nm, presumably it may be because of the strong absorption of water which dominates the effect. However, there is one observation from Figure 5-18 which is unclear to us for the moment: the change of the spectra between the rest state and the base line is positive, ie, an increase of reflectance from the ROI of the periorbital region; but it is just opposite for the mouth which exhibit a reduction of reflectance in these spectral region during anxiety! It is speculated that this may be related to the surplus of adrenaline and cortisol during the rest state after the ES session, which may cause an increase of blood perfusion into the perorbital region (see section 5.7 and chapter 7 for more information). The increased blood supplies in this region may well increase the glucose concentration.

Our data that showed in Figure 5-15 has demonstrated a higher reflectivity in the region of 1-1.4μm when a higher concentration of glucose is presented in the water solution. Hence it is plausible but without proof that, the behaviour that has been observed in Figure 5-18 may well be related to the increased glucose concentration in the periorbital region during the anxiety state.

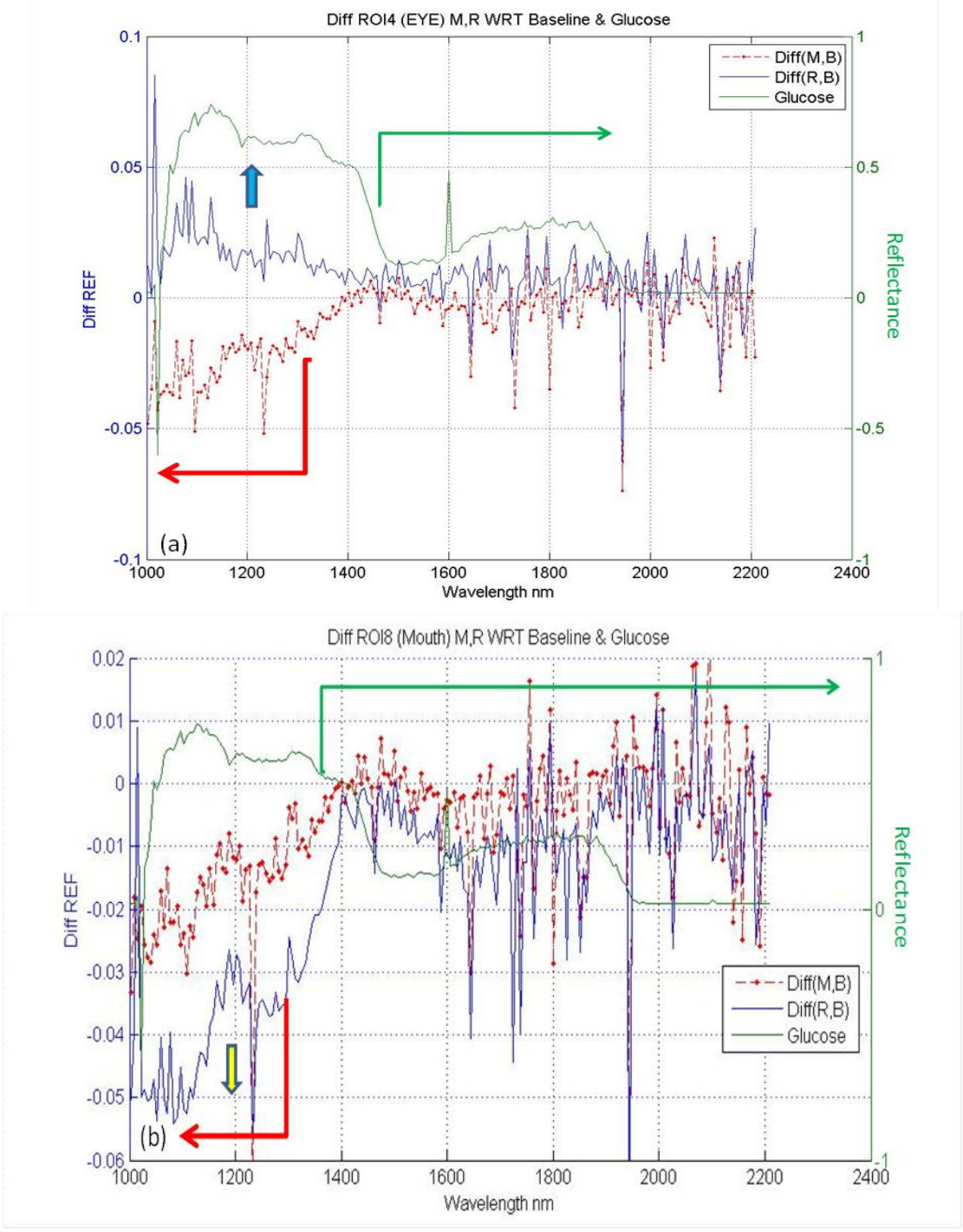

Figure 5-18 shows the differential reflectance between emotional anxiety state with respected to the base line for (a) periorbital region (b) mouth ROI. Diff(M,B) stands for differential of MS and base line.

5.9 Summary

This chapter investigates the electrical optical signatures that have been obtained during the course of this research. The chapter presents how human heart beat rate (HBR), glucose level in the face, blood perfusions in the facial region, hands and in the periorbital regions, are changed upon the onset of anxiety. All data presented in this chapter is recorded remotely using EO technique during experimental trials taken place in our laboratory.

6 Anxiety induced hot spots in periorbital region: revisited

6.1 Background

It is quite well-known that the temperature in the periorbital region can give information such as fever and anxiety in animals (Shylo R. Johnson, et.al, 2011, M. Stewart, et.al, 2007). Furthermore, the work published by the Texas team (Pavlidis et al., 2007) has claimed that emotional anxiety can bring about an 'instantaneous' increase in the periorbital blood flow. This surge of blood volume in the periorbital region has been measured by TI at the onset of anxiety (Pavlidis, 2001). Figure 6-1 shows the temperature profile in the periorbital region of a subject after he is given an emotional stressor. Pavlidis et al claimed that this is the hall mark of a 'fight or flight' syndrome and that the substantial increased of blood flow in the periorbital region can be considered as a signature for the instantaneous detection of emotional anxiety (Pavlidis et al., 2008) (Pavlidis, 2001). However, as it can be seen from Figure 6-1 that there is no indication of when the stressor was initiated and therefore it is difficult to verify the 'instantaneous' increase of blood flow upon anxiety as Pavlidis's team has claimed!

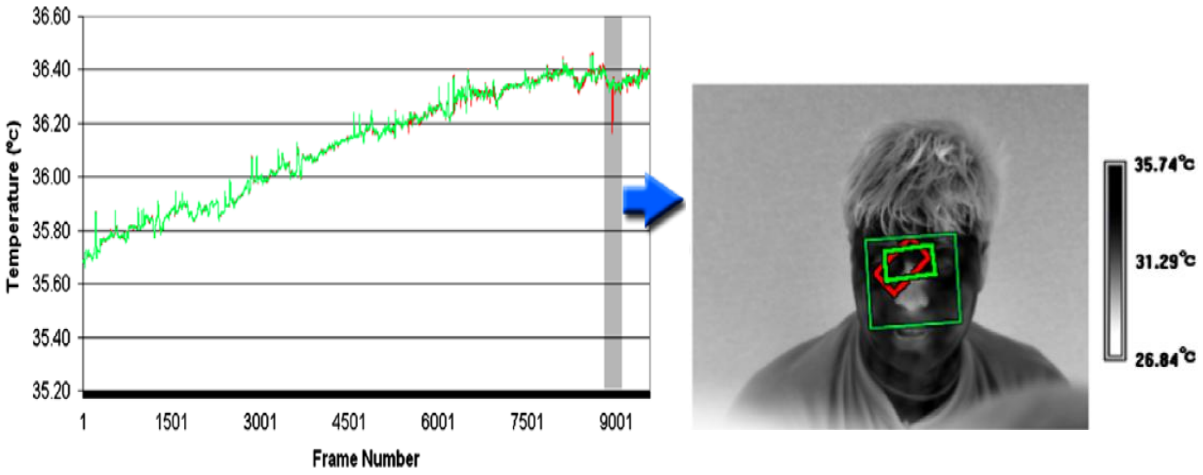

Figure 6-1 outline one of Pavlidis's work about the 'instantaneous' increase of temperature in the Periorbital region when one is under anxiety (Pavlidis et al., 2007). Left: temperature profile of the periorbital region, Right: depicts the location of the ROI in the periorbital region in red.

6.2 'Hot' spots in periorbital region

We have conducted a detailed analysis hoping to gain more understanding of the blood perfusions mechanisms in the periorbital region when one is under anxiety. Presented in Figure 6-2 is the false colour images of 3 subjects who have undergone

an emotional stressor (ES) session. The figure depicts the high temperature pixels in the periorbital through threshold the ROI in the eye region, and the threshold temperatures for the 3 subjects are 34.8, 34.4C and 34.4C respectively. The threshold temperature is arbitrary set and the exact value is dependent on individual's health conditions. The purpose is to observe any changes of temperature in the ROI while keeping the threshold temperature fixed throughout the experiment.

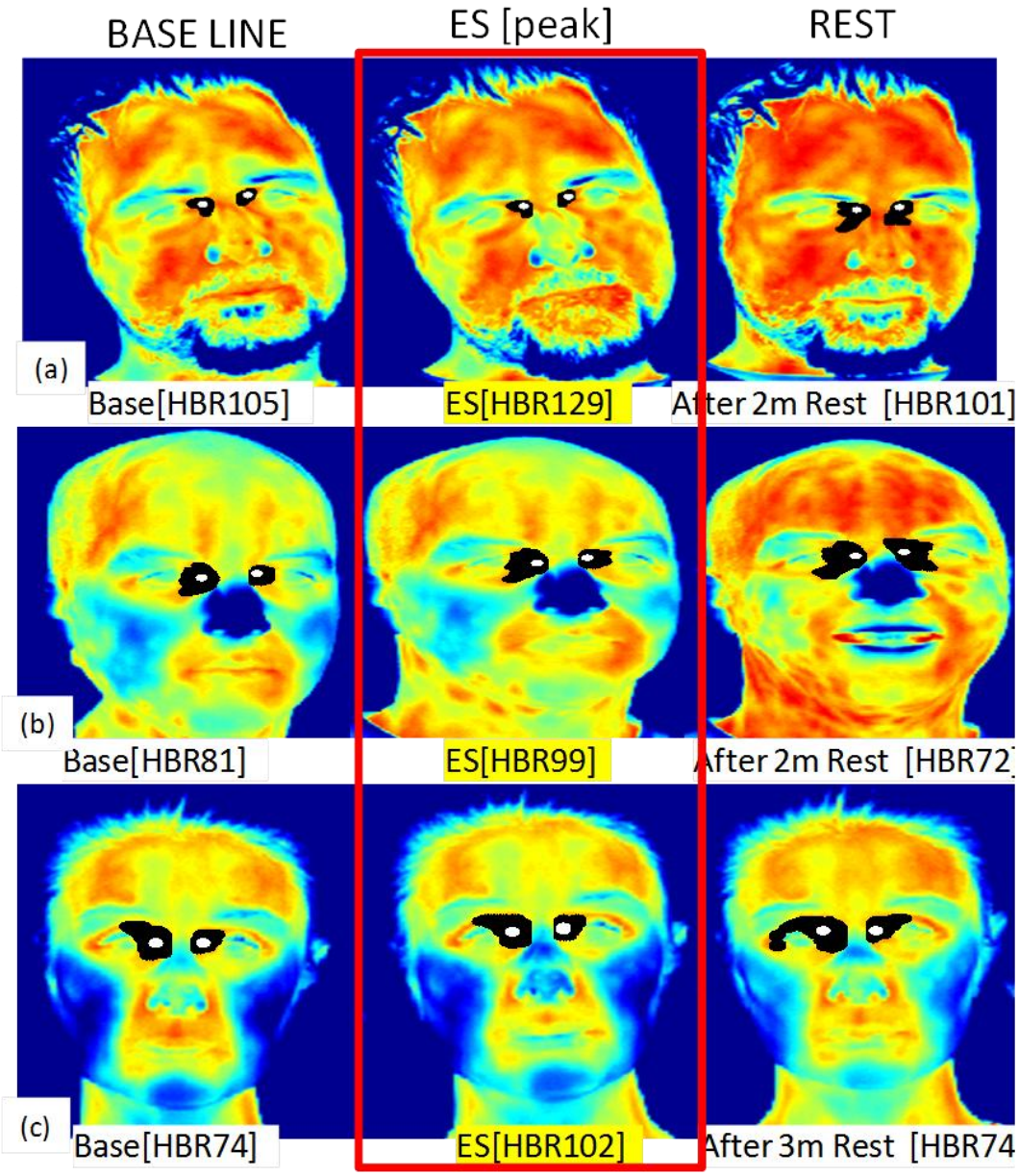

Figure 6-2: presents the hot spots in the periorbital region when one is under anxiety. Shown here are the TI images of 3 subjects (a) subject H, (b) subject P, (c) subject N. Left column: base line, Mid column: when the subject is at the peak HBR during the ES session, Right column: 2-3min rest time after the peaked HBR. All pixels higher than a threshold are labelled in black and the max temperature point is depicted in white. Note that the size of the hot spots has NOT been increased during ES.

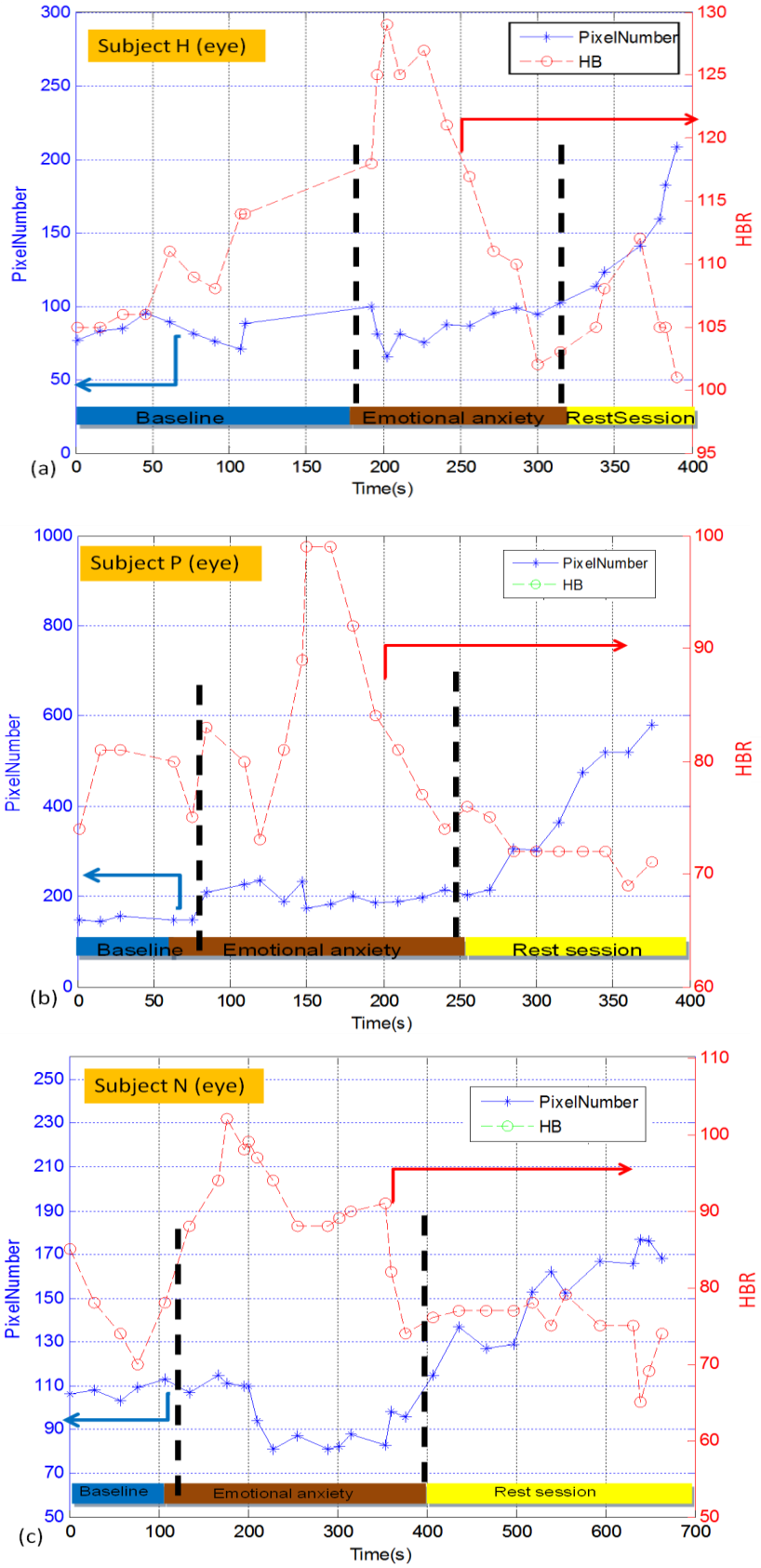

Figure 6-3: shows the number of hot pixels above the threshold in the periorbital ROI for (a)subject H, (b)subject P, (c)subject N. The 3 zones of baseline, under ES and rest are clearly identified. Note that substantial increase of hot pixels counts in the periorbital region happens only a few minutes AFTER the peak of the HBR.

It is observed from Figure 6-2 that the sizes of the hot spots above the threshold temperatures within the periorbital region are seen fairly constant when their HBR are surged to the peak during the ES. The hot spots have been labelled in black colour and the maximum temperature in the ROI is depicted in white. However, the sizes of the hot spots are seen to increase, only 2 to 3 minutes AFTER the peak of the anxiety when the HBR are surged to their maxima.

Figure 6-3 shows the pixel counts in the periorbital ROI of the participants throughout the complete experiment. The figure includes three zones of i) the base line when they are introduced to the trial, ii) the ES session where they are given the mental stressor and iii) the rest time after the ES session is over. The plot shows the HBR together with the hot spot pixel counts.

It is quite clear from the above figure that the number of hot pixels in the periorbital ROI has not been increased during the short ES session which lasts for ~5 minutes. The hot pixel count is seen to climb up 2-3 minutes AFTER the peaked HBR which may represent the moment when the anxiety has reached to its peak. Note that the amount of increase in the number of pixels is in the order of 100-400%!

This result appears to be not quite the same as Pavlidis's reported work. It is intuitive to follow through the temperature change in greater details for more understanding of what has happened exactly in the periorbital region during anxiety.

6.2.1 Temperature profiles in the periorbital: max and mean temperature

Figure 6-4 depicts the temperature profiles in the periorbital ROI of the three representative participants during the complete ES session. The maximum and the mean temperatures in the ROI shown in the figure have revealed that they are fairly stable and hardly changed during the 5 minutes ES session! There is even a temperature drop in the ROI which can be observed from subject N (Figure 6-4(c)). The temperature in the ROI is seen to increase during the rest session, somewhat 2-3 minutes after the peak of the HBR during the ES session.

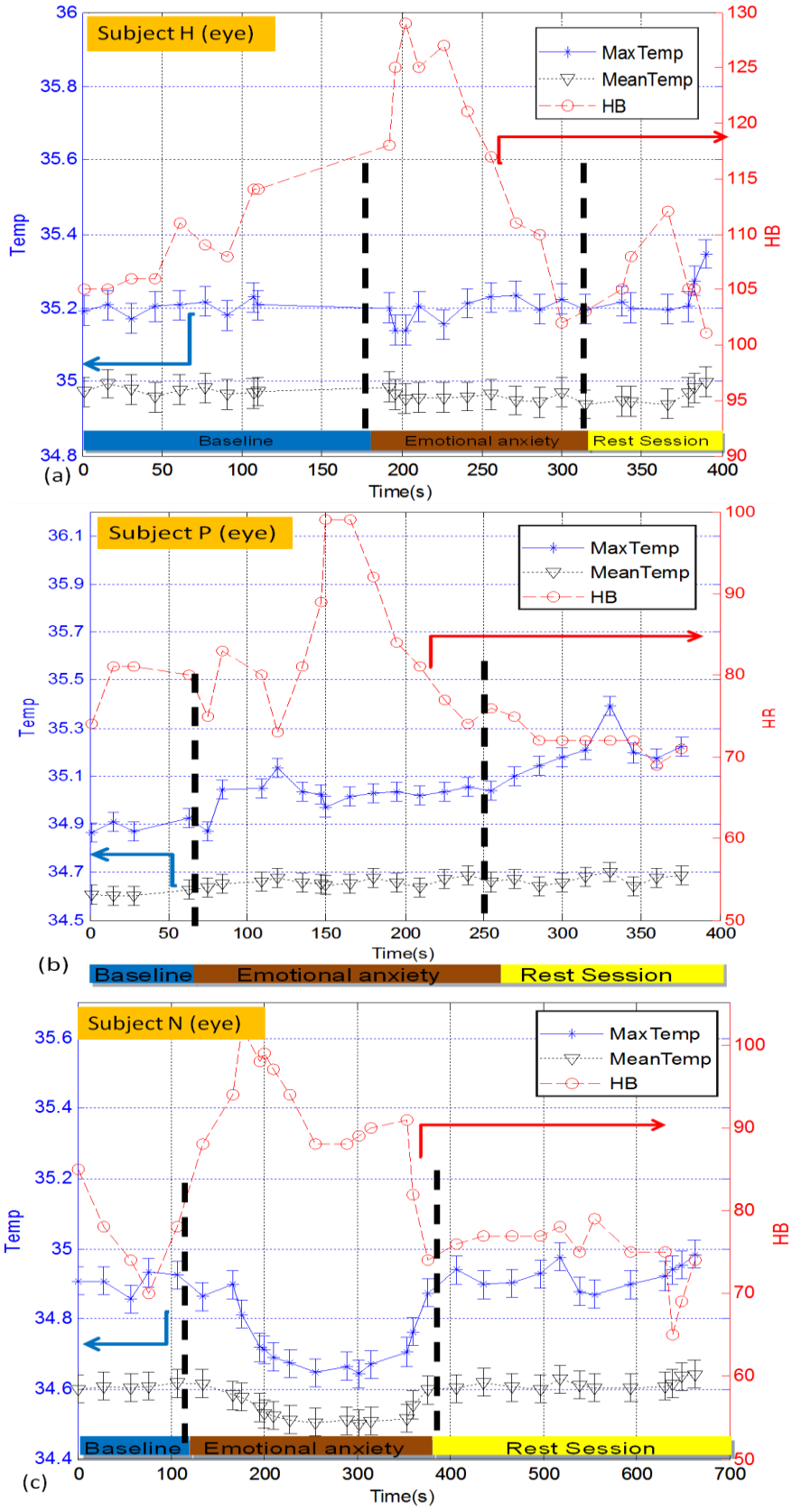

Figure 6-4 shows the temperature profile (max and mean) of hot pixels in the periorbital ROI for (a) subject H, (b)subject P, (c)subject N. Note that temperature in the periorbital hardly increase during the 5 minutes ES session.

6.2.2 Temperature profiles in the periorbital: temperature zones

The result that presented in Figure 6-4 however cannot explain the exact nature of the hot pixels that are seen increased in number after the ES session (see Figure 6-3). To understand this we have analysed the data by segmenting the periorbital ROI in several temperature zones and to monitor the pixel counts in each zone during the complete ES session. The temperature zones are segmented in steps of 0.1C from the threshold right up to the maximum temperature of the periorbital ROI.

The evolution of the hot pixel counts in each temperature zone for the 3 subjects throughout the ES session is presented in Figure 6-5. In common to all these participants, it is seen that the number of pixels in the higher temperature zones are very stable, while those in the lower quartile of the mean of the threshold temperature are observed to increase steadily after the peaked heart beat occurs. The behaviour of the pixel counts in these lower temperature zones can be seen from the blue and red star traces in Figure 6-5. It is interesting to see from Figure 6-5(c) that the number of pixels in the high temperature zones is reduced during the ES session, and only the lower temperature ones are seen to increase in number slightly. This explains the observation of the apparent drop in pixel count for this participant during the ES session (see Figure 6-4(c)).

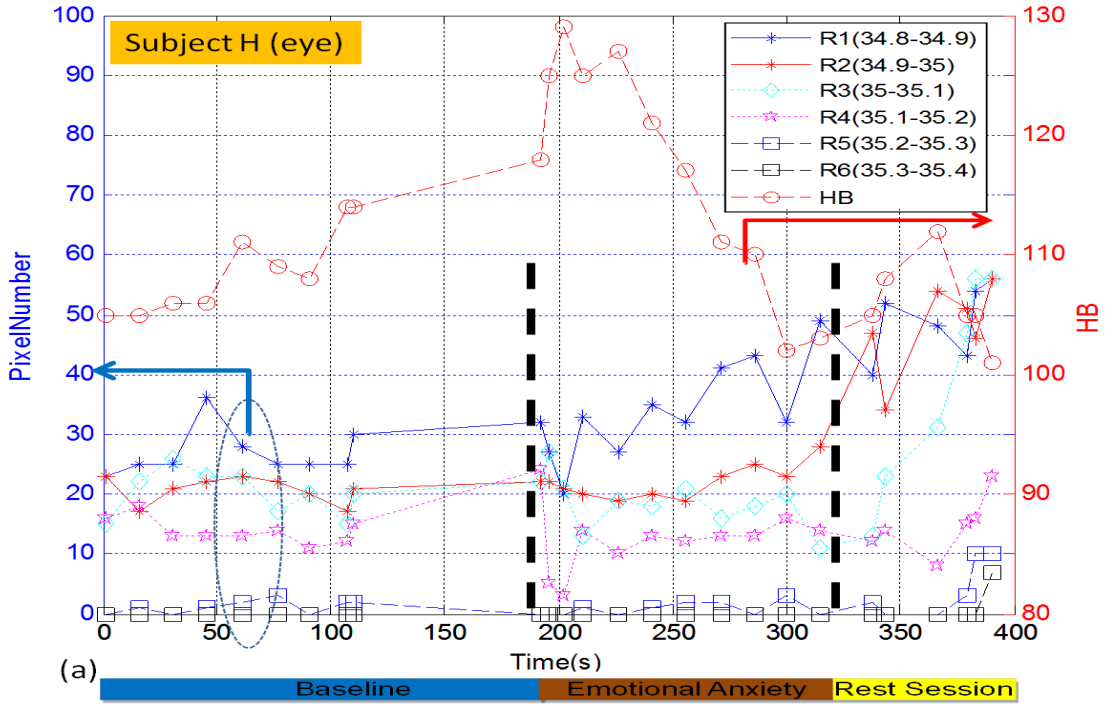

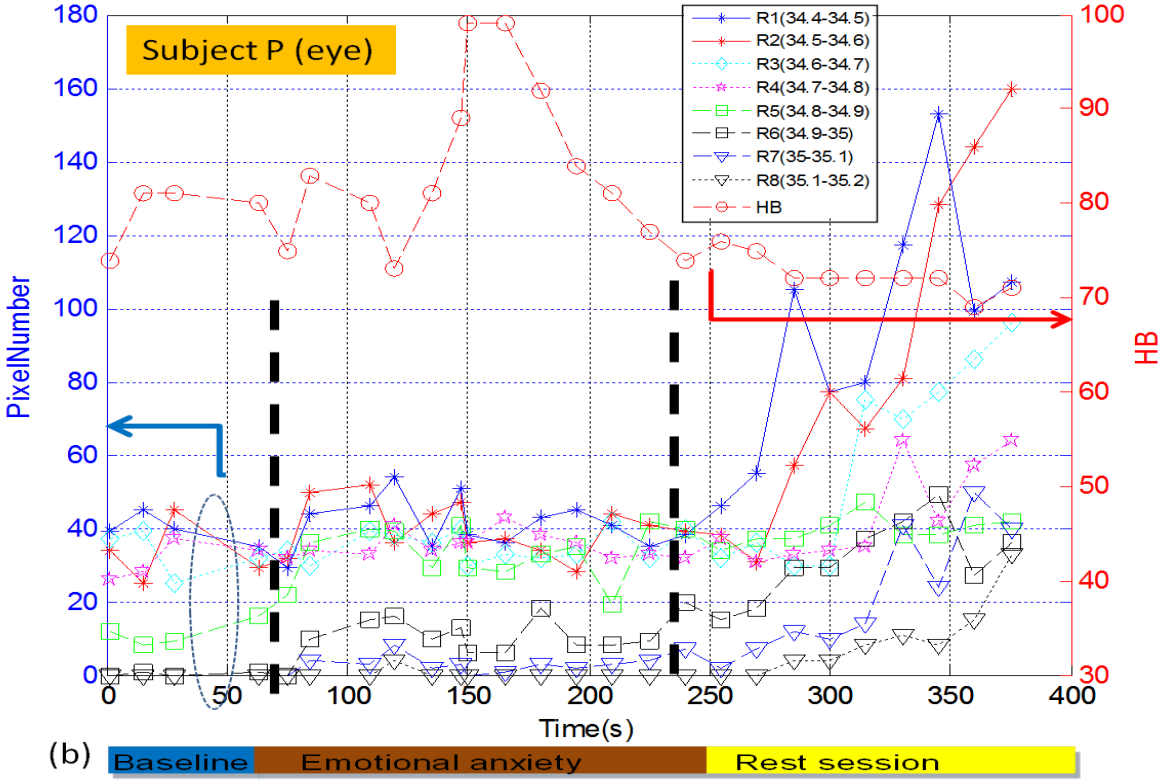

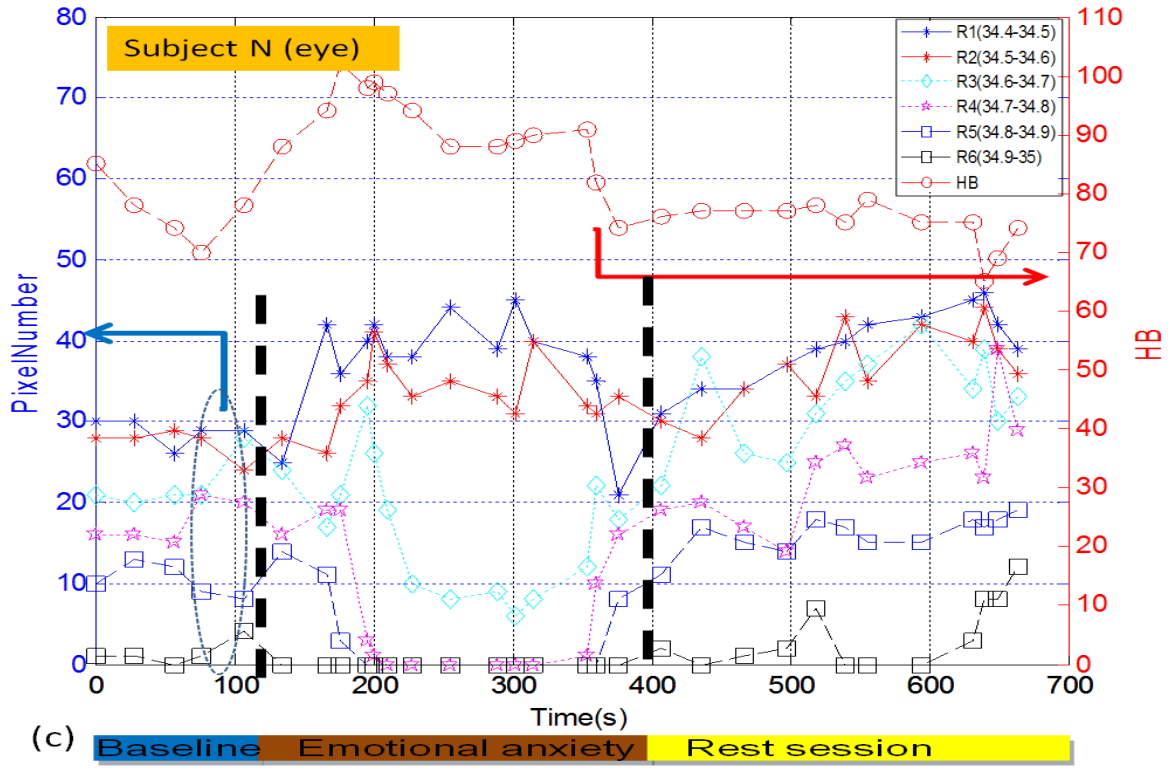

Figure 6-5: shows the hot pixel counts for each temperature zones in the periorbital ROI for (a) subject H, (b)subject P, (c)subject N throughout the ES session. Note that in most cases it is the pixels in the lower temperature zones that are increasing in number after 2-3 minutes of anxiety.

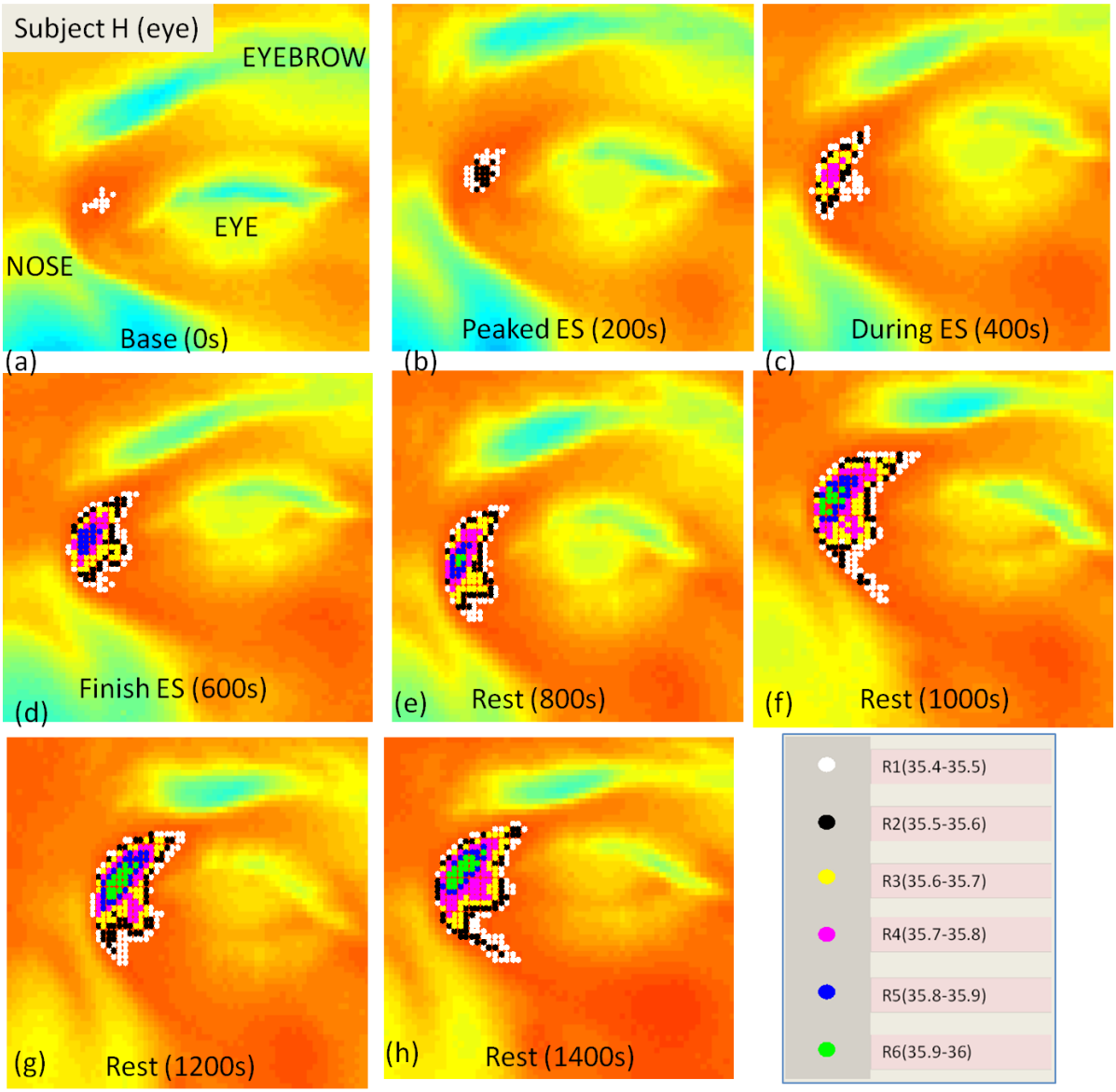

Figure 6-6: shows the false colour TI images of the periorbital ROI of subject H during the ES session ((a)-(h)). The TI image is overlaid by the hot pixels which are colour coded according to their temperature zones. The hot spots evolve like a growing pyramid with the highest temperature in the centre after the anxiety sets in.

Figure 6-6 shows the false colour TI image of the periorbital region of subject H during the ES session. The TI image overlays the hot pixels which have been colour coded according to their temperature zones. The hot spot begins with a small dot in the periorbital region, and it evolves and gets bigger in ~2 minutes after the peaked HBR occurs (Figure 6-6(c)). The growth of the hot spots is seen in the form of a pyramid, with highest temperature in the centre. This may explain why the number of the high temperature pixels in the ROI remains more or less constant throughout the ES session.

6.3 Hot spots in periorbital region: prolonged ES and long rest time

The data that presented in the previous two sections seems to be quite different from Pavlisdis's report which claimed a steady increase of temperature in the periorbital region as soon as the anxiety sets in. The time duration of the data that published by Pavlisdis's group in Figure 6-1 spans for ~6 minutes and it is slightly longer than the ES session that we conducted (~5 minutes). Subsequently we repeated another experiment to involve a stressor in terms of an interview presentation which lasted for about 15 minutes to see if we can repeat their data.

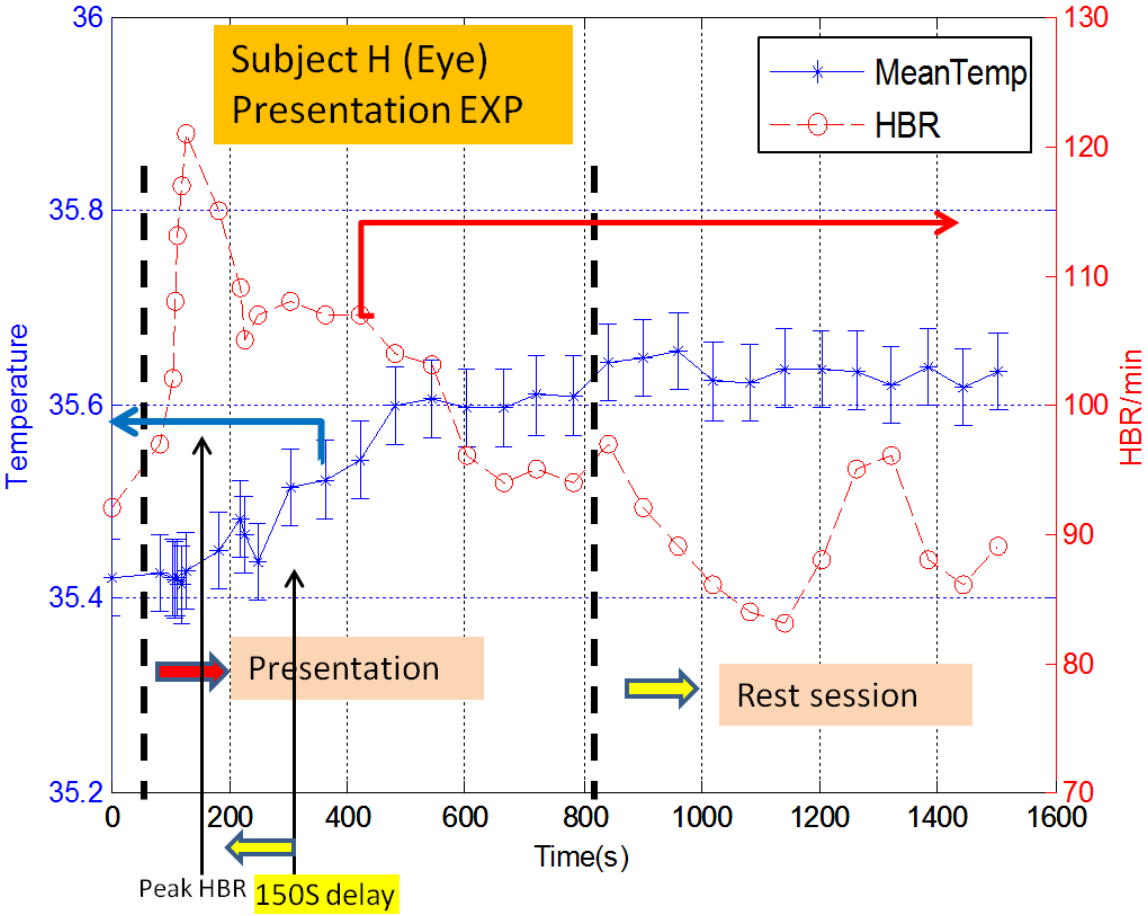

Figure 6-7: shows the mean temperature of the hot pixels in the periorbital ROI for subject H during a prolonged ES session. It is seen that the mean temperature of the hot spot begins to increase in about 2 minutes AFTER the peaked HBR occurs.

Figure 6-7 shows the mean temperature of the hot pixels in the periorbital ROI for subject H during a prolonged ES session. It is seen that the mean temperature of the hot spot begins to increase in about 2 minutes AFTER the peaked HBR occurs, thus this result confirms our previous findings presented in the last two sections. However, we have now observed a steady increase of the hot spot temperature after

2 minutes of the peaked HBR. The temperature in the periorbital region is seen to rise by about 0.2C (~0.5%) and it arrives to a plateau in about 10 minutes after the peak of the HBR. Furthermore, it is also seen that this elevated temperature in the periorbital region stays at the same level for very long time lasting for over 30 minutes!

The number of hot pixels in the periorbital region for this data set can be seen from Figure 6-8 that there is a huge increase of almost 10-fold after the ES: from a minimal of ~20 hot pixels in the base line and it increases to ~200 by the end of the presentation session. It is very likely that this huge amount of increase in hot pixel numbers may have given misleading information for the researchers to believe a significant increase of temperatures in the periorbital regions have been triggered by anxiety!

Again, this huge number of hot pixels has been seen to persist for over 30 minutes after the ES session!

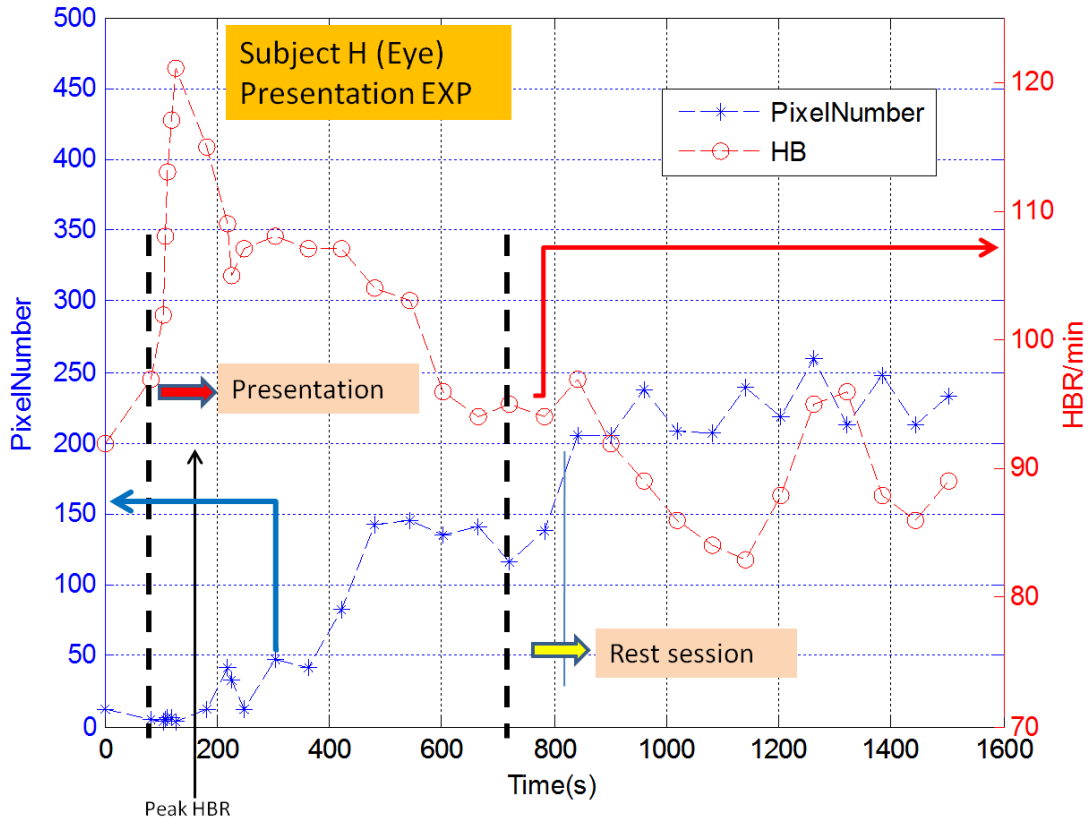

Figure 6-8: shows the number of the hot pixels in the periorbital ROI for subject H during a prolonged ES session. Note that the amount of increase in pixels is about 10 times of the base line!

Figure 6-9 shows the temperature profile of this data set which exhibits similar behaviour as that presented in Figure 6-5: the number of hot pixels in the lower temperature zones begins to increase in about 2 minutes after the peak of the HBR. However, the pixels in the higher temperature zones are seen to increase in number after about 5 minutes of the peaked HBR. The increased number of high temperature pixels induces an elevation of the mean temperature over the ROI, resulting in a steady increase of the mean temperature in the periorbital region as observed in Figure 6-7. This prolonged ES session data set thus explains why there is an absence of temperature rise in the periorbital region in the previous result presented in Figure 6-4 which involved short duration of ES session data less than 5 minutes!

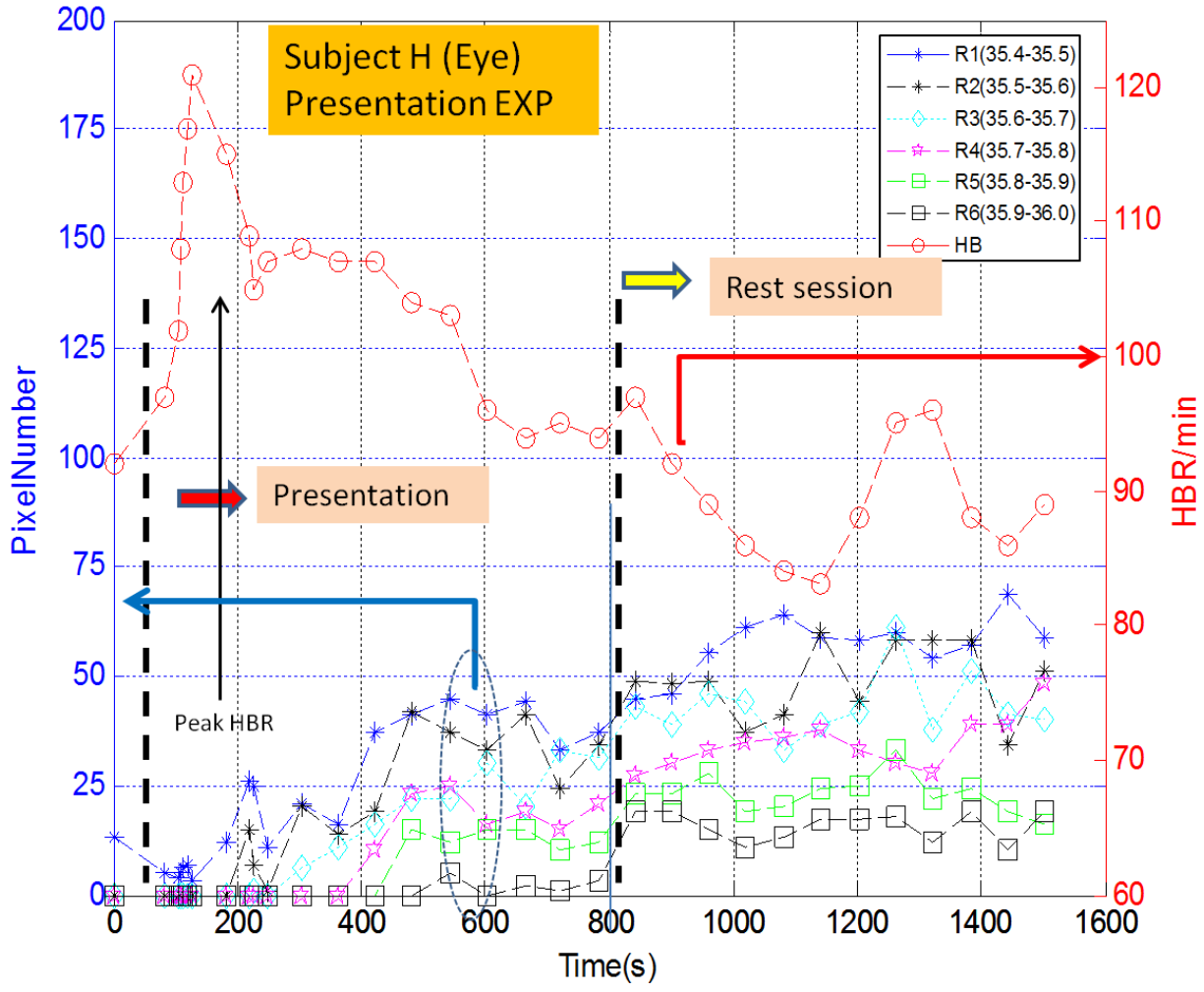

Figure 6-9: shows the hot pixel counts for each temperature zones in the periorbital ROI for subject H in the prolonged ES session. Similar to the previous results it is noted that the lower temperature pixels are increasing in number after 2-3 minutes of anxiety.

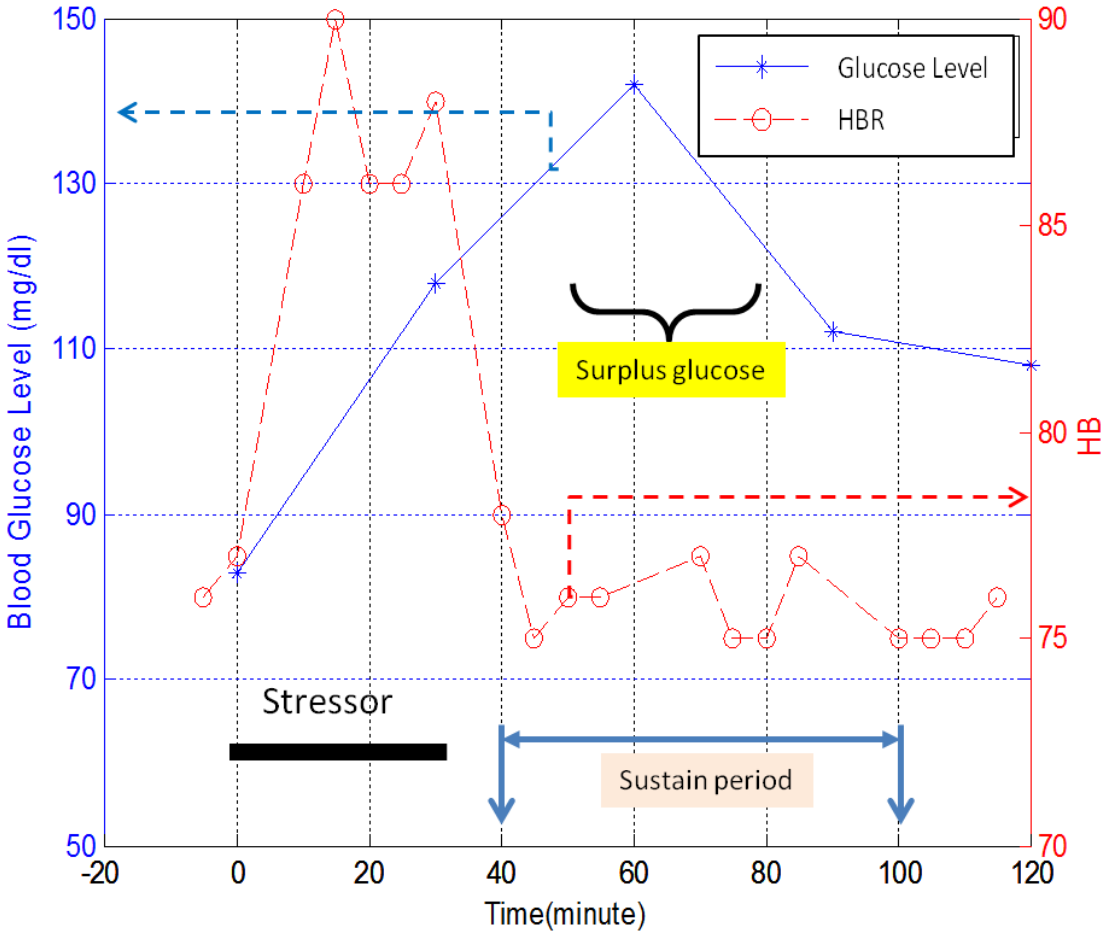

Figure 6-10: shows the long time lag (~60mins) of the blood glucose levels increase after the stressor is applied. The stressor is applied between 0 to 30 minutes (Wing, 1985). The surplus glucose can change many physiological responses in the body which can be very misleading as far as remote sensing of emotion as concern.

The persistent hot spots in the periorbital region even after ~30minutes of the anxiety (see Figure 6-7) is thought due to the surplus of the glucose left over in the ROI after the ES event. Recall the clinical work performed by Wing et al (Wing et al 1985) presented in Figure 4-12 and it is repeated here for the convenience of the discussion, that, the glucose level can sustain for about an hour after the trigger of the anxiety (see Figure 6-10). This surplus level of glucose will induce a number of metabolically and physiologically change in the body for a prolonged period of time. This artefact can be very misleading as far as the remote sensing of emotion as concern.

6.4 Physical stressor

Most research in the field has focused on the studies of physiological responses due to the mental stressor only. For completeness we have performed trials involving physical stressors such that the stressors impose direct impact to the body physically, with a view to understand whether there are any similarities or differences in the physiological responses to the mental ones.

6.4.1 PS induced temperature rise in the periorbital region

All the physical stressors involve physical exercise by requesting the participants to run 6-flights of stairs up and down in one or two minutes. This rigorous exercise impose heavy load to the participant's bodily strength and normally an increase of heart beat by 40-50% have been commonly observed. The EO imaging was performed shortly after the running was completed.

Figure 6-11 shows the mean temperatures of three participants who had performed the running after the completion of the ES session and a rest time of typically 20-30 minutes. The physiological responses of these participants due to the ES have been presented in the last two sections.

It is observed from Figure 6-11 that the temperatures in the periorbital regions of these participants exhibit very small increase with respected to that of the base line, typically less than 0.1C (~0.2%), after they have performed the running exercise and rest for ~5 minutes (Figure 6-11 (a)&(b)). In the previous section 6.3 it is realised that a long rest time may be needed so to give enough of time for the body to regain equilibrium. Figure 6-11 (c) shows the data after long rest of ~10 minutes, and similar result of very little increase of temperatures in the periorbital region with respected to the base line has been seen after the PS session.

6.4.2 PS induced number of hot pixels in the periorbital region

Figure 6-12 shows the number of the hot pixels in the periorbital region after the PS session. Again, it is seen that the number of hot pixels has increased from 2-5 times of the base line behaving very similar to that of the ES case presented in previous sections.

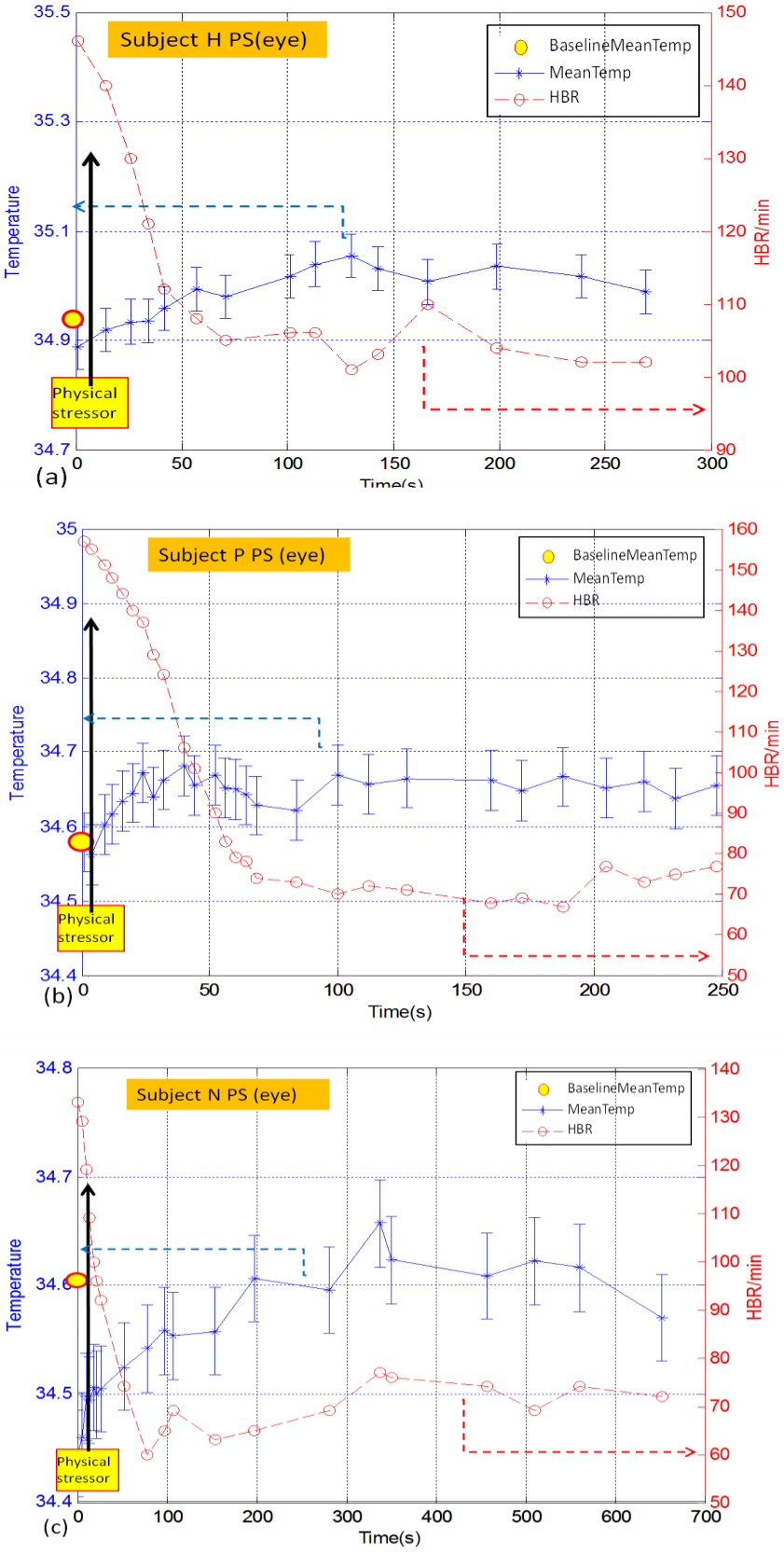

Figure 6-11: shows the mean temperature of the hot pixels in the periorbital ROI for (a) subject H, (b)subject P, (c)subject N during the PS session. Note that there is a long rest time of ~10minutes in (c).

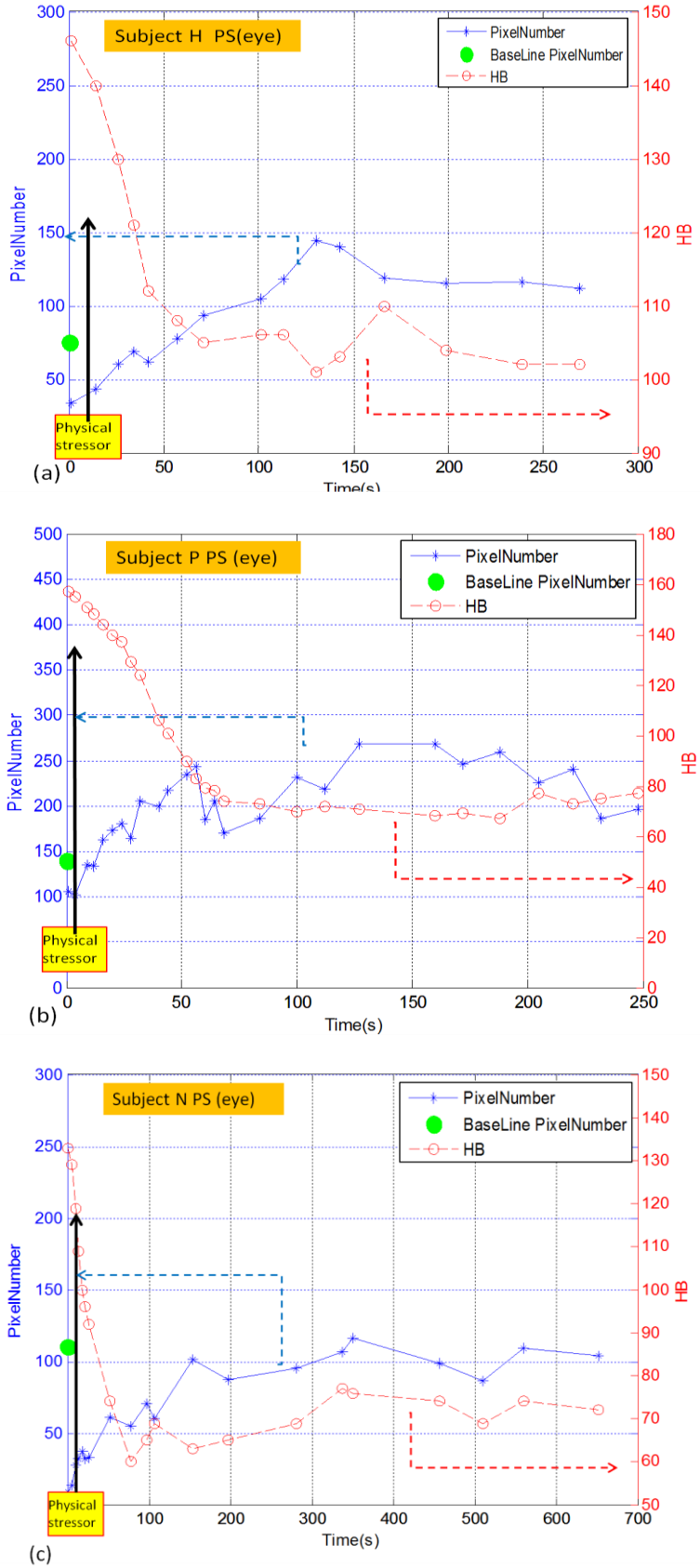

Figure 6-12: shows the number of the hot pixels in the periorbital ROI for (a) subject H, (b)subject P, (c)subject N throughout the PS session.

			ES: periorbital region			
Subject ID	δ HBR (%): ES	δ Cortisol(%): ES	δ Hot Pixel count @peak HBR	δ Hot Pixel count (%) after 5 mins	δ Mean temperature(%) after 5 mins	Threshold temp(C)
Subject H	22%	39.20%	No increase	130%	0.03%	34.8
Subject P	32%	114%	No increase	112%	0.23%	34.4
Subject N	32%	63%	No increase	50%	0.12%	34.4

Table 6-1: A summary of the temperature in the periorbital region after the ES session.

6.5 Summary

We have performed a detailed investigation about the anomaly temperature in the periorbital region upon the onset of anxiety. Previous work performed by Pavlidis group has claimed an 'instantaneous' increase of temperature in the periorbital region when anxiety sets in, but this claim cannot be validated according to our data. We have found that, the mean temperature in the periorbital region hardly increase within 5 minutes AFTER the initiation of anxiety. However, the number of pixels in the lower quartile of the mean temperature in the periorbital region is seen to increase after 2 minutes of the peaked HBR. The evolution of the hot pixels in the periorbital region during the ES session is seen to occur in the form of a pyramid with high temperature pixels located at the tip (centre) of the structure.

We have observed a small increase of the mean temperature in the periorbital region after 5 minutes of anxiety, but the amount of increase is very small in the region of 0.2C (0.5%) which is quite hard to detect in real environment. On the other hand, the number of hot pixels is seen to increase by a huge amount after 2 minutes lag of anxiety. In some cases, we have observed a ~10-fold increase of the number of hot pixels within the periorbital region in comparison to that of the base line (see Table 6-1). The number of hot pixels in the periorbital region can persist for long time, and in many cases it can sustain for 30 minutes and even longer! It is speculated that this huge number of hot pixels triggered by anxiety may have given misleading information to the researchers to believe the occurrence of a temperature rise in the periorbital region when one is under anxiety!

7 Detection of anxiety without base line information

7.1 Introduction

During this work it is commonly observed an increase of blood perfusions in the facial region particularly in the prefrontal forehead areas for almost ALL subjects in this study. The increased blood perfusions induce a rise in skin temperatures as well as accelerations of heart beat rate (HBR). The amount of increase varies from person to person and it is believed the variation is related to individual's cultural background, health conditions, and activities prior to the test and also genetic details.

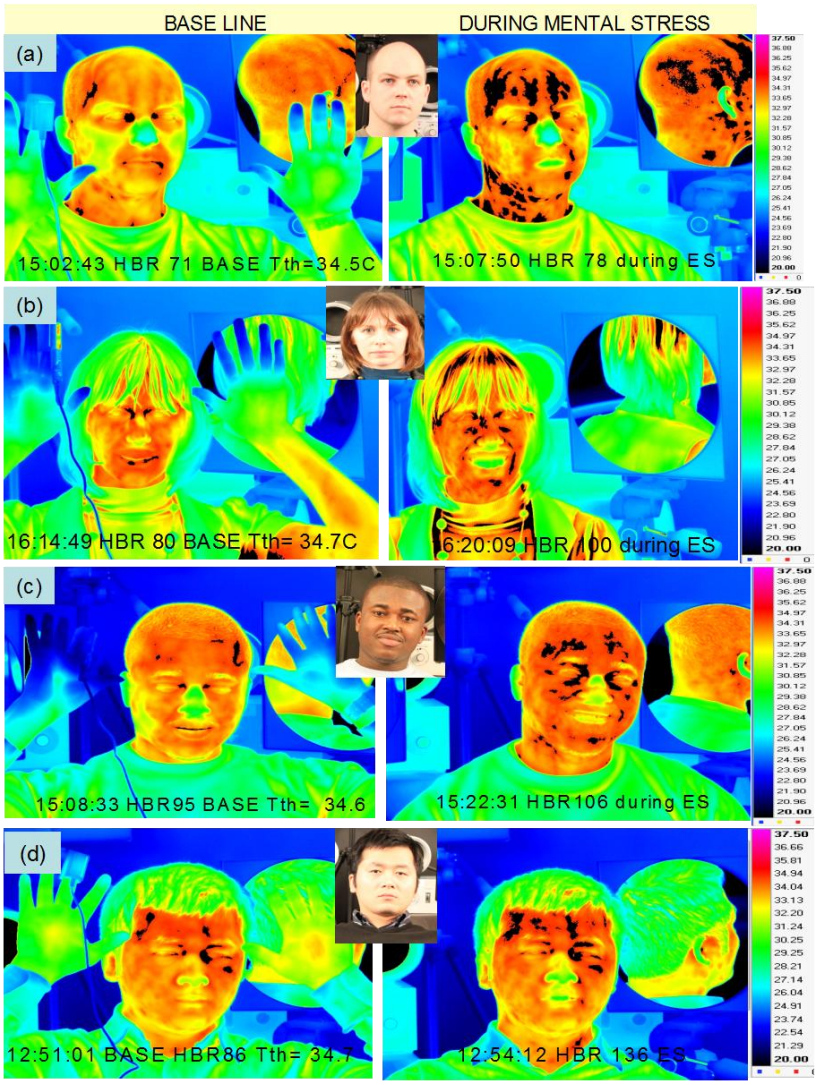

Figure 7-1. Shows the representative MWIR thermalgram of four different ethnical origins of participants before (left hand panel) and during the MS session (right hand panel). The thermalgram is in false colours representing the temperature, and the black pixels are those above the threshold temperature, which are NOT constant. (a) Male Caucasian b) Female Caucasian c) S American male d) Far-East Asian.

Figure 7-1 shows typical thermalgram of four different ethnical origins of participants before and after the stressor is applied to them. It is quite clear that an increase of skin temperatures at around their foreheads, periorbital regions and sometimes in the neck have been observed. These 'hot' pixels are labelled as black colour on the right hand panel of Figure 7-1. Note that the increased blood flow at around the forehead can be detected even through the hair obscures the forehead as it is demonstrated in Figure 7-1b, and some parts such as the nose and the mouth, have been found a reduction of blood flow when the participants are under anxiety.

Note that the presentation of the graphics in Figure 7-1 is made through a very careful selection of the threshold temperature, which is not a constant! Different people in different environment will need a complete different set of threshold parameter! Furthermore, the 'correct' parameter is obtained through a non-principle way of 'trial and error'! Therefore it is necessary to develop a more principle way to assess the people's emotional states.

7.2 Comparison of anxiety assessment by TI and HSI

Thermal imaging (TI) relies on sensing the skin temperatures in order to deduce the increased blood flow underneath the epidermis to assess one's anxiety state. This is quite different in the hyperspectral (HSI) technique which detects the oxygenation of the blood within the tissue directly. Shown in the upper panel of Figure 7-2 is the images of a subject in his base line relax state, and the image of the same subject under emotional anxiety (ES) is shown in the lower panel. The figure has exhibited some similarities between these two techniques, showing the StO2 detection maps in (b), the threshold StO2 level (above 55%) in black colour as depicted in (c), and the thermalgram of the subject in (d). The thermal image has been threshold at 34.34°C and the hot pixels are presented in black. The figure presents an almost one to one correspondence between the StO2 map and the thermalgram, both showing the significantly increase of blood flow at the corners of the forehead and at the neck regions when the subject was under anxiety. However, the figure also highlights some differences between the TI and the HSI technique for sensing the blood flow: it is seen that the StO2 map shows an appreciable increase of oxygenation level in the centre of the forehead, somewhere at around the centre of forehead, while the

thermalgram shows very little increase (~0.3°C) of the temperature in this region of interest (ROI). Although there is substantial increases of temperature in the face and chin regions (>1°C with respected to the base line), however, these areas have been avoided for further analysis due to various medical and physiological reasons.

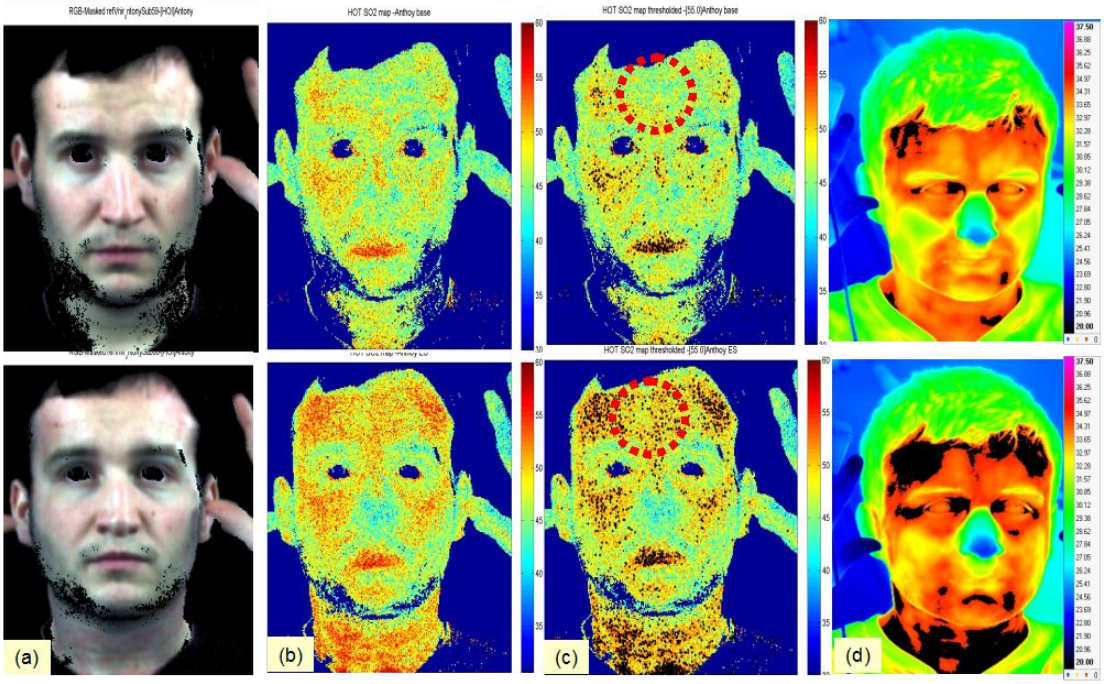

Figure 7-2. highlights the similarities between the TI and HSI techniques for anxiety assessment. Upper panel: base line, Lower panel: under anxiety. (a) RGB image of a subject, (b) the false colour StO2 map in scale of [30 60]%, (c) the thresholded StO2 map at 55% of StO2 and the high StO2 pixels are presented in black colour, (d) the threshold thermalgram at 34.34C and the hot pixels are presented in black. While both techniques are found capable to detect the change of blood flow that triggers by anxiety, the HSI seems to be more sensitive in detecting StO2 particularly at around the strategic ROI in the mid forehead (red circle in (c)).

7.3 Variable base lines issues

7.3.1 Environmental and dietary effects

It is well-documented that environmental effects such as ambient temperatures, humidity and air qualities can impose impacts to individuals and subsequently affecting one's psychological, emotional and physiological well-beings. The data presented in Figure 7-3 highlights how much of these ambient issues can affect one's skin temperatures and oxygenation levels apart from the emotional factors.

Figure 7-3 depicts the EO data of a subject recorded (a) early in the morning before his coffee, (b) at mid-day before food, (c) just after a sandwich lunch and (d) after food and just been outdoor for a cigarette. It is not too surprising to see a very rapid

change of the skin temperatures during one's normal routine activities, but the extent of the change is quite alarming: the skin temperatures in the face can fluctuate by as much as 5 °C (~15%) in one's normal daily life. Note that the anxiety induced change of temperature is in the region of ~1-5% of the body temperature.

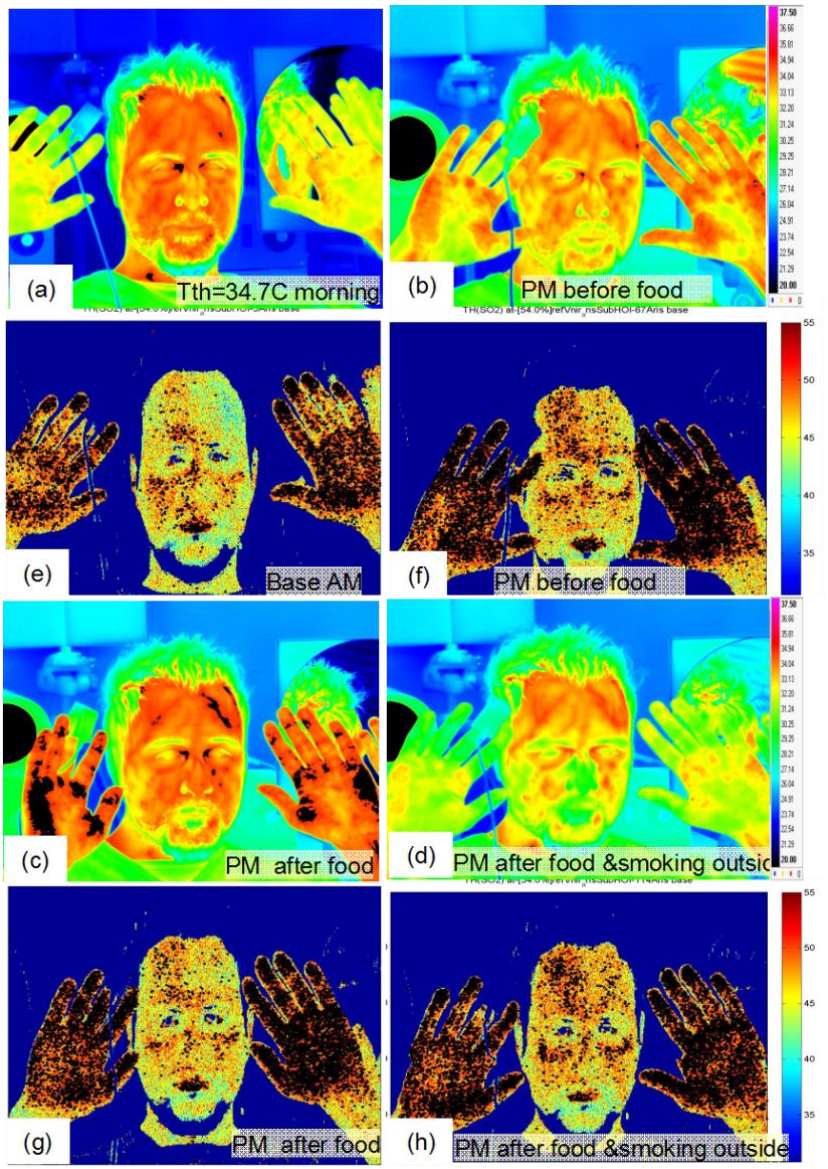

Figure 7-3. Outlines the variations of skin temperature and oxygenation in one's normal daily routines (a) thermalgram before coffee in the morning, (b) before food, (c) after food, (d) after food and had a cigarette outside. (e)-(h) are the StO2 maps thresholded at 54% (black pixels) corresponding to the thermalgrams presented in (a)-(d). Note the large fluctuation of the skin temperatures in the face and hand even when one is performing normal work in everyday's routine activity.

The oxygenation level in the facial region and hand are seen to be slightly less dependent on one's activity than that of theskin temperature. The StO2 presented in the figure is overlaid by the threshold StO2 at 54% (black pixels in Figure 7-3 e,f,g,h). However, as it can be seen in the following few sections that it is not quite

possible to assess emotional information using EO technique even for very small errors of ~ 1% uncertainty in the oxygenation data.

Furthermore, it is rather alarming to observe that the temperatures of the hands, as well as that in the facial region such as in the nose and the forehead, have exhibited large variations in the range of ~2-3C differences even though the subject was in fact very calm and relax. Table 7-1 & Table 7-2 tabulate the temperature change in the hands/fingers as well as in the forehead, nose and mouth under these conditions, and in the extreme cases a massive ~10% change of temperature in the finger is seen. Thus it can be concluded that although the skin temperatures of the hand are sensitive to the emotional anxiety, however, it is also strongly affected by external factors such as dietary and weather conditions too. The forehead temperature is seen to have 2% changes under these circumstances.

Furthermore, the skin temperature and the StO2 can also be affected by many other factors, such as sweating and change of ambient temperatures. In cases when the skin temperature is modulated by a sudden change of sweating or environmental factors, the assessment of anxiety without base line information can be very unreliable!

	Subject H: Base line				
Condition/MeanTemp (C)	Right fore finger temp (C)	Right little finger temp (C)	Left Palm temp (C)	Right Palm temp (C)	Forehead Temp (C)
morning	32.42	32.46	32.57	32.86	34.34
before lunch	34.16	33.97	33.05	33.60	34.00
after lunch	35.06	34.97	34.75	34.73	34.63
after been outside	32.31	31.73	32.13	32.34	33.89
Standard deviation	0.08	0.52	0.31	0.37	0.32

Table 7-1: Highlights how sensitive is the temperature of finger/hand to dietary and weather conditions other than that triggered by anxiety. Noted the very large standard deviation in these figures.

	Subject H Base line			
Condition/Mean Temp (C)	NoseTemp (C)	δ Mean temperature(%) Nose	MouthTemp (C)	δ Mean temperature(%) Mouth
Before go outside	33.06	---	32.91	---
After been outside	28.99	12.31%	30.75	6.56%
Before drink beer	33.39	---	33.68	---
After drink beer	33.56	0.50%	32.27	4.18%
Standard deviation	0.35		0.45	

Table 7-2: shows the variation of nose and mouth temperatures due to other environmental factors. Noted the very large standard deviation in these figures.

Figure 7-4. presents the base line images of 14 representative participants in two columns and each contains the RGB on the right, the false colour StO2 map presented in a fixed scale of [30-55]% in the middle and the thermalgram in the scale of [20 -37.5C] on the left. Note the wide range of the skin temperatures and StO2 variations in their foreheads across these 14 participants.

7.3.2 Personal health conditions

Given the wide range of people with enormous variations of cultural and ethnical backgrounds and health conditions, the physiological 'base-line' conditions for a very small sample size of people like the one we have (85 people), are found to be impossible to generalise. A good example can be seen from Figure 7-4 which shows the extremely large variations of the facial StO2 and skin temperatures across these 14 participants. The maximum oxygenation in their foreheads possesses a standard deviation of over 30% and therefore any attempt trying to detect a change of ~3% using their '*gross or face values*' without given the base line information sounds like an impossible mission!

7.4 Emotional anxiety assessment given base line information

With the presence of baseline information it is very straight forward to assess one's emotional state using EO technique. For instance, the change of the skin's electrical resistances such as that in the thumb has been traditionally regarded as one of the hallmarks for being under emotional anxiety. Given base line information to compare as it is shown in Figure 7-5(a), the emotional state such as anxiety can be readily assessed. In this case the hand's temperature is seen to drop by as much as 3 degree which amounts to a massive ~9% change when one is under emotional anxiety (Figure 7-5(b)). Other places such as the forehead temperature of the subject, is seen to rise rather extensively when the subject is under emotional anxiety. It is also noted that the temperatures at the nose and around the mouth regions, are seen to reduce too.

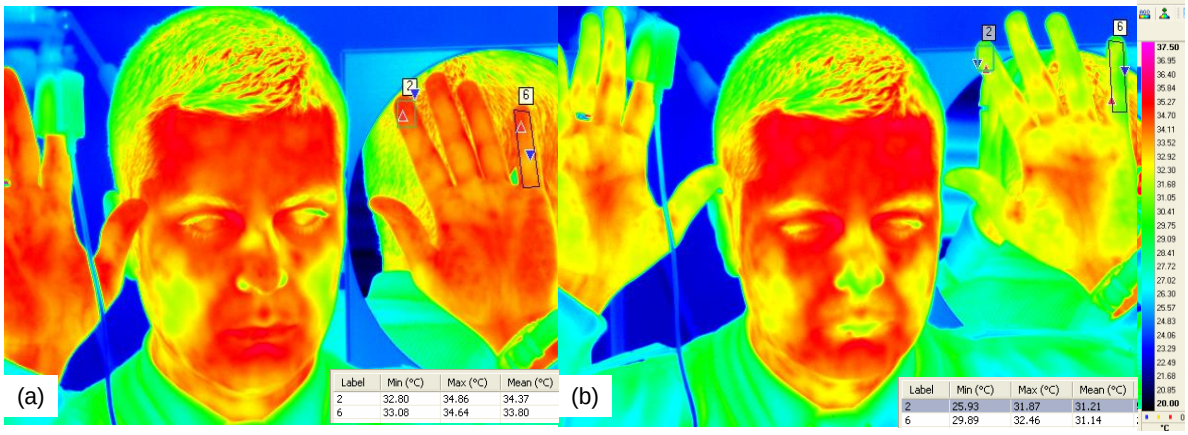

Figure 7-5 showing how straight forward it is for assessing one's emotional state when the base line information is given. The figure shows the false colour thermalgram of a subject (a) at rest and (b) after ES. The hand temperature is seen to reduce by as much as 3C (~9%) indicating that the subject is in anxiety unambiguously.

Figure 7-6 displays a collection of thumb and forehead temperatures of 20 participants when they are in their base lines and under anxiety. It is quite clear from the figure that the thumb temperatures fluctuate greatly with very large standard deviation across the sample size. However, the forehead temperatures seem to be rather stable amongst these 20 participants and furthermore, all of them appear to rise in temperature above their base line levels when they are in anxiety. This is depicted by the pink trace in Figure 7-6.

Note that the analysis in this chapter will be exclusively using TI data due to the reason that the HSI cannot record images when the subjects are in motion. In other

words, the HSI can only take snap shots of images when the subjects are requested to sit still, and it is not possible to record HSI images during the session.

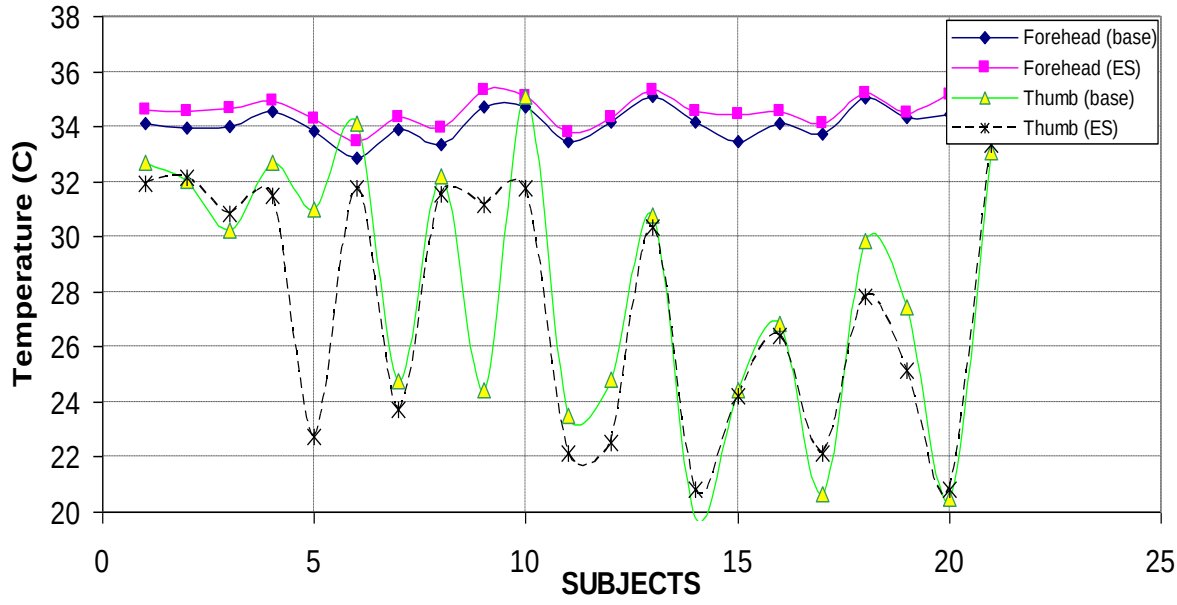

Figure 7-6 shows the forehead and thumb temperatures of 20 participants when they are in their base lines and under anxiety. Note the large variation of the thumb temperatures across this small sample size of participants.

7.5 Emotion assessment without baseline

7.5.1 Dynamic change of forehead temperatures during & after anxiety

As it can be seen from Figure 7-6 that the forehead temperatures are relatively stable amongst a sample size of 20 participants, it is of interest to look at how the forehead temperature behaves during and after anxiety sets in.

Figure 7-7 shows the evolution of forehead temperatures of three representative participants during the ES session. The change of the forehead temperatures is seen to be relatively small within the boundary of 0.2-0.5°C during the complete ES session. Note that the spread of the absolute temperatures of the forehead is about 2°C for this sample size of participants (see Figure 7-6 and Figure 7-7).

The forehead temperatures are seen to rise a few minutes after the peaked HBR, and the temperature is kept increasing for long time similar to the persistent increasing numbers of hot pixels in the periorbital region after anxiety sets in. However, this ‘memory’ effect in the forehead is not as extreme as that seen in the periorbital region and the temperature change is in the region of ~1%.

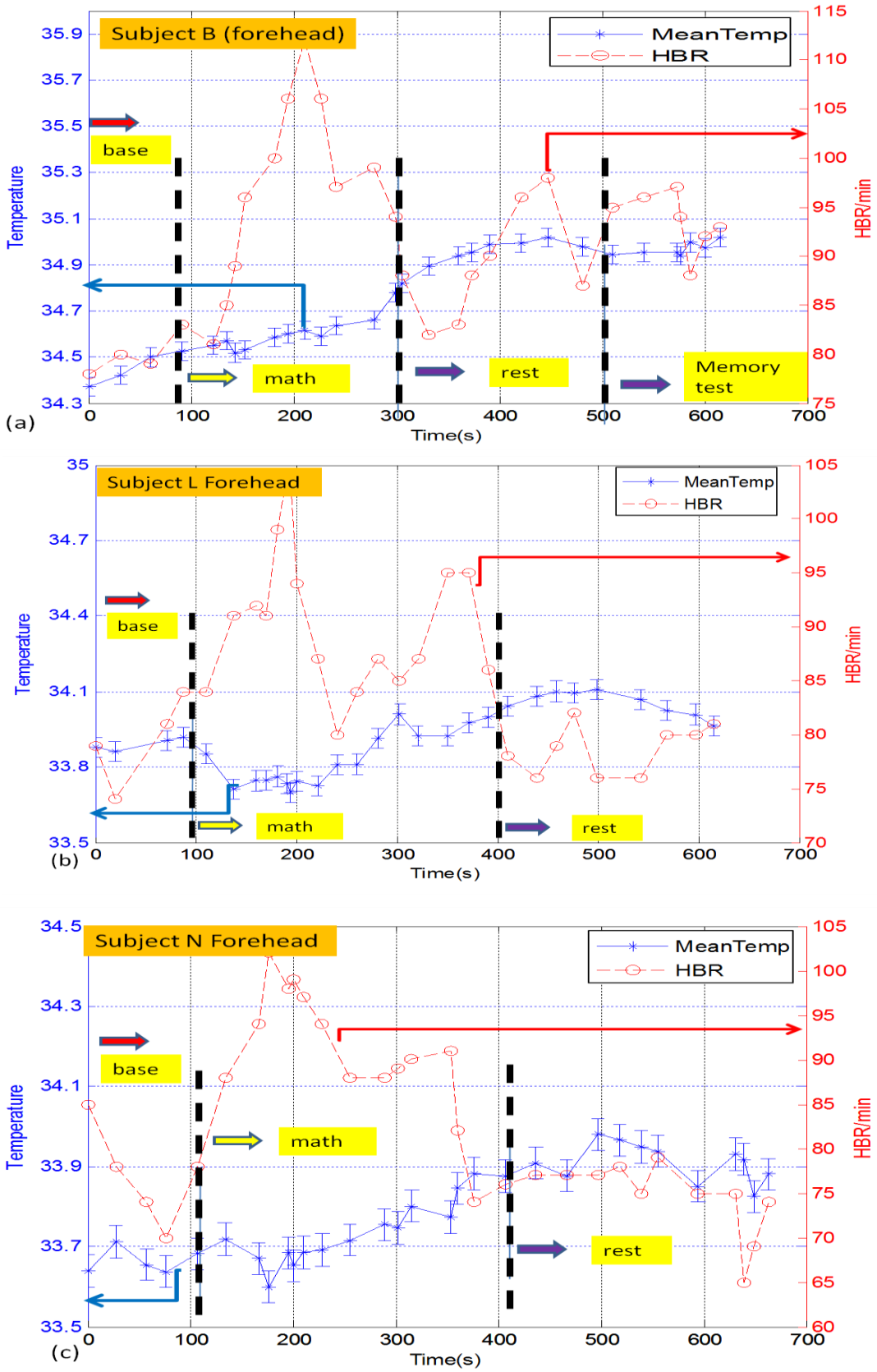

Figure 7-7 shows the behaviour of the forehead temperatures upon the trigger of anxiety: (a) subject B, (b) subject L and (c) subject N. The forehead temperatures are seen relatively stable with changes less than 0.5°C throughout the ES session.

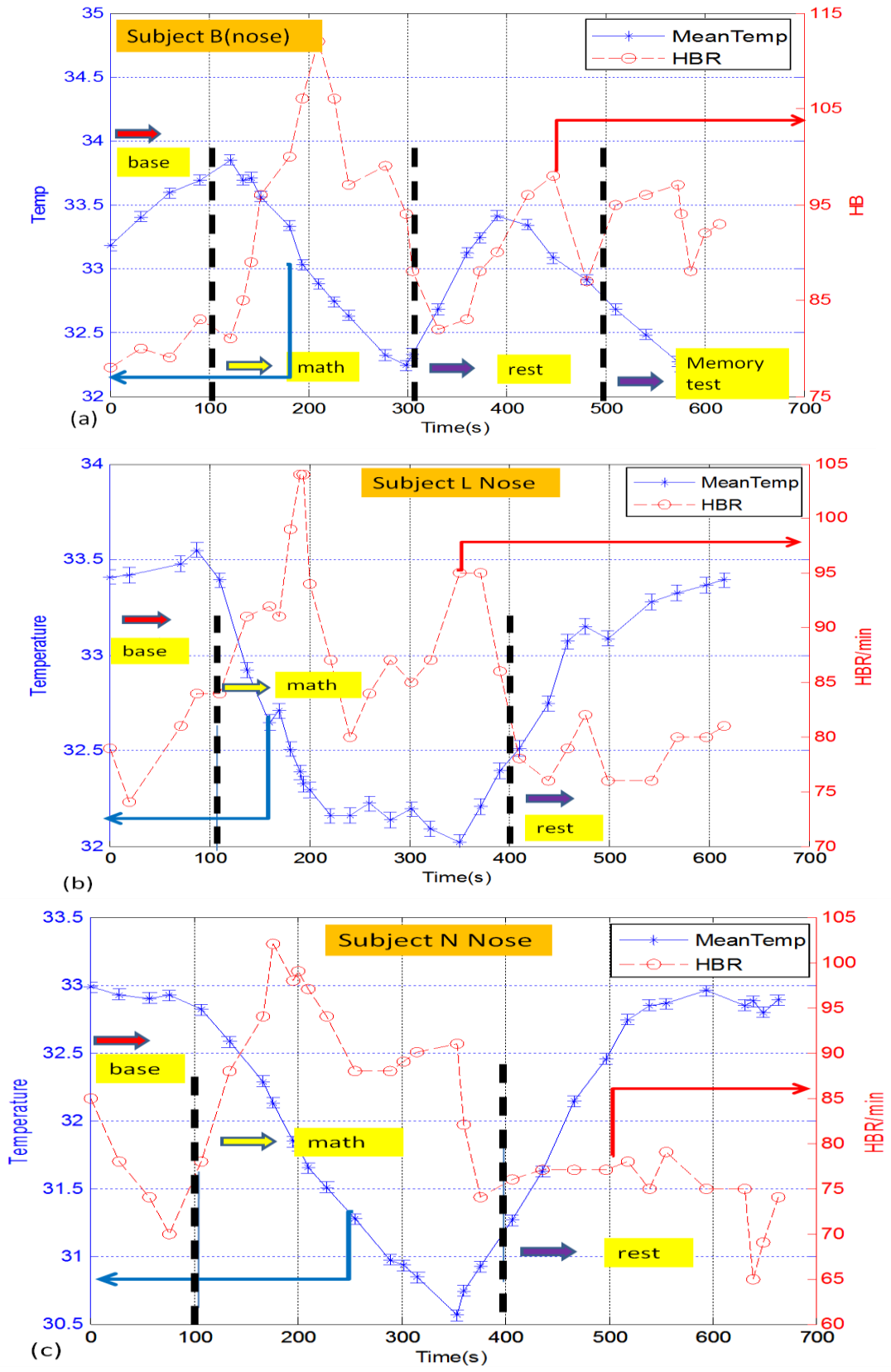

Figure7-8 shows the behaviour of the nose temperatures upon the trigger of anxiety: (a) subject B, (b) subject L and (c) subject N. The nose temperatures are seen very responsive to the HBR. Unlike in the forehead it shows very small residual memory effect.

7.5.2 Dynamic change of nose temperatures during & after anxiety

Figure7-8 shows the dynamic change of the nose temperatures of the same participants during and after the ES session. Unlike the time lag and the residual memory behaviours that have been seen in the forehead and periorbital regions, the nose temperature is observed to be very responsive to the change of heart rate throughout the trial. There are still time lags between the peak of the HBR and the minimum temperatures in the nose, but the lags are much shorter in the region of from 10's of seconds to ~100 seconds.

The responsiveness of the nose temperatures to the HBR is very fast: it begins to drop as soon as the HBR begins to increase (see Figure7-8(a-c)). The nose temperature also behaves very differently from that of the forehead and the periorbital region: the temperature reduces upon anxiety. The reduction of temperature in the nose AFTER the anxiety event has not been found from all the investigated participants during the course of this work. This unique property of the nose to the emotional state has been one of the most important findings in this research. Note that there are substantial reductions of the temperatures in the nose during the anxiety: reductions of 1.5C to 3C amount to ~4.5% to 9% change have been observed! This large amount of change can be readily detected without problem. However, the base line temperatures in the nose region amongst all the investigated participants are seen to span widely in the region of 5-10% variations (see Figure 7-4). Thus to detect the change of nose temperatures due to emotions will need some reference points.

7.5.3 Dynamic change of mouth temperatures during & after anxiety

Figure 7-9 displays the dynamic change of the lips (mouth) temperatures of the three participants during and after the ES session. It is seen that the behaviour of the mouth's temperature is very similar to that of the nose: it is also quite responsive to the change of HBR due to anxiety and temperature reductions of around ~2C (6%) have been seen from all the participants investigated in this study. Again, the base line of the lips temperature have a scatter of ~5% amongst the investigated population and therefore a reference point is needed in order to extract the net effect due to anxiety from the EO property of the mouth.

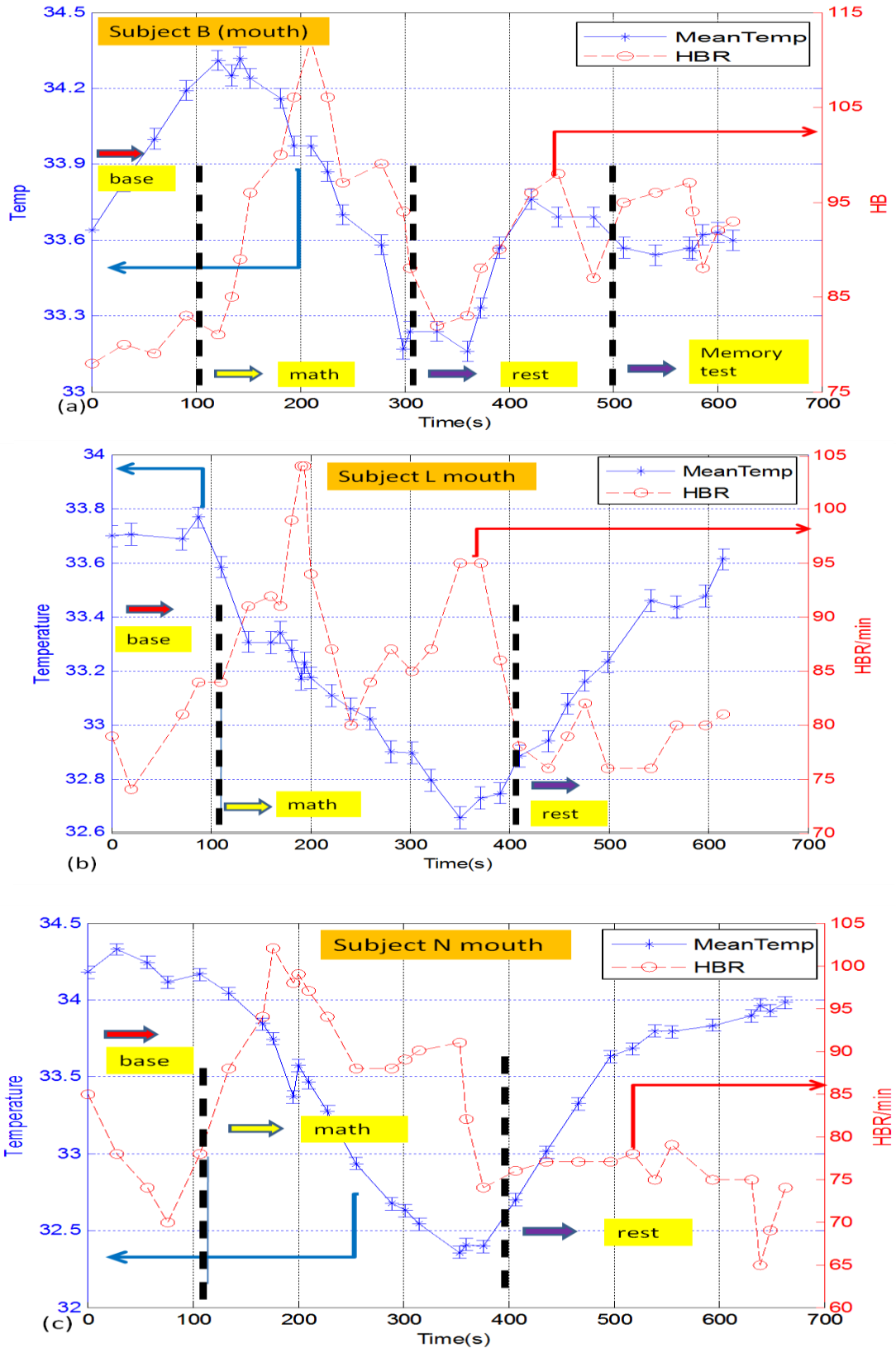

Figure 7-9 shows the behaviour of the mouth temperatures upon the trigger of anxiety: (a) subject B, (b) subject L and (c) subject N. The mouth temperatures are seen not as responsive as that of the nose to the HBR, and about ~6% reduction in the mouth's temperature due to anxiety has been observed.

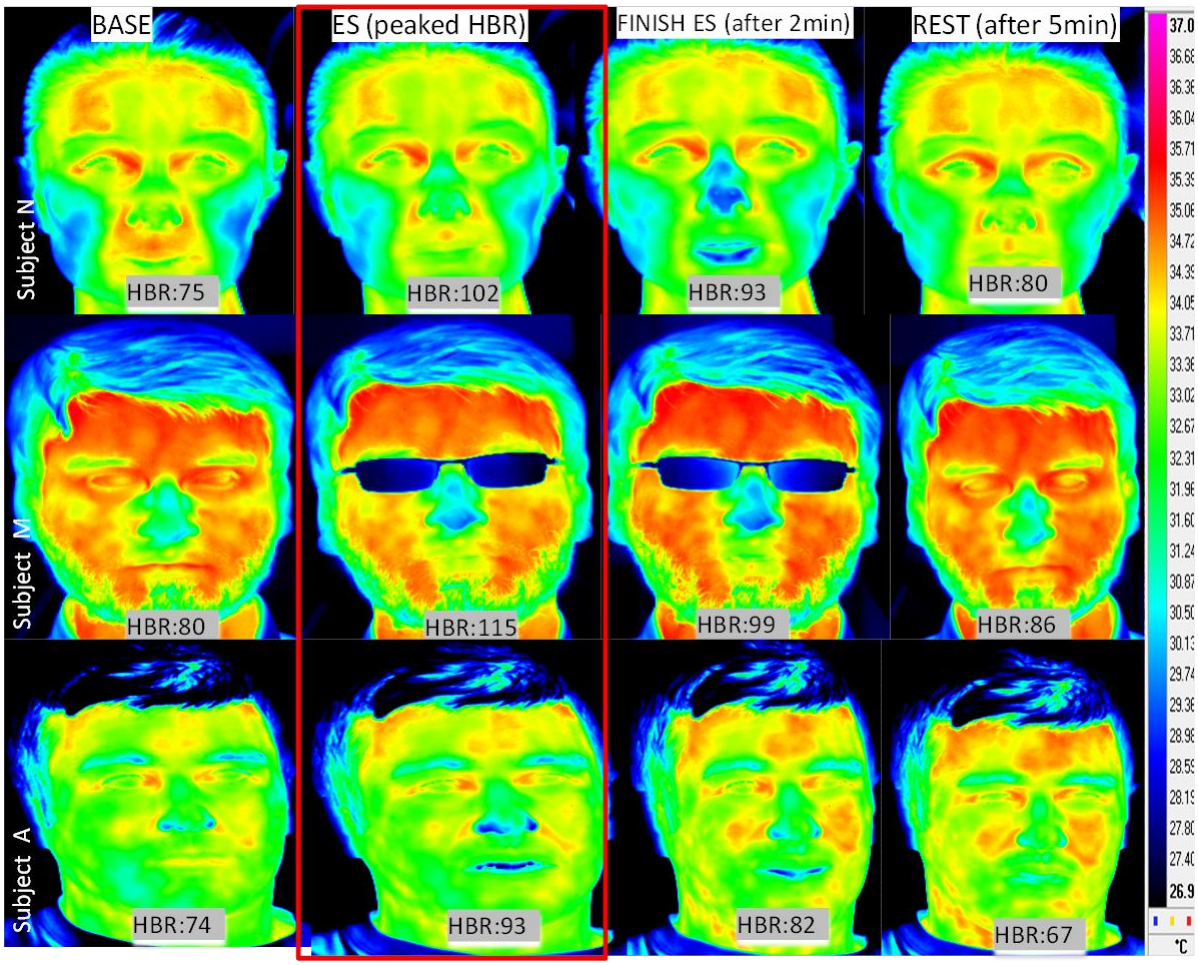

Figure 7-10 shows TI of three participants in four columns of: i) when they are in their baseline ii) during ES and at their peaked HBR, iii) after 2 minutes of the peaked HBR, and iv) after 5 minutes of the peaked HBR.

7.5.4 Summary of forehead, nose and mouth responses to anxiety

Figure 7-10 shows the representative TI images of 3 participants of different ethnic origins to provide supports of the data materials that have been presented in Figure 7-6 -Figure 7-9. Shown in the figure are the false colour images of TI before, during and after their ES sessions. Our main interest is the detection of the emotions when they are in extreme tension, and this is the moment as depicted by the red box in Figure 7-10 when their HBR are surged to the maximum. The immediate responses to the anxiety, as given by the features from the face that can be captured using EO imaging techniques, are the nose and mouth temperatures which are seen to react and drop instantaneously. The response from the nose is more acute as it can be seen quite clearly from the TI image shown in Figure 7-10.

A summary of these responses from a number of participants is presented in the following tables (Table 7-3, Table 7-4 and Table 7-5). It is obvious from Table 7-5 that there is an absence of direct correlations between the change of the heart rate and the change of the EO properties for the anxiety state with respected to the base line.

	ES: Nose region			
Subject ID	**Baseline Nose Temp (C)**	**Baseline HBR**	**ES Nose lowest Tempe (C)**	**ES HBR Peak**
Subject A	32.26	74	31.67	93
Subject B	33.23	77	32.29	112
Subject C	30.14	64	29.253	88
Subject D	32.55	86	31.94	108
Subject E	34.22	68	32.99	76
Subject F	32.64	81	32.03	136
Subject G	30.93	81	30.45	95
Subject H	33.74	101	33.16	129
Subject I	32.77	78	31.73	118
Subject J	28.17	77	27.87	121
Subject K	29.81	70	28.25	95
Subject L	33.39	79	32.02	115
Subject M	31.01	81	30	107
Subject N	33.18	75	30.57	102
Subject O	32.01	70	31.1	90

Table 7-3 tabulates the variations of the HBR and the mean nose temperatures for a number of participant during ES session.

	ES: Mouth region			
Subject ID	**Baseline Temperature (C)**	**Baseline HBR**	**ES Min. Temperature (C)**	**ES peak HBR /min**
Subject A	33.05	74	32.19	93
Subject B	33.71	77	33.267	112
Subject C	32.38	64	31.26	88
Subject D	33.08	86	32.23	108
Subject E	34.48	68	32.86	76
Subject F	32.68	81	32.09	136
Subject G	31.76	81	30.94	95
Subject H	33.36	101	33.15	129
Subject I	33.89	78	32.8	118
Subject J	32.68	77	31.78	121
Subject K	32.52	70	30.97	95
Subject L	33.7	79	32.72	115
Subject M	32.55	81	32.01	107
Subject N	34.39	75	32.39	102
Subject O	33.21	70	31.47	90

Table 7-4 tabulates the variations of the HBR and the mean lip temperatures for a number of participant during ES session.

ES: Nose and Mouth region			
Subject ID	**δ HBR (%): ES**	**δ NoseTemp (%): ES**	**δ MouthTemp (%): ES**
Subject A	25.67%	1.82%	2.60%
Subject B	45.45%	2.82%	1.31%
Subject C	37.50%	2.94%	3.45%
Subject D	25.58%	1.87%	2.56%
Subject E	11.76%	3.59%	4.69%
Subject F	67.90%	1.86%	1.80%
Subject G	17.28%	1.55%	2.58%
Subject H	27.72%	1.71%	0.62%
Subject I	51.28%	3.17%	3.21%
Subject J	57.14%	1.06%	2.75%
Subject K	35.71%	5.23%	4.76%
Subject L	45.56%	4.10%	2.90%
Subject M	32.09%	3.25%	1.65%
Subject N	36%	7.87%	5.81%
Subject O	28.57%	2.84%	5.23%

Table 7-5 tabulates the change of the HBR, the mean nose and lip temperatures for a number of participant between the baseline and when they are under anxiety.

To summarise, we have observed the following properties of EO features in response to the emotional anxiety in this study:

1. The temperature in the periorbital region is quite stable within 0.5%.
2. The number of hot pixels in the periorbital region begins to increase after a time lag of about 2 minutes upon the onset of anxiety. The hot pixel can keep increasing in numbers for 30-60 minutes after the triggering of anxiety, and the total hot pixels can be increased up to about 10 times of the base line level. This is one of the most undesirable memory effects to the remote sensing of emotions.
3. The forehead increases its temperature after a time lag of about 1-2 minutes upon the onset of anxiety. The amount of temperature increase is in the region of about 1%.
4. The temperatures in the nose and lip (mouth) regions are found very responsive to the anxiety induced change of HBR. The responses are found fairly instantaneous, and they start to drop in temperature as soon as the HBR begins to surge. The amount of the temperature drop is in the range of ~5-9%.
5. There is no direct correspondence between the change of the HBR and the change of temperatures in the facial region.

6. Environmental and variable base lines due to different physiques of individuals impose ~5-10% variations on the temperatures and StO2 in the facial region.

7.6 Differential temperature & oxygenation for emotion assessment

According to the neuroscience research, the behaviour of blood transfusions particularly in the facial region, is found very different when under anxiety. Thus it is possible to employ local differentiation method to eliminate this large and unsteady base line residue using a technique similar to that of 'lock-in' technology. During the course of this work we have developed two local differentiation techniques hoping to quantify the anxiety assessment. The objective of the method is to obtain a measure which ideally follows a net change of physiological responses to anxiety independent of individual's base line conditions.

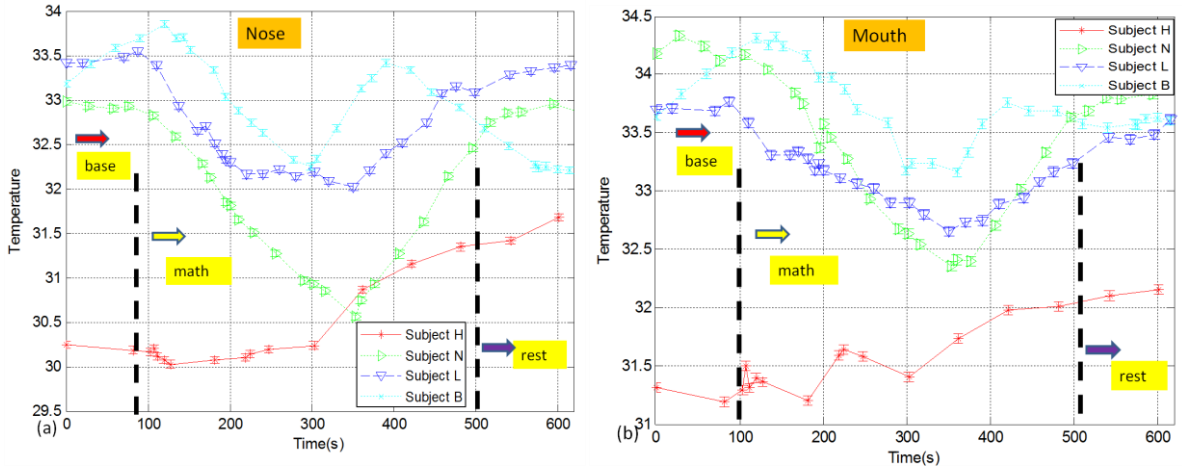

Figure 7-11. highlights the spread of the base line (at t=0) temperatures in (a) the nose and (b) mouth regions for a selection of subjects. This data implies the need of a reference point in order to relate the change of these temperatures to the degree of anxiety.

Figure 7-11 illustrates the appreciable spread in the base line levels of the nose and mouth temperatures amongst the selected four subjects as an example. The spread of the base line temperature, in many cases is far greater than the amount of the change due to emotional influences and therefore a reference point is needed before one can interpret the data sensibly.

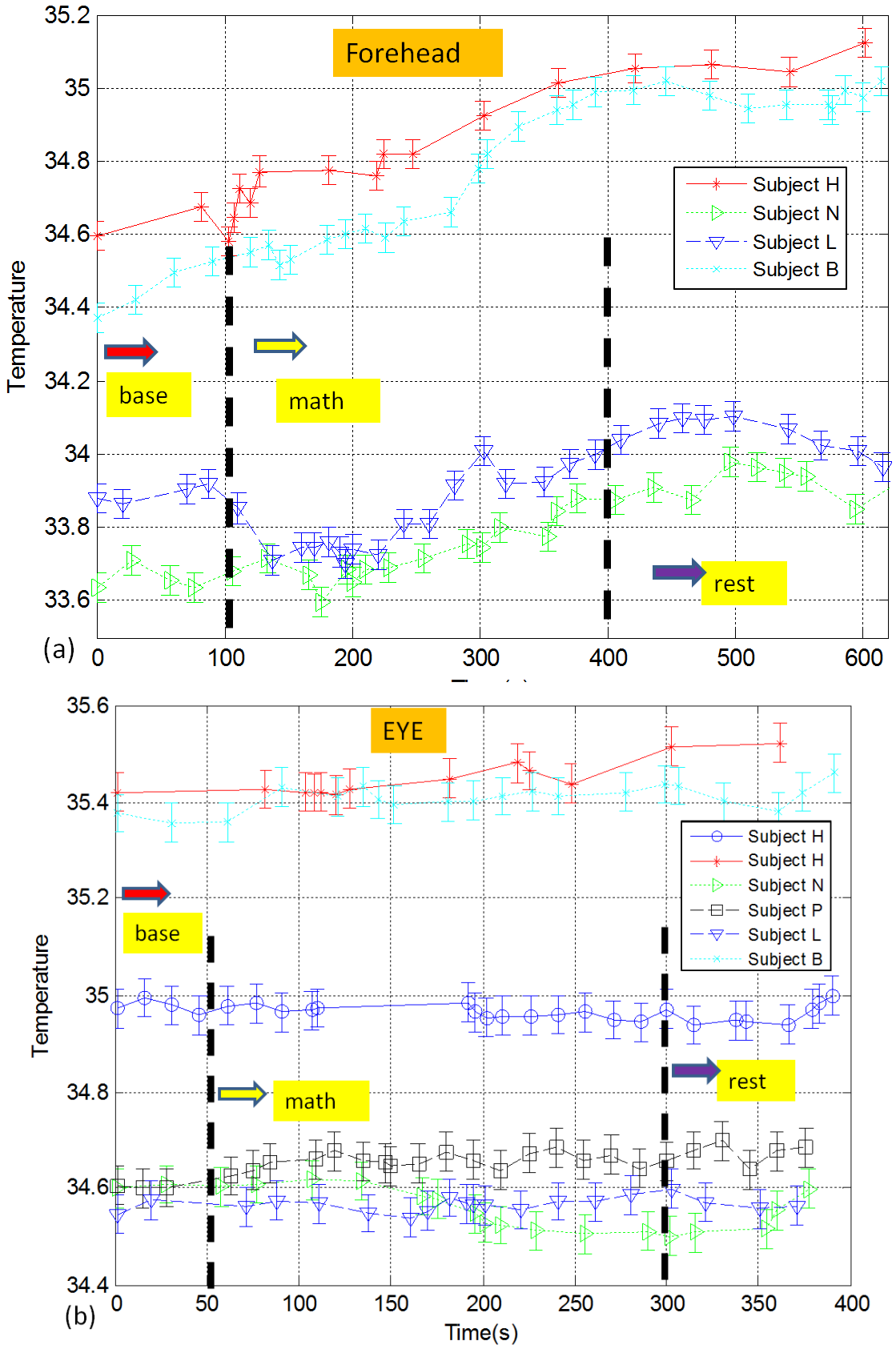

Figure 7-12. highlights the more stable of the temperatures in (a) the forehead and (b) eye regions for a selection of subjects during the ES session. Note that the base line temperatures of (a) & (b) are found closely correlated.

Figure 7-12 shows the fairly stable forehead and periorbital temperatures for a number of subjects during the ES session. Again the base line temperatures exhibit substantial spread like that of the nose and mouth as presented in Figure 7-11. It is observed from Figure 7-12 that the variation of the base line temperatures in the forehead is very similar to that of the periorbital: for example, subject H has the highest base line temperature within this group of people in his forehead and at the same time also in his periorbital. Thus one can choose either the forehead or the periorbital temperature as the reference point. In this work we opt to select the forehead temperature as the reference point due mainly to the ease to locate. Furthermore, the forehead is geometrically 'flatter' and therefore a bigger area of ROI can be selected so to minimise errors due to viewing angle dependent emission issues.

7.6.1 DFMT and DFNSO

After exhaustive data analysis we have developed two analytic techniques, one for the TI using differential temperatures of two selected ROIs in the facial region: the Forehead and the Mouth. This Differential Forehead Mouth Temperature (DFMT) has been tested for ~25 subjects and reasonable results have been obtained. Note that the DFMT works on a single frame of data without the need of base line information. DFNSO is the similar technique that has been developed for the HSI utilising the differential StO2 in two selected ROIs close to the Forehead and nose tip. Note that both the DFMT and DFNSO methods are designed for the elimination of artefacts due to external factors such as dietary, ambient temperatures, health conditions and activities (Yuen Peter, Hong Kan, Chen Tong, 2010).

It is hoped to calibrate the DFNSO and DFMT through some physiological properties such as the amount of cortisol or HBR. To achieve this we select four participants who experience various degrees of anxiety during the ES session as a test case. The details of their physiological properties together with the DFNSO and DFMT values are given in Table 7-6. A plot of their cortisol levels against their percentage ratio changes of HBR with respect to their HBR baseline (RHBR) is given in Figure 7-13. An attempt to plot between DFMT against the RHBR or cortisol level also results in failure.

Although there is no obvious relationship between the DFNSO/DFMT with respect to the cortisol level or HBR, however, it may be possible to 'classify' the anxiety level into 'high' and 'low' category according to their EO physiological feature values.

Strong Anxiety cases											
Subject	'Date'	Cortisol [Mental] pg/mL	Tth[C]	HBR [base]	Max HBR [mental]	(MaxHBR- Base HBR) /Base HBR	DFNSO [mental]	DFNSO [Physical]	DFNSO [base]	DFMT [Mental]C	DFMT [Base]C
A	'08/03/2010'	0.30	34.34	85.00	127.00	0.49	5.00	4.10	0.10	2.74	1.14
B	'04/03/2010'	0.83	34.50	75.00	112.00	0.49	3.50	2.20	1.20	2.08	2.11
C	'10/03/2010'	0.37	34.70	85.00	128.00	0.51	3.20	0.15	-2.00	1.75	0.50
D	'09/02/2010'	0.11	35.30	88.00	112.00	0.27	2.05	-1.00	-1.50	0.97	0.20

Table 7-6 Anxiety assessment data for 4 selected subjects (Yuen Peter, Hong Kan, Chen Tong, 2010).

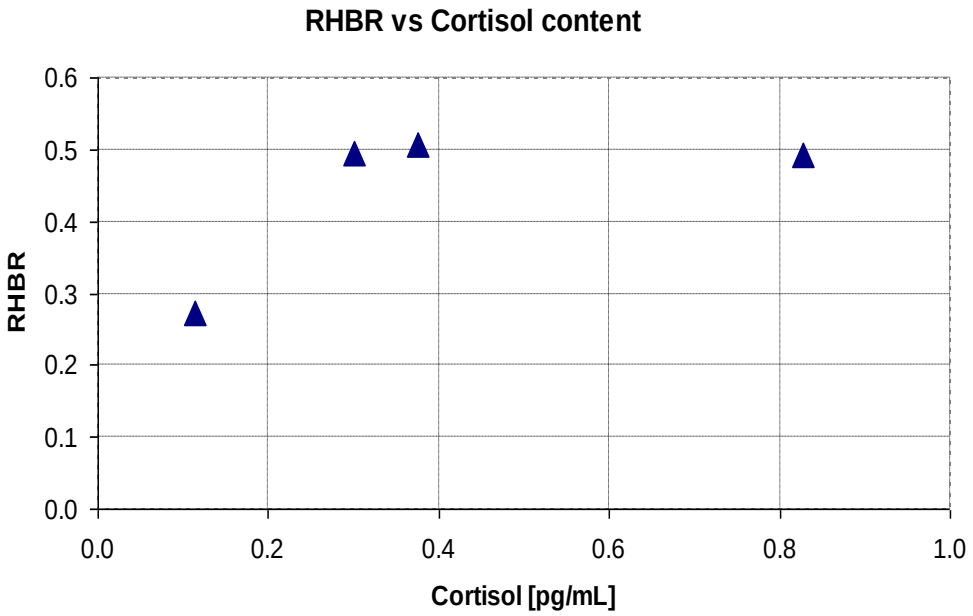

Figure 7-13. shows the ill-defined relationship between the physiological properties such as the change of the HBR with respected to the amount of the cortisol in the saliva for four participants who experience various degrees of anxiety during the ES session Correlations between DFMT & DFNSO.

It is intuitive to testify the validity of the two differential methods by using a number of data sets collected from various subjects of different backgrounds before and after performing a range of non-stressful activities. In all cases the participants remain claim and relax during the data collection, and their cortisol levels are measured via collection of their saliva samples in regular time intervals. The results processed by using the DFMT and DFNSO analytic techniques for these base line data sets, together with the gross-values of skin temperatures and StO2 measured during the experiment, are tabulated in Table 7-7.

Subject & conditions	Cortisol [Base] pg/mL	Mean Forehea	MaX Mouth	StO2 Forehead	StO2 Nose	DFMT	DFNSO
Sub P (Beer)		35.54	35.58	51.90	53.00	-0.04	-1.10
Peter base	0.13	33.45	33.04	46.00	46.50	0.41	-0.50
Sub A base AM	0.45	34.30	34.33	45.65	47.27	-0.03	-1.50
Sub A base PM before food		33.93	33.28	47.01	47.44	0.65	-0.50
Sub A base PM after food		34.26	34.38	45.96	47.33	-0.12	-1.40
Sub A base PM food+smoke		33.76	32.03	47.45	46.80	1.73	0.50
Sub T base before food	0.13	33.86	32.99	42.00	44.00	0.87	-2.00
Sub T base after food		34.30	34.19			0.11	
Sub I before food	0.09	33.99	32.35	40.80	40.00	1.64	0.80
Sub I after food		34.28	34.03			0.25	
Sub K before food	0.14	33.68	33.81			-0.13	
Sub K after food		34.47	34.96			-0.49	
Sub V	0.11	34.45	34.93	48.19	49.94	-0.48	-1.50
Sub M	0.14	34.09	34.25	53.86	51.54	-0.16	2.50
Sub S	0.13	34.49	34.87			-0.38	
Subject ML	0.12	33.46	32.10	48.98	48.92	1.36	0.40
Subject MB	0.18	33.59	34.37	51.85	49.14	-0.78	2.80
Subject R	0.08	34.39	33.73	47.50	46.80	0.66	0.70
Subject SM	0.10	34.12	32.16	46.40	46.00	1.96	0.40
Subject R	0.09	33.89	33.39	46.79	45.89	0.50	1.00
	Standard deviation	0.47	1.04	3.45	3.07	0.79	1.44

Table 7-7 Presents the base line data of several subjects and they are analysed by using the DFMT and the DFNSO method as a test bed. Scores of below 1.8 and 2.75 for the DFMT and DFNSO respectively imply the absence of anxiety. Yellow colour: Civilians subjects, green: military subjects, orange: high blood pressure subject, red: alcoholic test, pink: false alarm (Yuen Peter, Hong Kan, Chen Tong, 2010).

There are mixtures of civilian and military personnel ranging from 25-55 participating in this experiment, and they are all in good health except for one who has high blood pressure problem (coloured in orange in Table 7-7). Amongst them, there are male and female with various skin types (white, yellow and black) and of different professions.

As shown in Table 7-7 the standard deviations of the gross-data such as the StO2 at the Forehead and nose ROI are seen to be rather large (~3) in this experiment, but the DFNSO which exploits a simple differentiation technique manages to reduce this by over 50%. More importantly, this simple technique avoids the need to guess for a 'suitable' threshold value to fit for a situation during the anxiety detection process. Note that all the DFNSO values tabulated in Table 7-7 are quite small except for two 'outliners' data points (the pink data in Table 7-7) which belong to two rather nervous subjects. Obviously further effort is needed for a better understanding of the phenomena underlying the model.

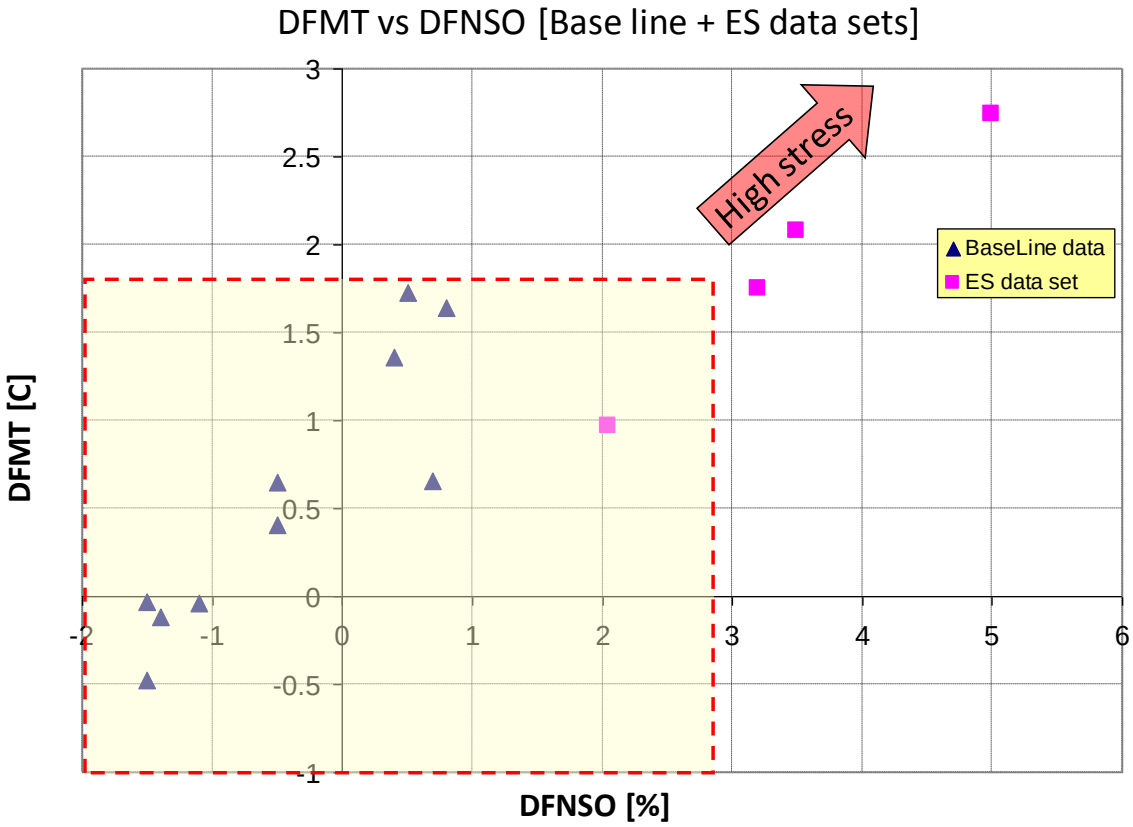

Figure 7-14. By using labelled data sets one can deduce the relationship between the EO quantities with respected to the level of anxiety. The figure plots the DFNSO & DFMT obtained from highly stressed subjects (see Table 7-6) together with those of the base line (see Table 7-7), and it results in a very well-defined two clusters representing two regimes of high and low anxiety. The boundary at the DFNSO of 2.75 which corresponds to the DFMT of 1.8 may then be used for anxiety classification into high and low categories (Yuen Peter, Hong Kan, Chen Tong, 2010).

7.6.2 Quantitative anxiety assessment using DFNSO and DFMT

It can be seen from the last section that although the exact location of the ROI and perhaps the correct way for the manipulation of EO quantities are still needed further refinement and optimisation, it is intuitive to explore if the EO quantity such as DFNSO/DFMT can be related to the anxiety level such that one can apply them for emotion assessment. This is one of the main objectives to achieve in this project. Despite of the unsuccessful attempt trying to correlate the measured physiological response of the EO quantity (DFNSO) with respected to the biological properties like the change of the heart beat rate (RHBR) that triggered by anxiety, it may be still possible to classify the DFNSO and the DFMT values to represent a high and low anxiety regime.

One method to achieve this is to analyse the data sets that belong to the highly stressed people, together with those of the base line data sets obtained from the subjects who are in their clam and relax states. In machine learning research this is termed as 'labelled' data. Through the cortisol assessment and the participant's questionnaire sheet, one can label the data into two groups of high and low anxiety sets. The data sets that presented earlier in Table 7-6 contains 3 subjects who are in acute anxiety during the ES session, and all of the data that presented in Table 7-7 are the bases line data sets. Thus a plot of the data using both Table 7-6 and Table 7-7 should exhibit a two regime plot with two clusters representing a high and low anxiety category.

This result is shown in Figure 7-14 which indeed exhibits a well-defined two cluster areas: the red squares in the plot belongs to the 3 highly stressed subjects, and the rest are those with low level of cortisol characteristic of having low anxiety. An extrapolation from these high anxiety data points is seen to coincide very nicely with the blue triangle base line data points, exhibiting an amazing consistency. The yellow box in the figure represents the boundary of the high and low anxiety clusters, suggesting that a DFNSO value of 2.75 which corresponds to the DFMT value of 1.8, can be used as threshold values for anxiety classification into a low and high regime in a semi-quantitative manner.

7.6.3 Anxiety detections using DFNSO & DFMT: an acid test

In the previous two sections it has been pointed out that while the principles of the differential technique that established from this work may represent a valuable tool for the remote sensing of emotion in a semi-quantitative manner; however the methodology in its present form needs further development and optimisation. Nevertheless it is still worthwhile to acid test the presently developed technique as the first result for future improvement.

Table 7-8 summarises the anxiety assessment results that have been performed at the time of writing the report. The result is colour coded, with green colour implying a positive positive detection and yellow implies a negative negative result. The level of anxiety is assessed through the level of the cortisol, and the heart beat change rate as well as through a direct consultation with the subject straight after the test.

Subjects	'Date'	Cortisol [Base] pg/mL	Cortisol [Mental] pg/mL	HBR [base]	Max HBR [mental]	(MaxHBR menta l- Base HBR) / Base HBR	DFNSO [mental]	DFNSO [base]	DFMT [Mental]C	DFMT [Base]C
1	'08/03/2010'	0.34	0.30	85.00	127.00	0.49	5.00	0.10	2.74	1.14
2	'10/02/2010'	0.18	0.38	70.00	100.00	0.43	4.80	2.80	1.45	-0.13
31	'02/03/2010'	0.12	0.11	70.00	86.00	0.23	4.28	3.78	3.66	2.93
24	'09/02/2010'	0.17	0.13	87.00	105.00	0.21	3.85		2.96	
3	'04/03/2010'	0.32	0.83	75.00	112.00	0.49	3.50	1.20	2.08	2.11
4	'10/03/2010'	0.13	0.37	85.00	128.00	0.51	3.20	-2.00	1.75	0.50
5	'04/03/2010'	0.14	0.19	66.00	93.00	0.41	3.20	2.50	1.62	0.29
20	'03/02/2010'	0.11	0.16	75.00	86.00	0.15	3.01	3.85	1.92	0.80
6	'03/02/2010'	0.08	0.12	72.00	100.00	0.39	3.00	0.70	1.17	0.15
16	'05/03/2010'	0.19	0.28	63.00	90.00	0.43	2.85	1.44	3.43	4.02
39	'09/03/2010'	0.05	0.06	95.00	98.00	0.03	2.79	1.09	2.35	2.84
7	'09/02/2010'	0.09	0.17	93.00	125.00	0.34	2.75	0.60	3.25	3.07
8	'09/03/2010'	0.45	0.62	86.00	120.00	0.40	2.70	-2.00	0.28	0.37
15	'04/03/2010'	0.40	0.31	90.00	122.00	0.36	2.39	1.51	1.58	1.28
19	'10/03/2010'	0.14	0.20	86.00	120.00	0.40	2.07	-1.00	1.82	0.60
9	'09/02/2010'	0.11	0.11	88.00	112.00	0.27	2.05	-1.50	0.97	-0.20
10	'09/03/2010'	0.10	0.09	91.00	99.00	0.09	1.70	0.40	1.9	2.47
14	'23/02/2010'	0.10	0.36				1.58	-1.37	2.69	2.84
11	'03/02/2010'	0.12	0.13	56.00	86.00	0.54	1.40	0.40	1.80	0.43
17	'25/02/2010'	0.16	0.25	75.00	103.00	0.37	1.31	-0.87	4.56	1.73
38	'24/02/2010'	0.06	0.06	70.00	93.00	0.33	1.14	-2.14	1.04	-0.10
33	'10/02/2010'	0.06	0.08	65.00	85.00	0.31	0.89	-0.33	2.62	1.19
29	'02/02/2010'	0.06	0.12	88.00	106.00	0.20	0.86	0.18	2.28	3.24
18	'09/02/2010'	0.34	0.23	90.00	109.00	0.21	0.30	0.10	2.39	4.16
26	'10/02/2010'	0.08	0.13	70.00	92.00	0.31	0.15	2.07	5.13	2.45
42	'10/02/2010'	0.05	0.05	82.00	102.00	0.24	-0.11	-2.80	2.21	1.16
21	'24/02/2010'	0.17	0.16	60.00	76.00	0.27	-0.20	-4.49	0.81	-0.16
25	'24/02/2010'	0.09	0.13	60.00	83.00	0.28	-0.35	-2.12	4.34	5.02
40	'05/03/2010'	0.13	0.06	73.00	81.00	0.11	-0.36	-1.77	2.75	1.64
27	'24/02/2010'	0.11	0.12	70.00	88.00	0.26	-0.72	-3.39	0.56	0.26
28	'05/03/2010'	0.11	0.12	90.00	127.00	0.41	-0.97	1.13	1.37	2.18
37	'03/02/2010'	0.09	0.06	64.00	79.00	0.23	-1.09	-3.58	1.95	1.09
12	'03/02/2010'	0.09	0.13	70.00	90.00	0.29	-1.20	1.00	1.29	0.23
13	'10/03/2010'	0.13	0.17	85.00	99.00	0.16	-2.20	-0.50	0.78	0.90
30	'05/03/2010'	0.11	0.11	88.00	91.00	0.03	-2.20	-2.23	1.34	2.03
32	'04/03/2010'	0.11	0.09	75.00	81.00	0.08	-2.25	-2.52	2.31	0.85
23	'03/02/2010'	0.16	0.14	77.00	103.00	0.34	-2.50	-2.35	0.35	0.73
36	'02/02/2010'	0.09	0.06	71.00	76.00	0.07	-2.75	-1.99	0.28	-0.32
22	'02/03/2010'	0.11	0.14	49.00	64.00	0.31	-3.04	-3.47	0.56	1.10
34	'10/02/2010'	0.08	0.07	67.00	77.00	0.15	-3.25	-3.37	0.29	-0.12
35	'10/03/2010'	0.05	0.06	94.00	128.00	0.36	no data			
41	'02/02/2010'	0.05	0.05	75.00	103.00	0.37	hair problem			
PP	NP	NN	NP	High cortisol		high blood pressure				

Table 7-8 Shows the anxiety assessment results without the base line information using the classification method that has been developed in this project. The anxiety is classified as **high** when the DFNSO and DFMT values are over 2.75 and 1.8 respectively; otherwise the anxiety status is classified as low or no anxiety. The result is colour coded, and the ground truth is based on the cortisol level together with a consultation with the subject. Green=positive positive, Yellow=negative negative, Pink=positive negative, red=negative positive, purple=high cortisol above 0.17mg/mL (Yuen Peter, Hong Kan, Chen Tong, 2010)

The DFNSO result has shown to be very promising giving apparently '1' false alarm out of 41 subjects, while the DFMT scores 15 false alarms which mainly due to the difficulty of extracting the desire ROI particularly when the subject is in motion.

7.6.4 The reliability of DFMT for assessing physiological property

If EO quantities like the DFMT and the DFNSO truly reflects the physiological properties then it is possible that they may correlate well to other physiological or biological functions, such as the heartbeat. Since the DFMT is based on the measurement of skin temperature at a rate of 50 frames/sec, it is of interest to study the dynamic change of the DFMT as a function of time. To achieve this the TI data is manually analysed frame by frame to obtain the measurement of skin temperatures at the two selected ROI, and typical results together with the heart beat plot for a subject is shown in Figure 7-15.

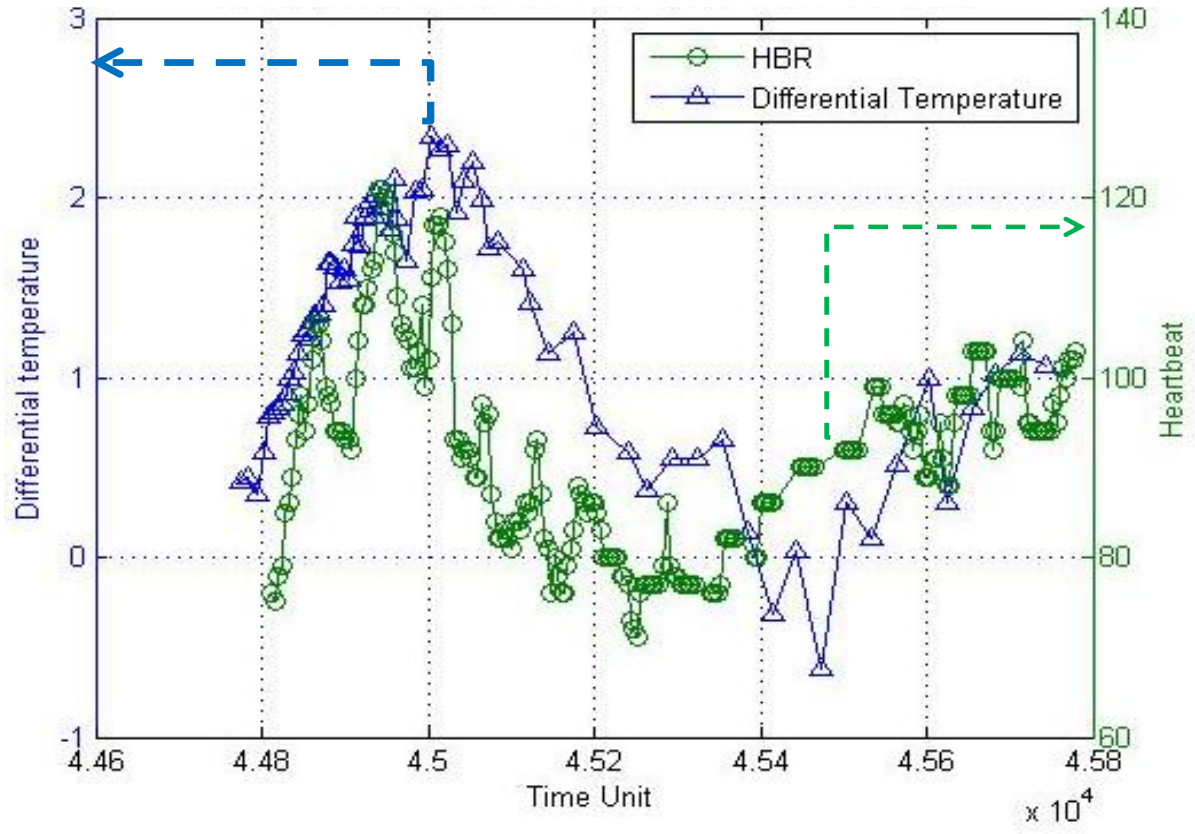

Figure 7-15. Showing how the DFMT can be correlated to physiological properties such as the heart beat rate. The figure presents the DFMT and the HBR of one subjects during the ES session, and it is seen that the DFMT follows the HBR with a small time lag as mentioned in previous sections.

7.7 Summary

This chapter concerns with the assessment of strong emotional state such as anxiety without the need of base line information. The study involves a detailed investigation and understanding of the EO features that can be extracted from the facial region. It is found that not all EO features response to emotions in the same way: some reacts

positively and some behave in a negative manner. The EO features from the forehead, periorbital region and face responses to strong emotions positively in terms of increasing blood perfusions into these parts of tissues. However, the nose and the lip (mouth) reduce blood perfusion upon anxiety.

The timing of the responses also vary from region to region: the blood perfusions into the periorbital region can persists for long time and in many cases over an hour after the anxiety sets in. The nose and the mouth part however response almost instantaneously.

By extracting EO features from different parts of the facial region, it is feasible to arrive at some quantity which can be related to the physiological property or functionality. In this study we have derived a methodology for cancelling out artefacts due to environmental, ambient and health influences to the integrity of the EO features. The method has been tested using a sample size of about 40 subjects, and the accuracy for the detection of anxiety is about 99% and 80% by using the HSI and TI based techniques respectively. The highly successful rate stems from the fact that the manipulated EO quantity agrees with the physiological heart beat data very closely.

8 Classification of emotions using EO imaging technique

8.1 Introduction

Roger Sperry initiated the research of the relationship between brain's left side and right side (Roger Sperry, 1980). He demonstrated that left half brain is used to process information through analytical, logical, rational, sequential method. However, the right half of the brain tends to understand outside information by recognising relationships, integration and synthesis of information, and also for arriving at intuitive insights. His study then further explained how the right and left side of brain is used in our daily life. His theory postulates that the left brain mainly deals with information that requires rational thinking and logical analysis. However, the right side of the brain mainly to processe the same information with intuitive insights and perceptions. Because of this fundamental difference the left side brain tends to split information into small pieces for further analysis, while the right half of the brain is able to digest all the information as a whole.

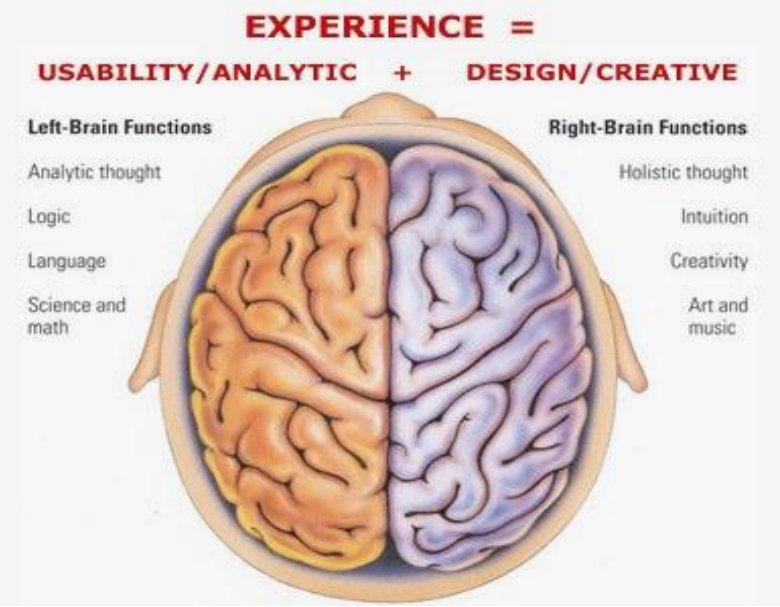

Figure 8-1 outline the functionality of right and left brain according to Sperry's theory. (Sperry, 1980)

Further Research into the brain's function was enhanced by Ned Hermann (Ned Hermann, 1996), the former manager of management education at General Electric's Management Development Institute. He developed an instrument for assessing the usage of brain at brain-dominance profile. He then concluded that people tend to be a half brain oriented dependent on their occupation. For instance,

CEO may use their left brain a lot more than their right side brain, as they have to be particularly organized and systematic. But social workers tend to be right-brain oriented, simply because of the fact that they need to concentrate on the insights about situations.

Humans transform visual targets into action order through the visual--motor integration. In order to under this process, Patrick Bedard assessed the brain activation, together with gaze orientation, using functional magnetic resonance imaging (Patrick Bedard, 2010). He found fixated gaze to left or right side from centre is a sign of goal-directed movements for visible or remembered targets. He then further demonstrated the strong effects of gaze orientation on brain activation during planning, and the interactive effects of target visibility.

The new evidence for distinct right and left brain systems, base on deductive versus probabilistic reasoning, has been exploited by Lawrence M. Parsons (Lawrence M. Parsons, 2001). These two definitions are poorly understood if placed in the context of cognition for functional neuroanatomy underlying them. He further illustrated that deduction gives a simulation on the area of right brain homologues, inferior frontal cortex and basal ganglia, as well as right amygdale. By contrast, probabilistic reasoning tends to activate left hemispheric areas. Deduction and induction are then further classified as two distinct processes, because of the fact that probabilistic reasoning mostly associate with left brain movement whereas right brain is often activated by deductive reasoning.

The purpose of this chapter is to investigate different natures of stressful tasks whether they can be classified using the EO imaging data?

8.2 Experimental procedure

The procedures of this experiment are as follows:

A. The participant is asked to wear a heart rate monitor before the experiment, and then the subject is led to a good lighting conditions room for a short time relaxation.

B. The subject is requested to stay still as much as possible during the experiment. A set of baseline images are taken after the subject accommodates the new environment.
C. The participant is then asked to do mental mathematics for few minutes, allowing the heart rate increase significantly.
D. The participant is requested to take a break and let the heart rate back to the baseline level.
E. Shortly, the participant is then asked to perform recognition-memory task for few minutes, allowing the participant get stressed and heart rate increase significantly again.
F. Following the recognition-memory task and rest, participant is asked to play a game for a few minutes.
G. Finally, the participant is requested to take a break and let himself back to baseline.

8.3 Results and discussion

TI images have been utilised throughout this experiment due to the higher quality of the data. Figure 8-2 outlines the locations of the four ROIs on the forehead of a subject, and together with the typical skin temperatures of these ROI as measured by the TI is shown. Note that there is indeed some temperature differences across these ROIs, and the differences are seen to be very dependent on the specific tasks.

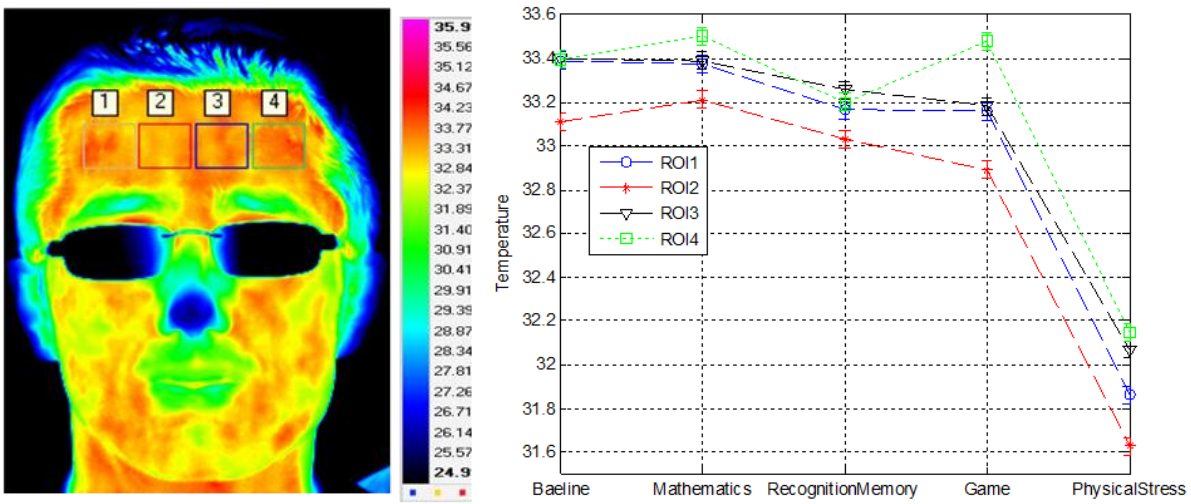

Figure 8-2 (Left) Shows the false colour TI image of a subject and the assignment of the ROI on his forehead. (right) typical skin temperatures of the 4 ROIs while they are performing different natures of tasks.

Figure 8-3 plots the differential temperature between ROI1 and ROI4 for the four different task. It is seen that the differential temperature between the left and right forehead seems to be very small when all the participants are performing the recognition/memory task. This observation appears to be much clearer when the data is plotted against the HBR, as it is shown in Figure 8-4. The almost equal blood perfusions in both left and right forehead may suggest an equal use of the left and right brain when the pattern recognition task is performed.

The maths data cluster is found at the centre of Figure 8-4, which suggests that both sides of the brain may have been used for performing the mental mathematics task.

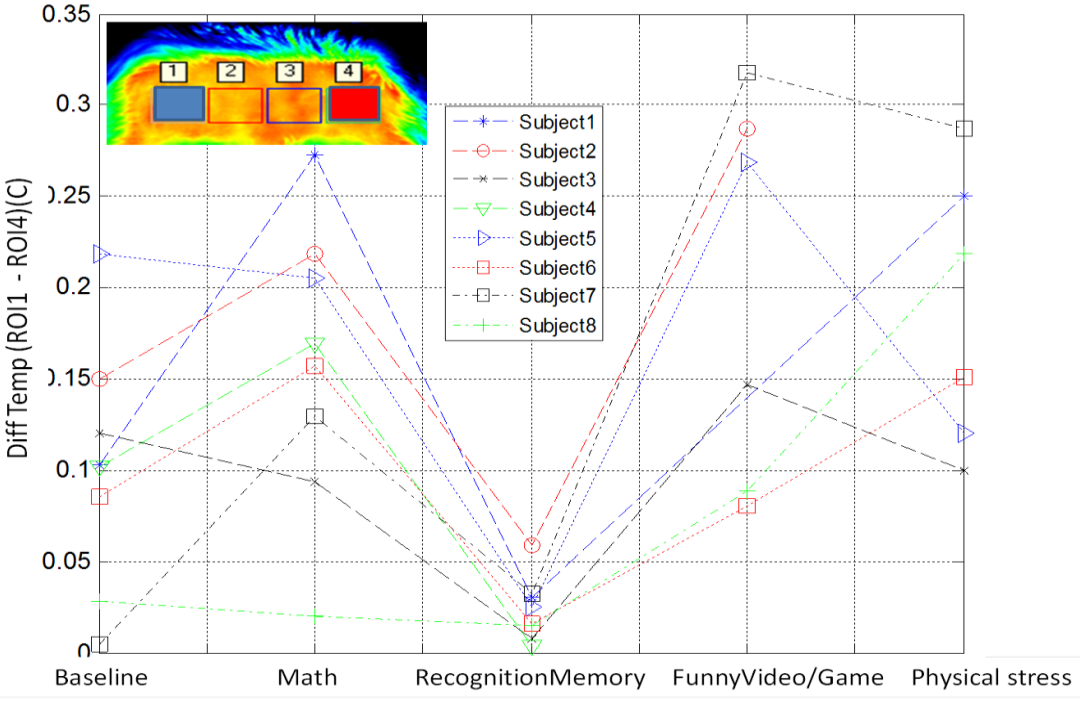

Figure 8-3 shows the differential temperatures between the left (ROI 4) and the right (ROI 1) for a number of subjects after they performed 4 different kinds of tasks. Note that the temperature difference seems to be very small for the recognition task.

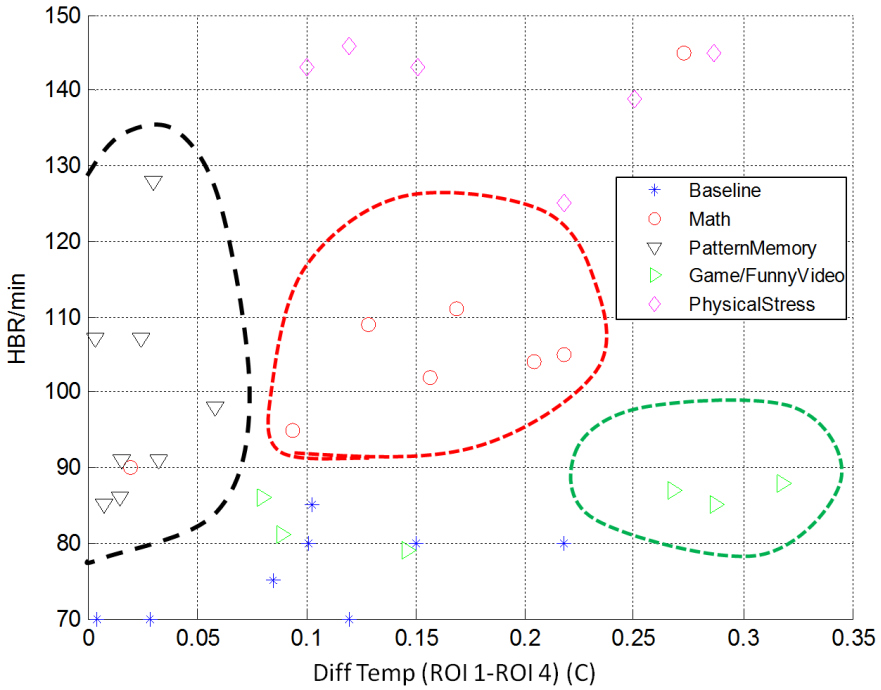

Figure 8-4 plots the differential temperatures between ROI1 and ROI4 against the HBR. The data due to the recognition/memory task seems to be well clustered (in black) with clear boundary well separated from the mental maths task (in red).

8.4 Summary

Previous medical research has demonstrated the correlation of left brain and right brain. It has also been suggested that this relation can be classify through the usage of brain. The purpose of this chapter is to investigate different natures of stressful tasks whether they can be classified. The idea has been based on the fact that skin temperature is heavily modulated by superficial blood flow. Furthermore, the superficial blood flow is greatly affected by brain activity. Two different types of anxiety inducing experiments are established: mental math and pattern recognition experiment. The equal blood perfusion data extracted from facial TI data suggest an equal use of the left and right brain when the pattern recognition task is performed.

9 Conclusions and future work

Emotional anxiety can be defined as a temporarily-induced physiological or psychological imbalance that is caused by any action/ situation which an individual regards as a possible danger or threat. A physical emotional stress is one that has a direct effect on the body. This may be the reaction to an external environmental or the physiological request of the human body to cope with the stimulant. Mental emotional stress can be a situation when information is passed into the brain without direct physical effect on the human body. It is well-known that both emotional and physical stressors will induce a surge of adrenaline in the blood stream under the command of the sympathetic nerve system. The response is involuntary which means that it cannot be suppressed by training. The onset of this alleviated level of adrenaline triggers a number of physiological chain reactions in the body, such as the dilation of pupil and an increased feed of blood to muscles etc.

One area of the present work has been the understanding of how the EO characteristics of physiological responses that triggered by these two different kinds of emotional stressors can be assessed and/or classified. In 2008 we were the first group within UK to initiate a programme for assessing people's intent through one's physiological or neurological states, for example via the detection of people's anxiety.

Previous work performed by Pavlidis group has claimed an 'instantaneous' increase of temperature in the periorbital region when anxiety sets in, but this claim cannot be validated according to our data. We have performed a detailed investigation about the anomaly temperature in the periorbital region using TI and HSI techniques in this study. We have found that, the mean temperature in the periorbital region is hardly increased during the anxiety state. However, the number of pixels in the lower quartile of the mean temperature, is seen to increase in the periorbital region after 2 minutes of the onset of anxiety. The evolution of the hot pixels in the periorbital region during anxiety is seen to occur in the form of a pyramid, with high temperature pixels located at the tip (centre) of the pyramid structure. The number of hot pixels within the periorbital region can be increased by ~10-fold in comparison to that of the

base line. The hot pixels in the periorbital can persist for long time, and in many cases it can sustain for 30 minutes and even longer!

We have observed the following EO characteristics from the facial region during emotional anxiety:

1. The temperature in the periorbital region is quite stable within 0.5%.
2. The number of hot pixels in the periorbital region begins to increase after a time lag of about 2 minutes upon the onset of anxiety. The hot pixel can keep increasing in numbers for 30-60 minutes after the triggering of anxiety, and the total hot pixels can be increased up to about 10 times of the base line level. This is one of the most undesirable memory effects to the remote sensing of emotions.
3. The forehead increases its temperature after a time lag of about 1-2 minutes upon the onset of anxiety. The amount of temperature increase is in the region of about 1%.
4. The temperatures in the nose and lip (mouth) regions are found very responsive to the anxiety induced change of HBR. The responses are found fairly instantaneous, and they start to drop in temperature as soon as the HBR begins to surge. The amount of the temperature drop is in the range of ~5-9%.
5. There is no direct correspondence between the change of the HBR and the change of temperatures in the facial region.
6. Environmental and variable base lines due to different physiques of individuals impose ~5-10% variations on the temperatures and StO2 in the facial region.

We have also developed techniques to allow the assessment of strong emotional state such as anxiety without the need of base line information. The study involves a detailed understanding of the EO features that can be extracted from the facial region. It is found that NOT all EO features response to emotions in the same way: some reacts positively and some behave in a negative manner. The EO features from the forehead, periorbital region and face responses to strong emotions positively in terms of increasing blood perfusions into these parts of tissues. However, the nose and the lip (mouth) reduce blood perfusion upon anxiety.

The timings of the responses also vary from region to region: the blood perfusions into the periorbital region can persists for long time and in many cases over an hour after the anxiety sets in. The nose and the mouth part however response almost instantaneously.

By extracting EO features from different parts of the facial region, it is feasible to arrive at some quantity which can be related to the intrinsic physiological property or functionality. In this study we have derived a methodology for cancelling out artefacts due to environmental, ambient and health influences to the integrity of the EO features. The method has been tested using a sample size of about 40 subjects, and achieved promising result. The highly successful rate stems from the fact that the manipulated EO quantity agrees with the physiological heart beat data very closely.

During the course of this study, we have also developed a technique that allows the detection of HBR directly using TI data. The technique involves the monitoring of the frequency change of the skin temperature signal and it is then converted into time signal. Furthermore, we have also attempted for the first time to sense glucose concentration from the blood sample in-vivo remotely using HSI technique.

We have obtained some encouraging results and further works are needed for more understanding of the remote sensing of strong emotions technology. The study of glucose detection method by using hyperspectral imaging system needs further investigation as it is speculated that the water absorption may dominate and obscure the interpretation. Further analysis particularly the robustness for the local differential methodology for assessing emotions using EO data is needed. In particular the evolutions of blood perfusions in various parts of the facial regions needs to be monitored for much longer time than the ~30 minutes duration as it was performed in this study. There is a number of affective sensing research being taken place world-widely, unfortunately none of it addresses the assessment of the instantaneous emotions and all the reported results is in fact due to the after-maths of having strong emotions such as anxiety which has happened quite a while ago. New methodology, such as the one that proposed in this thesis, may suggest an alternative new direction to realise the assessment of human’s emotions in real time.

10 Appendix I

10.1 Software design: VNIR, SWIR & AOTF MSI systems

All camera control software undertaken by the author has been developed on the VS.NET platform and all the basic camera functions, such as spectral and spatial binning, mirror controls and image acquisitions, have been established and subsequently implemented in the very first version 1.0 of the package for both the VNIR and SWIR cameras. Typical GUI for the two cameras are shown in figure 10-1. The MSI control software has been written in Visual basic due to historical reasons, and data can be captured at the camera speed without any time wasted for data storage etc. Figure 10-2 shows the GUI of the MSI and samples of typical images taken by the three spectral cameras are outlined in figure 10-3.

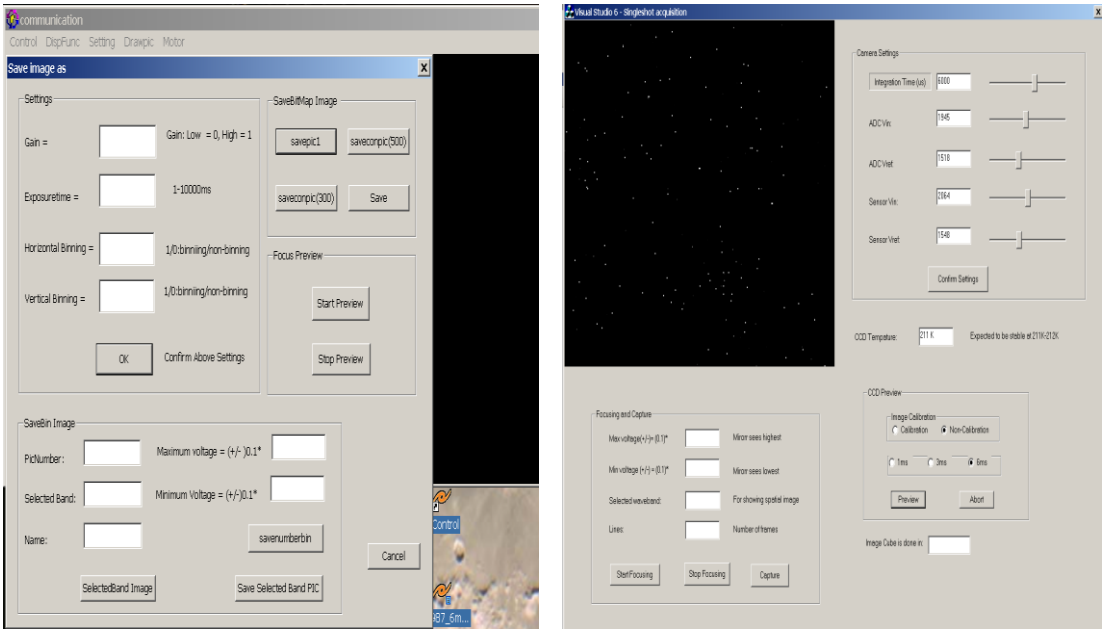

(a) (b)

Figure 10-1: shows the set up menu of the HSI control software designed and developed by the author: (a) VNIR HSI camera. (b) SWIR HSI.

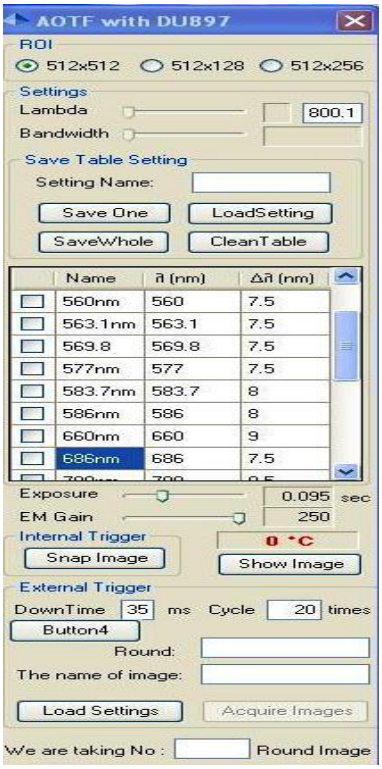

Figure 10-2:shows the setup menu for the control of the AOTF MSI system that has been developed by the author.

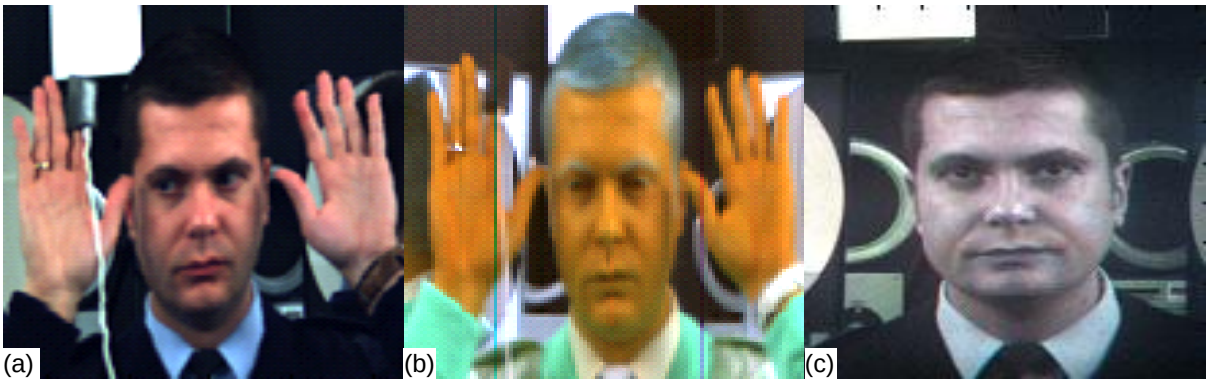

Figure 10-3:Shows the typical 'composite' images collected by the three spectral cameras (a) VNIR HSI (b) SWIR HSI (C) AOTF MSI using the acquisition software established by the author.

10.1.1 Software configuration

The software for controlling the systems are developed by the Kan Hong using C++ based on the Software Development Kit (SDK) of the hardware. The VNIR, SWIR and MSI AOTF camera systems software are designed through the Vc++.net and Vb.net platform. The SDK are provided by camera system, which are shown at figure 10-4 and 10-5 and can be further developed in practical application.

Programs / Digital Camera ToolBox / PixelFly SDK	
pccam.h	SDK-function definitions
pccamdef.h	SDK defines and macros
pccam.lib	Library File for Microsoft Visual++ Compiler 6.0
Pccam.dll	DLL with SDK calls for PixelFly
Readme.txt	Readme file with additional information

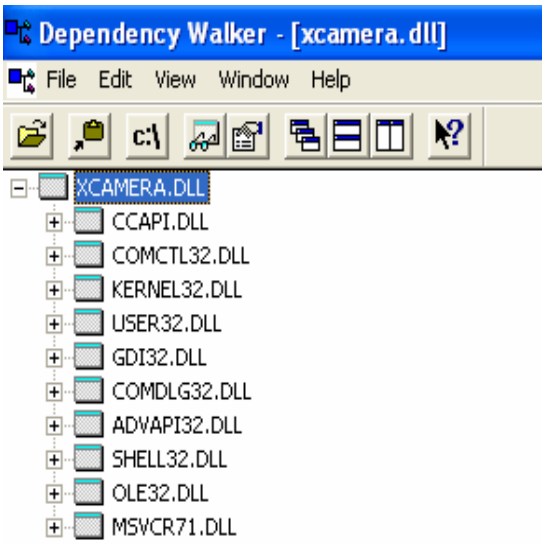

Figure 10-4: gives the SDK layout of VNIR and SWIR

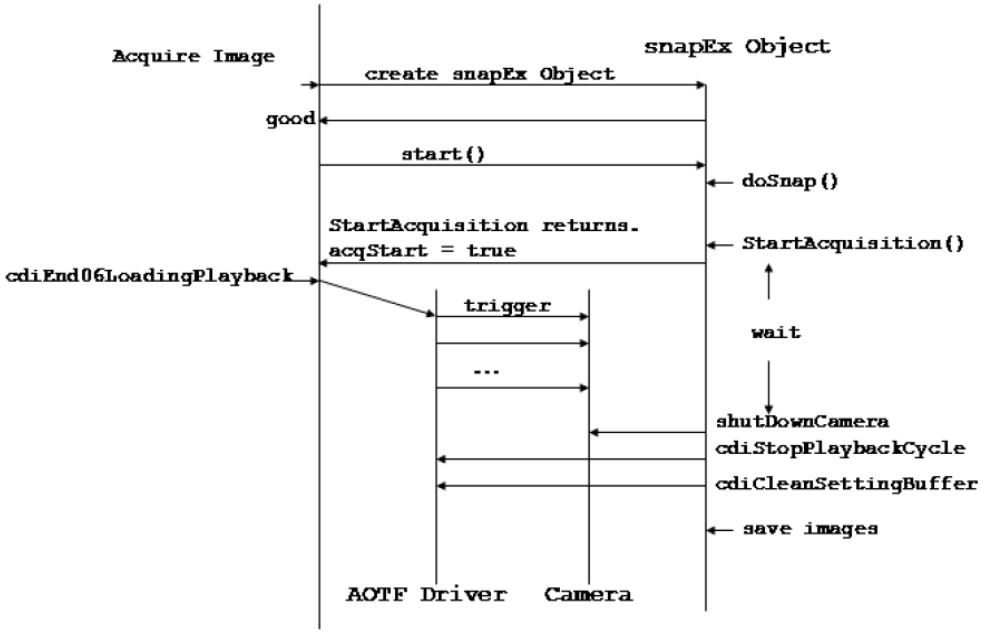

Figure 10-5: highlights the flow chart of MSI SDK

In this section, the configuration of SWIR and VNIR software will be presented in details. Multi-threading platform and the improvement of frame rate will be given as well.

10.1.2 The configuration of SWIR and VNIR

Unlike the MSI system, two identical optical scanners are employed to acquire 3D hyper-spectral image cube in SWIR and VNIR. Each scanner, including a motor and a mirror, can capture the light from different spatial positions where only one frame data can be acquired. Therefore, the software must be built up in conjunction with

the framework of motor. The configuration of SWIR and VNIR are similar with each other, as the fundamental working procedure is almost the same. The figure 10-6 shows the configuration of SWIR and VNIR.

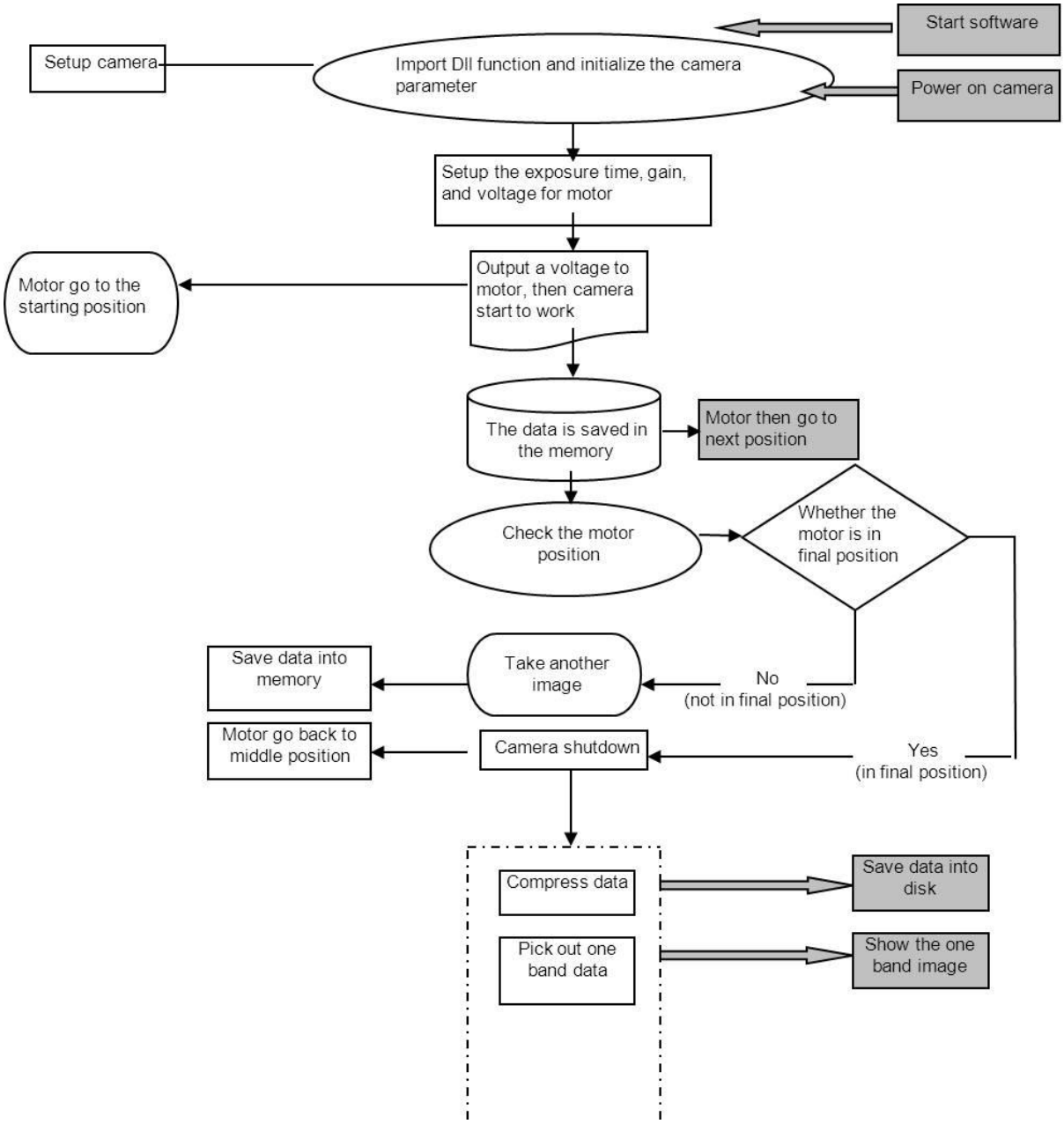

Figure 10-6highlights the flow chart of VNIR and SWIR

10.1.3 Multi-threading configuration for AOTF MSI system

A thread is a type of context where code is running. It will not affect the process with whatever code is in the thread. All the thread in the context must follow the program flow. Within the operating system, there is only one thread running for each process before the invention of multi-threading technology. Multi-threading can works in a

real-time sense when multi-processor box have more than one processor. The multi-thread may still “available” when the context runs like a substitute sequence: 20%code for thread A, then 20% code for thread B, then back to thread A for another 20% code etc. Actually, this is not the real multi-thread process. But it still works in an inefficient situation. Nevertheless, if both threads are “compute bound” then multi-threading will not speed up the program at all but push the operating system switching resource between two threads.

Once the start method is invoked, the thread is available but may not actually be running as it requires the operating system to give the thread time to run. In fact, it would be desirable if running threads can occasionally pause to make other threads valid. All the thread scheduling is dependent on the operating system. Each runnable thread will be given a slice of time to implement its process through the preemptive scheduling systems. Once the time slices are finished, the sleeping thread will be activated. All the operating systems rely on this structure.

Therefore, multi-processor machine could enable each processor run a thread and, then multiple threads can run in parallel. However, if the processor is less than thread, the scheduler has to perform time-slicing, which driver the thread from one state to another state. The following figure shows the possible states that a thread can have. Whenever a thread is blocked, another sleeping thread can be activated. Whenever a blocked thread is worked, the scheduler will check whether this thread is the most significant thread. If not, the operating system preempts the current thread and activates a new thread to run. Figure 10-7 gives the possible states of thread that OS may give.

In the view of this, all the softwares for our hyperspectral imaging system are built up in this configuration. There are two computers running the SWIR, VNIR and MSI systems. The running computers in the project all have dual core processor. Therefore each computer can run 2 threads in parallel. It is applicable to run SWIR and VNIR in one software but, the programme needs further development due to some historic reasons. This chapter uses MSI system as an example to show how multi-thread works in the software and how this configuration improves the acquisition speed.

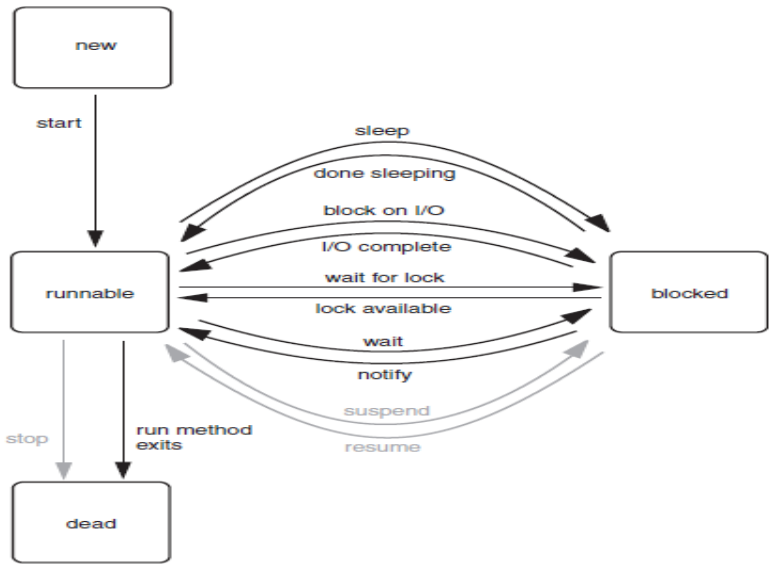

Figure 10-7: exhibits the possible states of thread that operating system may give

As one of the most fast hyper-spectral imaging system, MSI system requires more robust software to support its near-real time speed. The exposure time and transmission speed has been fixed by the operator and hardware. Therefore, it is significant to arrange acquisition and transmission thread. The following figure shows the general procedure of probing image by using single thread software.

Figure 10-8: shows the single thread software procedure

According to the above image, the single thread procedure requires the data storage after the image acquisition. This procedure may waste many times in the data storage. Therefore, multi-threading is employed in this software. The following figure gives the flowchart for multi-threading configuration of our MSI system, which specifies the two multi-threads for acquisition and data storage, respectively.

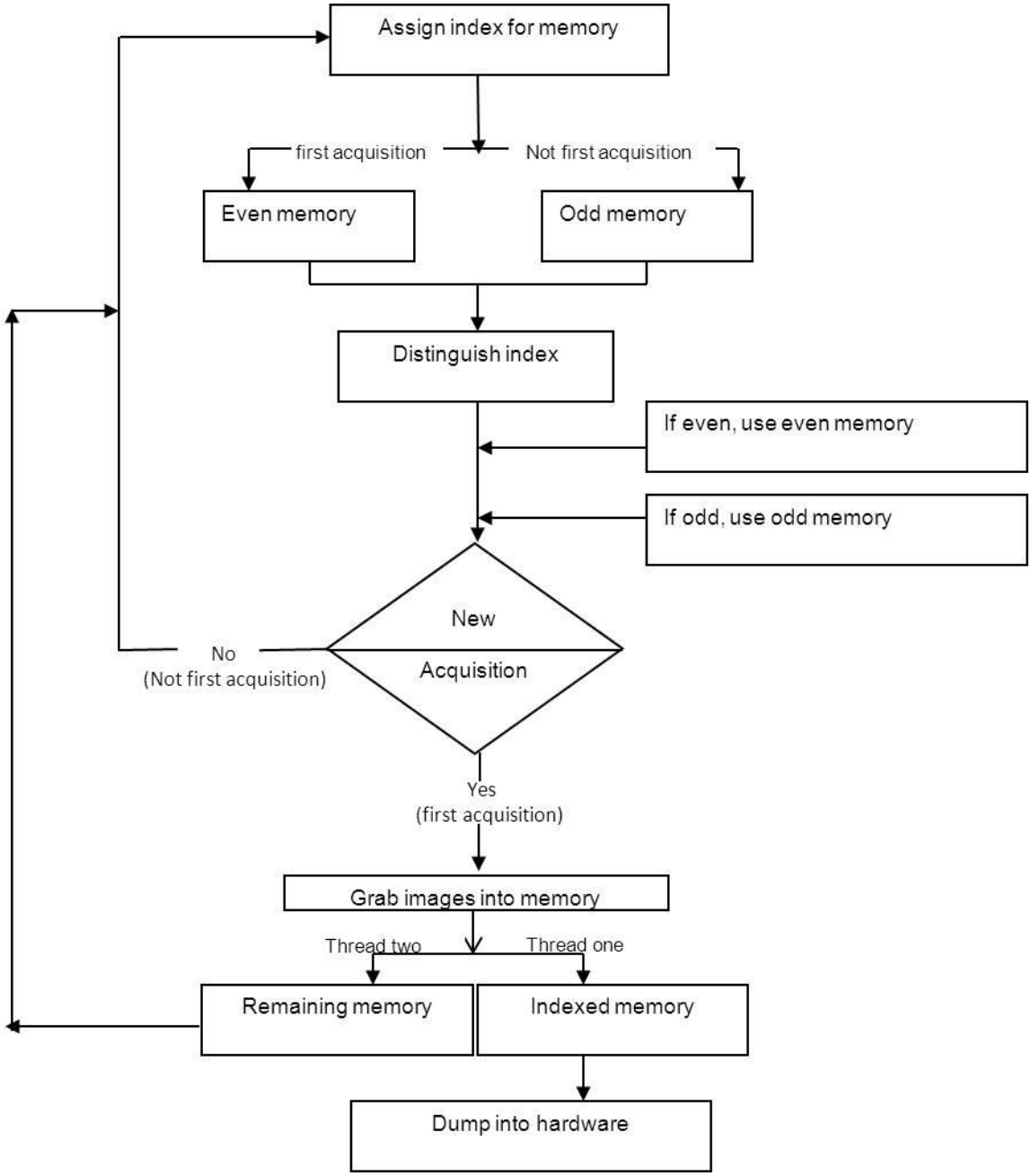

Figure 10-9: gives the flowchart of multi-threading configuration of MSI imaging system

10.2 Angular variation of thermal emissivity

As described in the previous section that the emissivity of a material is a function of the angular emission, wavelength and temperature. For example the emissivity of water varies considerably from band to band, and at wavelength of 10 um it is a perfect blackbody while it becomes a mirror at 'low' angle of emission (ieφ~90).

Substantial interests in the field of biomedical area have been drawing on the human skin energy absorption and reflection. In the thermal radiation range, the angular

emission and its emissivity can introduce bias to determine the temperature of the skin. Therefore, it's necessary to understand how its angular emissivity works.

The participant with mask ROI is sit in front of the camera comfortably. Throughout the experiment the participant is asked to avoid substantial body movement and to sit down calmly as much as possible. Then a rest time of about 5 minutes is given to allow the subject to settle in the new environment and subsequently the skin temperature information as functions of the angular emission is taken. In order to locate the angle properly, the mat with calculated angle curve was placed in front of participant. Specifically, the participant rotates the head according to the angle marked on the mat, and the temperature was measured simultaneously from both Lwave and Mwave camera.The schematic diagram of the experiment is shown in the following figures.

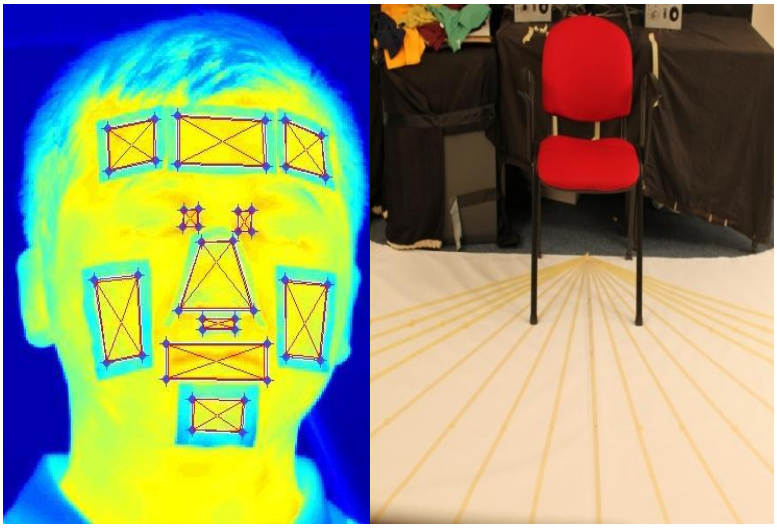

(a) (b)

Figure 10-10 Shows the sample thermal image of participant and the experimental setup of angle measurement.

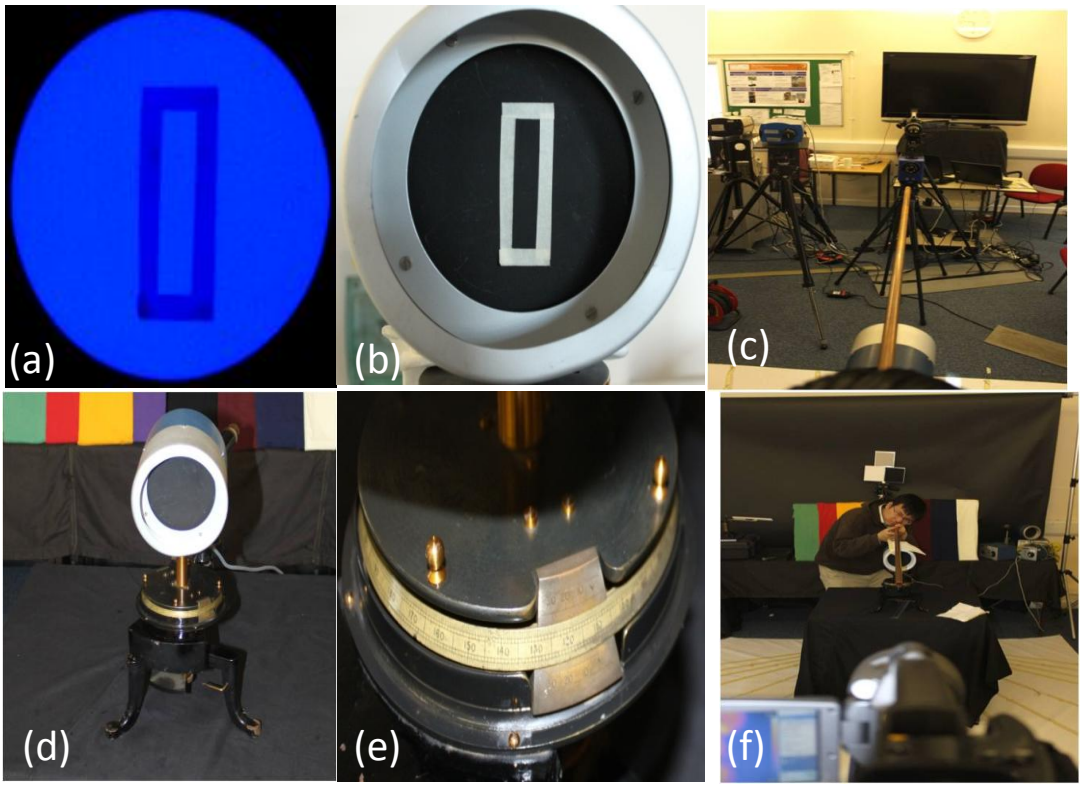

Figure 10-11: Shows the sample thermal image of black body and the experimental setup for the black body temp measurement.

Similar to the human skin temperature measurement, the black body temperature is captured by using both Lwave and Mwave simultaneously. The black body is placed at a rotation platform with accurate angle meter. The cameras are then capture sequentially images after the black body is rotate to the target angle from 0 to 40 degree (in steps of 10 degree).The mask is used to accurately locate the ROI from the thermal image.

10.3 Result analysis and discussion

The effect of angular dependence in the emissivity can be seen in the aforementioned experiment which measures the 'apparent' temperature of a subject's forehead as functions of emission angle. Shown in figure 10-12 is the temperature measurement by using a TI with a 'fixed' emissivity (skin: 0.98 & blackbody: 1) as functions of the angular emission. The result of this temperature measurement is also shown in figure 10-13. Linear regression analysis was performed on the temperature data in both blackbody and human forehead region to produce a proper relationship with viewing angle. The differences in the Lwave and

Mwave regression analysis were characterized empirically, and least squares were also employed to study linear regression.

10.3.1 The relationship between angle and temperature

The black body and human forehead temperature (Mwave) appearing in figure 3-4 correspond to the temperature value investigated in the different viewing angle. For Y axis, the value of cosine at various degree of angle was plotted on a linear scale to allow simultaneous viewing of the relationship between angle and temperature. The least-squares regression lines were also overlaid together with real data value (blue star on the figure).

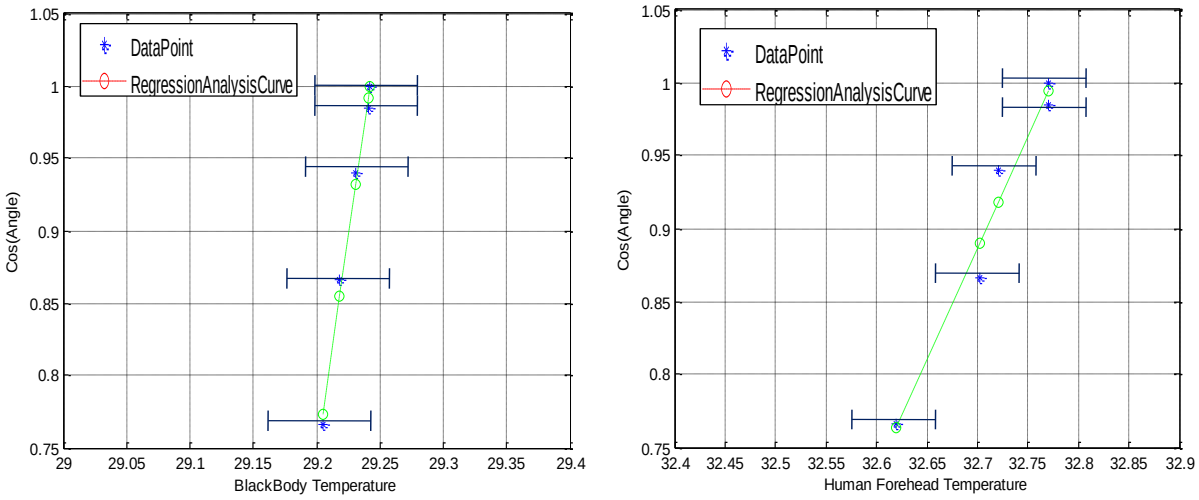

Figure 10-12: Shows the least-squares regression line for blackbody and human forehead temperature (Mwave) and the value of cosine angle.The blue star illustrates the real temperature value against the cosine value of angle.

To better quantify the relationship between viewing angle and temperature, the least-squares regression line for blackbody and human forehead are given and it appears that higher R^2 value could be observed for both two equations. This means regression line is a good fit for the points.

Unlike the temperature value presented in the above graph, figure 3-5 gives the regression analysis of temperature change percentage and the value of cosine angle data. This result demonstrates that a similar interpretation of the regression analysis infrared information.

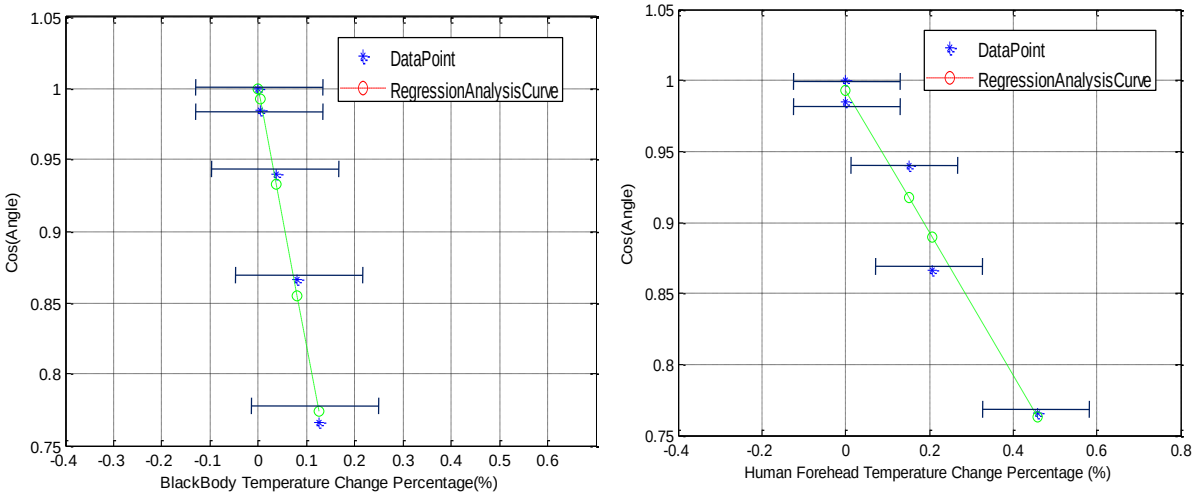

Figure 10-13: illustrates the least-squares regression line for blackbody and human forehead temperature change percentage (Mwave) and the value of cosine angle. The blue star shows the real temperature change percentage value against the cosine value of angle.

In order to further understand the source of the discrepancy between the measured data (fig. 10-13), another set of data which was recorded at the same time but using a LWIR (FLIR SC640) TI is analysed (see figure 3-6).The linear regression model was also used to calculate relationship from the viewing angle and temperature data captured from the Lwave thermal imaging system. The as-measured temperature as function of emission angle given by the LWIR TI is shown in figure 10-14 10-15, which shows remarkably the same trend as that depicted in figure 10-13. Again, this data set also exhibits a linear relationship between cosine angle and temperature, and it is consistent with the MWIR data but in contradict to the slop of the least-squares regression line. Although this data set is recorded using an integrated 7-14um wavelength, however it shows the same trend as that of the MWIR result, suggesting that the emissivity difference between black body and human skin needs further investigation.

Within the field of optics, Lambert's cosine law describes the radiant intensity captured from a Lambertian radiator (or surface) is proportional to the value of cosine angle between the surface normal and viewing line. Although the Lambertian radiator is not an incident energy-dependent emitter, its emission depends upon the radiation originating in the emitting body itself. A black body is an example of a Lambertian radiator. Again, our TI data prove that skin is also a near Lambertian radiator.

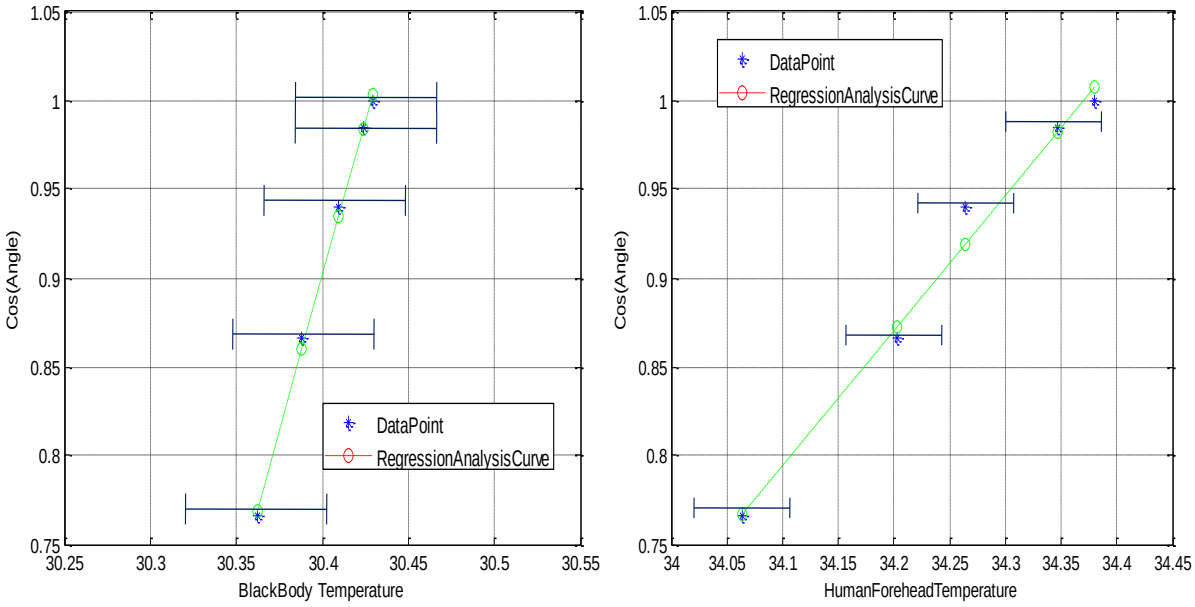

Figure 10-14: Shows the least-squares regression line for blackbody and human forehead temperature (Lwave) and the value of cosine angle. The blue star illustrates the real temperature value against the cosine value of angle.

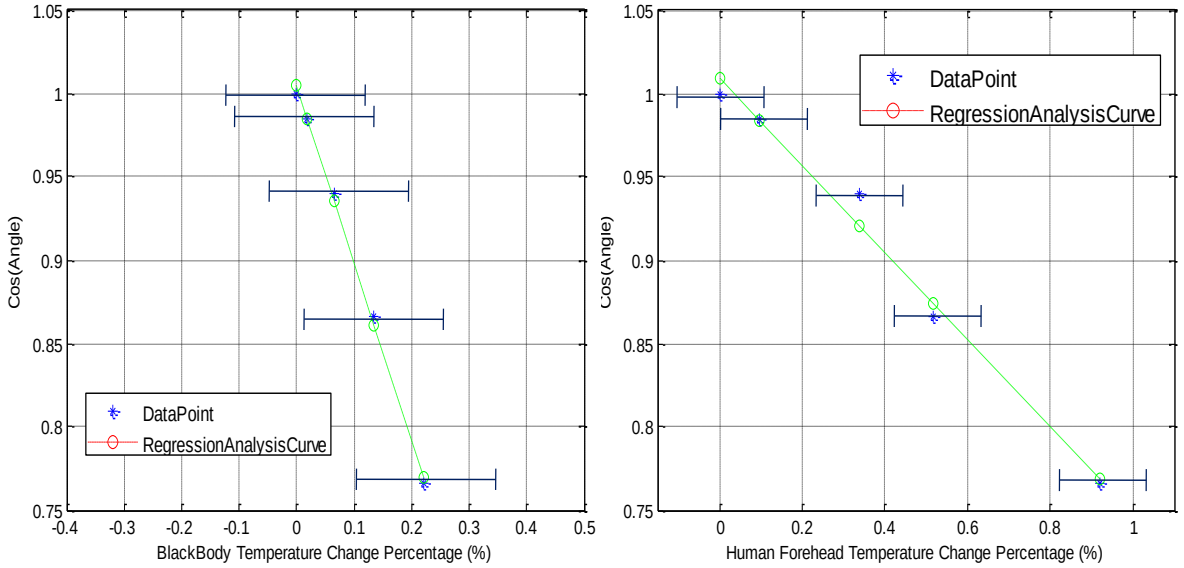

Figure 10-15: illustrates the least-squares regression line for blackbody and human forehead temperature change percentage (Lwave) and the value of cosine angle. The blue star shows the real temperature change percentage value against the cosine value of angle.

10.4 The correlation between long wave & middle wave thermal data

Thermal imagers have been established as the primary tool used in military and securityactivities that involve surveillance, targeting and tracking, and night-time operations. Unlikeimage intensification (I2) devices, which depend on ambient light levels, thermal imagers exploitthe fact that all objects with a temperature above 0 K emit thermal radiation by creating apseudo-image of the scene based on this thermal emission. The two thermal imaging windowsare the mid-wave IR (MidIR), 3–5 µm, and the long-wave IR (LWIR), 8–14 µm, both chosen forthe relatively low amounts of absorption from atmospheric species, such as carbon dioxide (CO_2)and water (H_2O).

Contrast between the objects within a thermal image is determined by their temperatures, which also reflect a characteristic that describes how efficiently an object radiates absorbed energy as compared to a blackbody.

In order to understand the difference between long wave and middle wave data, the temperature of blackbody is set from 26 to 45 and measured by both long wave and middle wave camera. Figure 10-16 illustrates the result and linear relationship between long wave and middle wave thermal data.

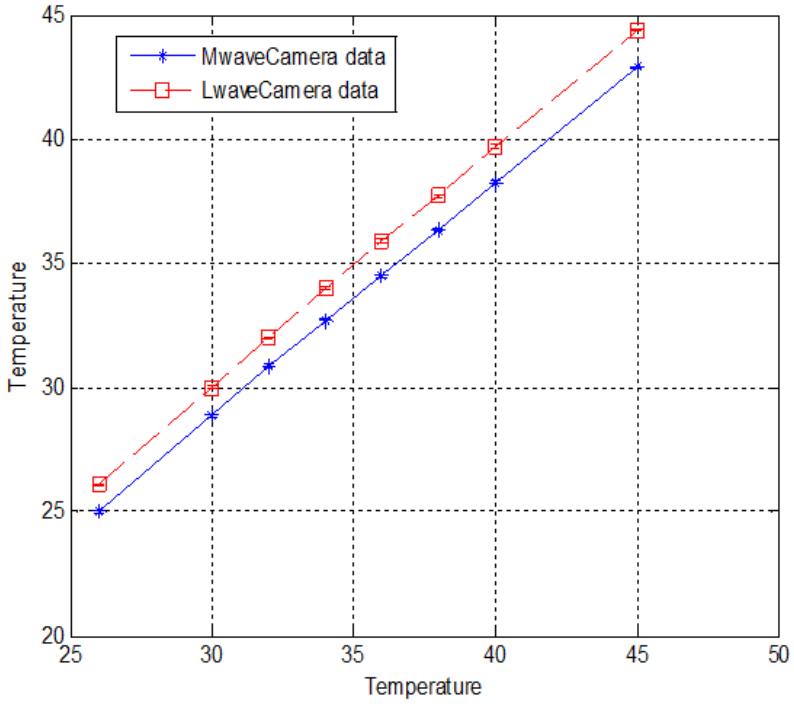

Figure 10-16shows an example of the black body temperature measured by a cooled MwaveTI camera (NETD ~20mK and LWIR uncooled TI camera (NETD~35mK). The blackbody temperature is set from 26 to 45 degree, shown in the x axis. The y axis gives the corresponding temperatures Measured by the two TIs.

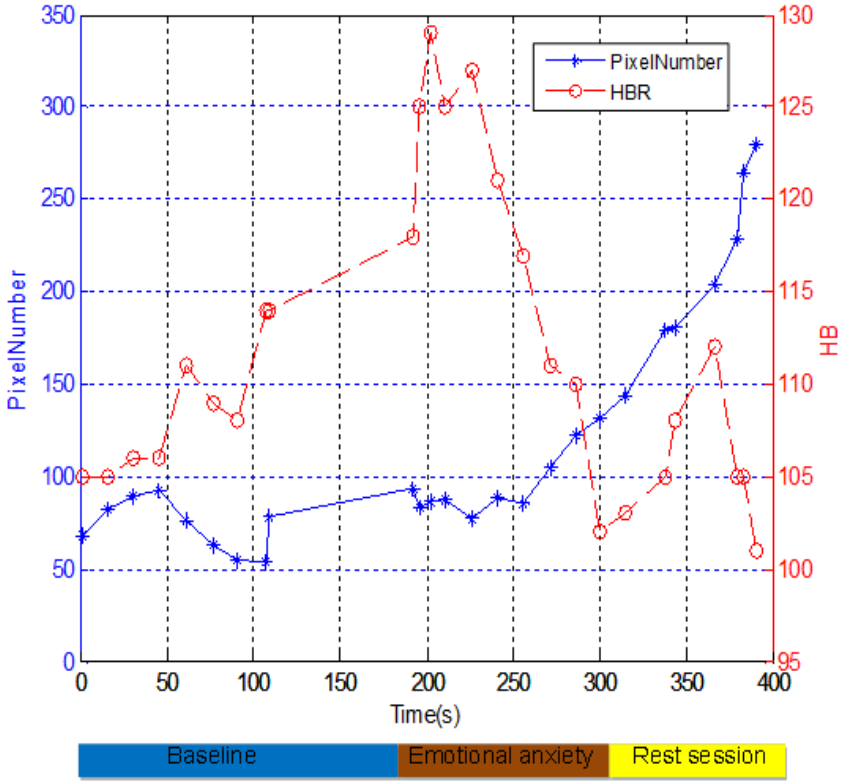

Figure 10-17Shows the hot pixel number of periorbtial region of the subject H measured by LWIR uncooled TI camera (NETD~35mK).

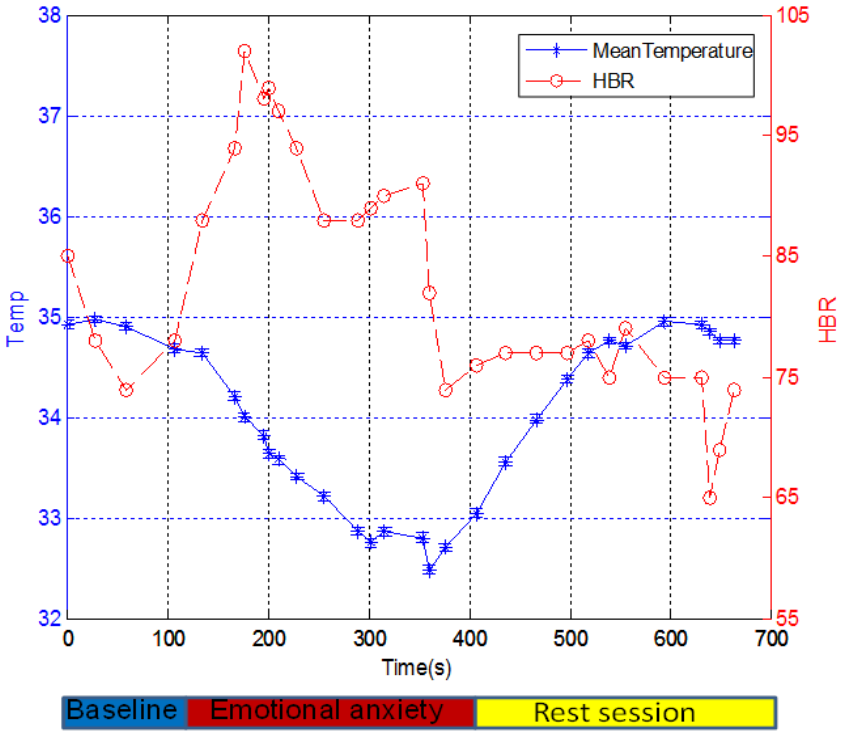

Figure 10-18Shows the nose Mean temperature of the subject N Measured by LWIR uncooled TI camera (NETD~35mK).

Figure 10-17 Shows the hot pixel number of periorbtial region of the subject H measured by LWIR TI camera. The hot pixel maintain in a low level, but increase sharply after the anxiety is taken from the participant, which demonstrates the same conclusion as the data of MWIR. The same conclusion could be achieved by using subject N's LWIR data. The nose and mouth temperature drop down greatly during the emotional anxiety session, as shown in the figure 10-18.

11 Reference

Baba. J, et al, 2002, “Effect of temperature, pH, and corneal birefingence on polarimetric glucose monitoring in the eye”, J Biomed Opt. Vol 7(3), Pages 321–328.

Burmeister. J, et al, 2000, “Noninvasive blood glucose measurements by near-infrared transmission spectroscopy across human tongues”, Diabetes Technol Ther, Spring, Vol 2(1), Pages 5-16.

Berry. J. W, et al, 2001, “Forgivingness, relationship quality, anxietywhile imagining relationship events, and physical and mental health”, Journal of Counseling Psychology, Vol 48, Pages 447-455.

Bédard. P, et al, 2010, “Brain activation related to combinations of gaze position, visual input, and goal-directed hand movements”, Cereb Cortex. Vol 21(6), Pages 1273-82.

Buddharaju. P, Pavlidis. I, Tsiamyrtzis. P, and Bazakos. M, 2007, “Physiology-based face recognition in the thermal infrared spectrum”, IEEE Transactions on Pattern Analysis and Machine Intelligence, Vol. 29, no. 4, Pages 613-26.

Bezemer. R, Karemaker. J. M, et al, 2009, “Simultaneous multi-DFMTh assessment of tissue oxygen saturation in thenar and forearm using near-infrared spectroscopy during a simple cardiovascular challenge,” Critical Care, Vol. 13, no. Suppl5, p. S5.

Cameron. B, Gorde. H, 1999, “The use of polarized laser light through the eye for noninvasive glucose monitoring”, Diabetes Technol Ther, Vol 1(2), Pages 135-43.

Carl. D, et al, 2002, “A novel noninvasive blood glucose monitor”, Diabetes Care, Vol 25(12), Pages 2268-75.

Carlos. E, Wolf. B, 2008, “Current development in non-invasive glucose monitoring”, Medical Engineering &Physics, vol. 30, pp. 541-549.

Cadeddu. J and Livingston. E, 2009, “Hyperspectral Imaging Utilizing LCTF and DLP Technology for Surgical and Clinical Applications,” in Proc of SPIE 7170, doi:10.1117/12.816279.

Cancio. L. C, Batchinsky. A. I and Mansfield. J. R, 2006, “Hyperspectral imaging: A new approach to the diagnosis of hemorrhagic shock,” The Journal of Trauma: Injury, Infection, and Critical Care, Vol. 60, no. 5, Pages 1087-1095.

Creates. M, Grayson. J, 1980, “The effect of adrenaline and noradrenaline on coronary vascular reserve in the dog”, J Physiol, Vol 309, Pages 557-68.

Celso. M. M, et al, 2009, “Expression of Emotions using Wrinkles, Blushing, Sweating and Tears”, IVA '09, Pages 188-200.

Cho. O, Kim. Y, et al, 2004, “Noninvasive Measurement of Glucose by Metabolic Heat Conformation Method”, Clin Chem. Vol 50(10), Pages 1894-1898.

Condren. R, et al, 2002, “HPA axis response to a psychological stressor in generalised social phobia”, psych neuroendocrinology Vol 27(6), Pages 693-703.

Chen. T, Yuen. P, Hong. K, et al, 2009, “Remote sensing of emotional anxiety using Electro-optics imaging technique,” Proceedings of the SPIE, 7486, pp. 0601-06-12.

Chen. T, 2012, “Hyperspectral imaging for the remote sensing of blod oxygenation and emotions” , Ph.D Thesis, Cranfield University.

Delpy. D. T, Cope. M, Zee. V, Arridge. S, et al, 1988, “Estimation of optical path length through tissue from direct time of flight measurements,” Phys. Med. Biol, Vol 33, Pages 1433-42.

Ding. H, Lu. J. Q, Wooden. W. A et al, 2006, “Refractive indices of human skin tissues at eight wavelengths and estimated dispersion relations between 300 and 1600nm,” Physics in Medicine and Biology, Vol. 51, Pages 1479-1489.

Dickerson. S, Kemeny. M, 2004, “Acute stressors and cortisol responses: a theoretical integration and synthesis of laboratory research”, Psychol Bull, Vol 130(3), Pages 355-91.

Drummond, P, 1997, “The effect of adrenergic blockade on blushing and facial flushing”, Psychophysiology, Vol 34(2), Pages 163-168.

Drummond, P, 1994, “The effect of anger and pleasure on facial blood flow”, Australian Journal of Psychology. Special Issue: Research in psychophysiology, Vol 46 (2), Pages 95-99.

Drummond. P, Lance. J, 1987, “Facial flushing and sweating mediated by the sympathetic nervous system”, Brain, Vol 110 (Pt 3), Pages 793-803.

Edwards J. J, Jackson. HJ, 2002, “PEEmotion recognition via facial expression and affective prosody in schizophrenia: a methodological review”, Clin Psychol Rev, Vol 22(6), Pages 789-832.

Ekman. P, Friesen. W, Hager. J, 2002, Facial Action Coding System. The Manual on CD Rom. Salt Lake City: Network Information Research Corporation.

Elofsson. U, et al, 2007. “Physiological correlates of eye movement desensitization and reprocessing”, Journal of Anxiety Disorders, Pages 622–634.

Fasela. B, et al, 2003, “Automatic facial expression analysis: a survey ”, Pattern Recognition, Volume 36, Issue 1, Pages 259–275.

Fujimasa. I, et al, 2000, “Converting far infrared image information to other physiological data,” IEEE Engineering in Medicine and Biology Magazine, Vol.19, Pages, 71–76.

Fujita. K, Tamura. K, Wataru. K, Ishizawa. H, and Toba. E, 2004, “Development of noninvasive blood glucose sensor using the infrared spectroscopy,” Transactions of the Institute of Electrical Engineers of Japan C, Vol. 129, no. 9, Pages. 1759–1765.

Gabriely. I, Wozniak. R, 1999, “Transcutaneous glucose measurement using near-infrared spectroscopy during hypoglycaemia”, Diabetes Care, Vol 22(12), Pages 2026-32.

Garbey. M, Merla. A, Pavlidis. I, 2004, “Estimation of blood flow speed and vessel location from thermal video,” Proceedings of the IEEE Computer Society Conference on Computer Vision and Pattern Recognition, Vol. 1, Pages. 356–363.

Garbey. S. M, Merla. A, Pavlidis. I, 2005, “Imaging the cardiovascular pulse,” Proceedings of the IEEE Computer Society Conference on Computer Vision and Pattern Recognition, San Diego, Vol. 2, Pages 416-421.

Gault. T, et al, 2010, “Extraction of the Superficial Facial Vasculature, Vital Signs Waveforms and Rates Using Thermal Imaging,” IEEE Computer Society Conference on Computer Vision and Pattern Recognition Workshops, Pages 1-8.

Hattery. D, Hassan. M, Demos. S and Gandjbakhche. A, 2002 “Hyperspectral Imaging of Kaposi’s Sarcoma for Disease Assessment and Treatment Monitoring,” in AIPR 2002 Proceedings 31st Applied Imagery Pattern Recognition Workshop From

Harvey. L, McNeil. B, 2006, “At-line monitoring of ammonium, glucose, methyl oleate and biomass in a complex antibiotic fermentation process using attenuated total reflectance-mid-infrared(ATR-MIR) spectroscopy” Anal Chim Acta, Vol 561, Pages218–24.

Hale. G. M and Querry. M. R, 1973, “Optical Constants of Water in the 200-nm to 200-µm Wavelength Region,” Appl. Opt, Vol 12, Pages 555-563.

Head. J, Wang. F, et al, 2000, “The important role of infrared imaging in breast cancer,” IEEE Engineering in Medicine and Biology Magazine, Vol.19, Pages, 52–57.

Hong. K, Yuen. P, Chen. T, et al, 2009. “Detection and classification of emotional anxietyusing thermal imaging technique”, Proceedings of the SPIE, 7486, pp. 0I01-0I09.

Huang, R and Jacques. S, “Skin optics summary,” 1998. [Online]. Available: http://omlc.ogi.edu/news/jan98/skinoptics.html. [Accessed 20 March 2012].

Herrmann. N, 1996, “The Whole Brain Business Book”, McGraw-Hill, New York, NY. ISBN 0-07-028462-8. ISBN 978-0-07-028462-3.

Hejazi. S, Spangler. R, 1992, “THEORETICAL MODELING OF SKIN EMISSIVITY,” Engineering in Medicine and Biology Society, Proceedings of the Annual International Conference of the IEEE, Vol.1, Pages 258 – 259.

Ives. C. L, Harrison. D. K and Stansby. G. S, 2007, “Tissue oxygen saturation, measured by near-infrared spectroscopy, and its relationship to surgicalsite infections,” British Journal of Surgery , Vol. 94, Pages 87-91.

Ishii. H, Niioka. T, Izumi. H, 2009, “Circulating adrenaline released by sympathoadrenal activation elicits acute vasodilatation in the rat masseter muscle”, Arch Oral Biol, Vol 54(5), Pages 486-94.

Jarlier. S, et al, 2011, “Thermal Analysis of Facial Muscles Contractions”. IEEE transactions on affective computing, Vol.2,No.1.

Johnson. S , et al, 2011, “Thermographic Eye Temperature as an Index to Body Temperature in Ponies” ,Journal of Equine Veterinary Science ,Volume 31, Issue 2, Pages 63–66.

Jiang. B, Valstar. M, and Pantic. M, 2011, "Action Unit detection using sparse appearance descriptors in space-time video volumes," in Proceedings of IEEE International Conference on Automatic Face and Gesture Recognition, Pages 314-321.

Jason. E, 2005, “Matched filter stochastic background characterisation for hyper-spectral target detection”, Master thesis, Rochester Institute of Technology.

Kudielka. B. M, et al, 2004, “Sex differences in HAP axis response to anxiety: a review.” Biological Psychology, vol. 69, pp. 113-132.

Kudielka. B. M, Hellhammer .D. H., 2004, “Acute HPA axis responses, heart rate and mood changes to psychosocial anxiety (TSST) in humans at different times of day,” Psychoneuroendocrinology, vol. 29, Pages 983–992.

Kozel. F. Andrew, et al, 2005, “Detecting Deception Using Functional MagneticResonance Imaging”, Biol Psychiatry, Vol 58(8), Pages 605-13.

Kozel. F. Andrew, et al, 2009, “Replication of Functional MRI Detection of Deception”, The Open Forensic Science Journal, Vol 2, Pages 6-11.

Klein. J, Moon. Y, Picard. R, 2002, “This computer responds to user frustration,” Interacting with Computers, Vol 14, Pages 119–140.

Kajiwara http://www.ncbi.nlm.nih.gov/pubmed?term=Kajiwara%20K%5BAuthor%5D& cauthor=true&cauthor_uid=8231320,

Khan. M, 2009, “Cluster Analytic Detection of Disgust-Arousal”, ISDA '09, Pages 641-647.

Khan. M, 2006, “Automated Facial Expression Classification and affect interpretation using infrared measurement of facial skin temperature variations”, ACM Transactions on Autonomous and Adaptive Systems, Volume 1 Issue 1, Pages 91 – 113.

Kohl. M, Nolte. C, et al, 1998, “Determination of the wavelength dependence of the differential pathlength factor from near-infrared pulse signals,” Phys. Med. Biol., Vol. 43, Pages 1771–1782.

Kasemsumran. S. S, et al, 2006, “Improvement of partial least squares models for in vitro and in vivo glucose quantifications by using near-infrared spectroscopy and searching combination moving window partial least squares”, Chemom Intelligent Lab Syst , Pages 82:97–103.

KNOEFEL, W. T, KOLLIAS, N, et al, 1996, “Reflectance spectroscopy of pancreatic microcirculation,” J.Appl. Physiol, Vol 80, no. 1, Pages 116-123, 1996.

Levine JA. J, Pavlidis. I, et al, 2009, “Description and clinical studies of a device for the instantaneous detection of office-place anxiety.” Work, Vol 34(3), Pages359-64.

Levine. J. A, Pavlidis. I, and Cooper. M, 2001, “The face of fear,” The Lancet, Vol 357, no. 9270, Pages 1757–1757.

Lawrence. M, etc, 2001, “New Evidence for Distinct Right and Left Brain Systems for Deductive versus Probabilistic Reasoning”, Cereb. Cortex , Vol 11 (10), Pages 954-965.

Lliou. T, 2010, “Classification on Speech Emotion Recognition - A Comparative Study”, International Journal on Advances in Life Sciences, Vol 2 no 1 & 2.

Leonardo. T, 2005, “Automatic Feature Localization in Thermal Images for Facial Expression Recognition”, CVPR Workshops 2005, Pages 14.

Merla. A, 2007, “Thermal signatures of emotional arousal: a functional infrared imaging study”, Conf Proc IEEE Eng Med Biol Soc, Pages 247-9.

Maruo K, K, Tsurugi. M. M, et al, 2003, “In vivo noninvasive measurement of blood glucose by near-infrared diffuse-reflectance spectroscopy”, Appl Spectrosc, Vol 57(10), Pages 1236-44.

Mehmood. K, 2008, “Cluster-analytic classification of facial expressions using infrared measurements of facial thermal features”, Ph.D Thesis, department of computing and engineering, University of Huddersfield, Huddersfield, UK.

Maruo K. K, Tsurugi M. M, et al, 2003, “Noninvasive blood glucose assay using a newly developed nearinfrared system”, IEEE J Selected Top Quantum Electron, Vol 9:3, Pages 22–30.

Nozawa. A and Tacano. M, 2009, “Correlation analysis on alpha attenuation and nasal skin temperature,” J. Stat. Mech.: Theory Exp., vol. P01007, pp. 1–10.

Nozawa. A, et al, 2011, “Dynamic analysis of dorsal thermal images”, Artif Life Robotics vol.16, pp 147-151.

NatrualTech, “ The adrenal anxiety profile Available at:,” 2010. [Online]. Available: http://www.natratech.com/Products/saliva_test.htm . [Accessed 7 March 2012].

Nakanishi. R, Imai-Matsumura. K, 2008, “Facial skin temperature decreases in infants with joyful expression,” Infant Behav. Dev., Vol. 31,Pages 137– 144.

Nhan. B, Chau. T, 2010, “Classifying affective states using thermal infrared imaging of the human face”, IEEE Trans Biomed Eng, Vol 57(4), Pages 979-87.

Nakayama. K, Goto S. S, et al, 2005, “Decrease in nasal temperature of rhesus monkeys (Macaca mulatta) in negative emotional state”, Physiol Behav, Vol 84(5), Pages 783-90.

Olesberg. T, Liu. L, et al, 2006, “In Vivo Near-Infrared Spectroscopy of Rat Skin Tissue with Varying Blood Glucose Levels”, Anal. Chem, Vol 78 (1), Pages 215–223.

Pavlidis. I, et al, 2002, “Human behavior: Seeing through the face of deception,” Nature, Vol 415, no. 6867, p. 35.

Pavlidis. I et al, 2003, “Continuous Physiological Monitoring”,Proceedings of the 25‘ Annual International Conference of the IEEE EMBS Cancun, Mexico, Pages 17-21.

Pavlidis. I, Levine. J, Baukol. P, 2001, “Thermal image analysis for anxiety detection,” Proceedings of the 2001 IEEE International Conference on Image Processing, Vol. 2, Pages 315–318.

Power. S, Falk. T, et al, 2010 “Classification of prefrontal activity due to mental arithmetic and music imagery using hidden Markov models and frequency domain near-infrared spectroscopy.” Journal of Neural Engineering, Vol 7, Pages 1–9.

Pavlidis. I, Levine. J, 2001 ,“Monitoring of periorbital blood flow rate through thermal image analysis and its application to polygraph testing,” Proceedings of the 23rd Annual International Conference of the IEEE Engineering in Medicine and Biology Society, Vol. 3, Pages 2826–2829.

Pavlidis. I, Dowdall. J, et al, 2007, “Interacting with human physiology”, Computer Vision and Image Understanding, Vol 108, Pages 150-70.

Pavlidis. I, 2001, “Monitoring of periorbital blood flow rate through thermal image analysis and its application to polygraph testing “, Engineering in Medicine and Biology Society, Proceedings of the 23rd Annual International Conference of the IEEE, Vol 3, Pages 2826-2829.

Pavlidis. I, 2001, “Thermal image analysis for anxiety detection “, International Conference on Image Processing, Vol.2, Pages 315 – 318.

Pavlidis. I, et al, 2000, "Thermal imaging for anxiety detection", IEEE Workshop on Computer Vision Beyond the Visible Spectrum: Methods and Applications, Pages:104-109.

Pavlidis. I, et al, 2001, "Monitoring of periorbital blood flow rate through thermal image analysis and its application to polygraph testing ", Engineering in Medicine and Biology Society, Proceedings of the 23rd Annual International Conference of the IEEE, Vol 3, Pages 2826 - 2829.

Puri. C, Olson. L, Pavlidis. I, et al , 2005, ”AnxietyCam: non-contact measurement of users' emotional states through thermal imaging”, Proceedings of the 2005 ACM Conference on Human Factors in Computing Systems (CHI), Portland, Oregon, pp. 1725-8.

Palmer. G. M, et al, 2010, “Optical imaging of tumor hypoxia dynamics,” Journal of Biomedical Optics, Vol. 15, no. 6, p. 066021.

Randolfi. A, 2007, “The Psychophysiology of Emotional anxiety Part II” [online]. Available at: http://www.msubillings.edu/cahpfaculty /randolfi/436/psychphys2.html [access on 01/07/2009].

Robinson. M, Eaton. R, et al, 1992, “Noninvasive Glucose Monitoring in Diabetic Patients: A Preliminary Evaluation”, 1618 CLINICAL CHEMISTRY,Vol.38, No. 9.

Sassaroli. A and Fantini. S, “Comment on the modified Beer–Lambert law for scattering media,” Phys. Med. Biol., vol. 49, p. N255–N257.

Sämann. A, Fischbacher. C, Jagemann. K, et al, “Non-invasive blood glucose monitoring by means of near infrared spectroscopy: investigation of long-term accuracy and stability”, Exp Clin Endocrinol Diabetes, Vol 108(6), Pages 406-13.

Sherwoo. L, Kell. R, 2009, “Human physiology: From cells to systems”, Toronto: Nelson Education Ltd., 1st Canadian edition.

Sauro. M, Jorgensen. R, et al, 2001, “Sociotropic cognition moderates anxiety-induced cardiovascular responsiveness in college women”, J Behav Med, Vol 24(5), Pages 423-39.

Stewart. M, Webster. J, et al, 2007, “Non-invasive measurement of anxiety in dairy cows using infrared thermography”, Physiol Behav, Vol 92(3), Pages 520-5.

Smith. R. B, “Introduction to Hyperspectral Imaging,” 5 Jan 2012. [Online]. Available: http://www.microimages.com. [Accessed April 2012].

Sottilare. R, 2012, “Passively Classifying Student Mood and Performance within Intelligent Tutors”, Educational Technology & Society, Vol 15 (2), Pages 101–114.

Shaw. R. A, Mansfield. J. R, et al, 2000, “In vivo optical/near-infrared spectroscopy and imaging of metalloproteins,” Journal of Inorganic Biochemistry , Vol. 79, Pages 285-293.

Sperry. R, 1980, “Mind-brain interaction: Mentalism, yes; dualism, no". Neuroscience 5 (2): 195–206. doi:10.1016/0306-4522(80)90098-6. PMID 7374938. edit

Sun. T, etc, 2006, “Genomic and Evolutionary Analyses of Asymmetrically Expressed Genes in Human Fetal Left and Right Cerebral Cortex”, Cereb. Cortex, Vol 16 (suppl 1): i18-i25.

Schrader. W, Meuer. P, et al, 2005, "Noninvasive glucose determination in the human eye", J. Mol. Struct. Pages 735–736.

Swan. J, 2007. The circulation [online]. Available at: http://classvideos.net/anatomy/pdf/circulation-pdf.pdf [accessed on 02/07/2009].

S. Prahl, 1999, “Optical Absorption of Hemoglobin,” Oregon Medical Laser Center, 15 Dec 1999. [Online]. Available: http://omlc.ogi.edu/spectra/hemoglobin/ . [Accessed 20 March 2012].

She. Y, et al, 2003, “The use of Fourier-transform infrared spectroscopy for the quantitative determination of glucose concentration in whole blood”, Phys Med Biol, Vol 48, Pages 2023–32.

Tsitiridis. A, Yuen. P, Hong. K, et al, 2009. “A biological cortex like target recognition and tracking in cluttered Background,” Proceedings of the SPIE,7486, Pages 0G01-0G12.

Tenhunen. J, etc, 1998, “Non-invasive glucose measurement based on selective near infrared absorption; requirements on instrumentation and spectral range”, Measurement, Vol 24, Issue 3, Pages 173–177 .

Tamura K. K, Fujita. K, et al, “Noninvasive measurement of blood glucose based on optical sensing”, Proceedings of the 21st IEEE, Vol. 3, Pages 1970–1974.

Tsiamyrtzis. P, Dowdall. J, Pavlidis. I, et al, 2007, “Imaging facial physiology for the detection of deceit”, International Journal of Computer Vision, Vol.71, no.2, Pages 197-214.

Tsiamyrtzis. P, Dowdall. J, Shastri. D, Pavlidis. I, et al, 2005, “Lie detection—recovery of the periorbital signal through tandem tracking and noise suppression in thermal facial video,” Proceedings of SPIE Sensors, and Command, Control, Communications, and Intelligence Technologies for Homeland Security and Homeland Defense IV, Pages. 5778.

Thennadil. S, Rennert. J, et al, 2001, “Comparison of glucose concentration in interstitial fluid, and capillary and venous blood during rapid changes in blood glucose levels”, Diabetes Technol Ther, Vol 3, Pages 357–65.

Troy. T. L and Thennadil. S. N, 2001, “Optical Properties of Human Skin in the Near Infrared Wavelength Range of 1000 to 2200nm,” J. Biomed. Opt, Vol. 6, Pages 167-176.

Torella. F, Haynes. L, et al, 2002, “Cerebral and Peripheral Oxygen Saturation during Red Cell Transfusion,” Journal of Surgical Research, Vol 110, Pages 217–221.

Tuchin. V, 2007, “Tissue Optics:light scattering metrhods and instruments for medical diagnosis”, SPIE Press.

Tong. Y, Liao. W, et al, 2007, “Facial action unit recognition by exploiting their dynamic and semantic relationships”, IEEE Trans Pattern Anal Mach Intell, Vol 29(10), Pages1683-99.

Uemura T.T, et al, 1993, “Noninvasive measurement of blood glucose concentrations by analysing Fourier transform infra-red absorbance spectra through oral mucosa” ,Med Biol Eng Comput, Vol 31, Pages17-22.

Vianna. D and Carrive. P, 2005, “Changes in cutaneous and body temperature during and after conditioned fear to context in teh rat,” European Journal of Neuroscience , Vol. 21, Pages 2505-251.

Vagni. F, 2007, “Survey of Hyperspectral and Multispectral Imaging Technologies,Volume TR-SET-065-P3,” Research and Technology Organisation, North Atlantic Treaty Organisation,BP 25, F-92201 Neuillysur- Seine Cedex.

Williams. H, Read. G, et al, 1984, “Effect of inhaled beclomethasone dipropionate on saliva cortisol concentrations”, Arch Dis Child. Vol 59(6), Pages 553–556.

Wolff. K. D, Marks. C, Uekermann. B, et al, 1996, “Monitoring of flaps by measurement of intracapillary haemoglobin oxygenation with EMPHO II: experimental and clinical study,” British Journal of Oral and Maxillofacial Surgery, Vol. 34, Pages 524-529.

WING, RENA R, 1985, “Psychologic Anxiety and Blood Glucose Levels in Nondiabetic Subjects” Psychosomatic Medicine, Vol. 47, No. 6.

Wray. S, Cope. M, et al, 1988, “Characterization of the near infrared absorption of cytochrome aa3 and haemoglobin for the non-invasive monitoring of cerebral oxygenation,” Biochim. Biophys. Acta Bioenerget, Vol. 933, no. 1, Pages 184-192.

Wang. T and Hung. C, 2004, “Role of Tissue Oxygen Saturation Monitoring in Diagnosing Necrotizing Fasciitis of the Lower Limbs,” Annalys of Emergency Medicine, Vol. 44, no. 3, Pages 222-228.

Wikipedia-the free encyclopaedia, 2009, “Emotional anxiety (biological)” [online]. Available at: http://en.wikipedia.org/wiki/Emotional anxiety_(biological) [accessed on 01/07/2009].

Wikipedia-the free encyclopaedia, 2010, “Wien's displacement law” [online]. Available at: http://en.wikipedia.org/wiki/Wien%27s_displacement_law [accessed on 03/5/2010].

Wikipedia-the free encyclopedia, 2009, “Peripheral nervous system” [online]. Available at: http://en.wikipedia.org/wiki/Peripheral_nervous_system [accessed on 01/07/2009].

Waldhausl. W, Bratusch-Marrain. P, et al, 1992, ’ Glucose Response to Anxiety Hormone Exposure in Healthy Man and Insulin Dependent Diabetic Patients: Prediction by Computer Modeling’, IEEE TRANSACTIONS ON BIOMEDICAL ENGINEERING, Vol. 39, NO. 8.

Yudovsky. D, Nouvong. A, Schomacker. K and Pilona. L, 2011, “Assessing diabetic foot ulcer development risk with hyperspectral tissue oximetry,” Journal of Biomedical Optics , Vol 16, no. 2, p. 026009.

Yudovsky, D, 2010, “Hyperspectral Imaging in Diabetic Foot Wound Care”, Journal of Diabetes Science and Technology ,Volume 4, Issue 5.

Yang. M, Kriegman. D, Ahuja. N, 2002, “Detecting faces in images: a survey,” IEEE Transactions on Pattern Analysis and Machine Intelligence, Vol 24, Pages 34–58.

Yuen. P, Chen. T, Hong. K, et al, 2009, “Remote detection of anxiety using Hyperspectral imaging technique”, 3rd International Conference on Imaging for Crime Detection and Prevention (ICDP 2009), London, UK, ISBN: 978 1 84919 2071.

Yuen. P and Bishop. G, 2006, “Hyperspectral multiple approach fusion for the long-range detection of low observable objects: MUF2,” in Proceedings of the SPIE, Vol 6396.

Yuen. P, Chen. T, Hong. K, et al, 2009, “Final report on the feasibility study remote sensing of intent using Electro-Optics technique” Final CTC report contract DSTLX-1000013688.

Yeh. S, Hanna. C, 2003, “Monitoring Blood Glucose Changes in CutaneousTissue by Temperature-modulated Localized Reflectance Measurements”, Clinical Chemistry Vol 49:6, Pages 924–934.

Zhang, Lei, 2008, “Interactive labeling of facial action units”, ICPR 2008. 19th International Pattern Recognition conference, Pages 1-4.

Martin WB. W, Mirov. S, et al, 2002, “Using two discrete frequencies within the middle infrared to quantitatively determine glucose in serum”, J Biomed Opt, Vol 7, Pages 613–8.

Zhao, Z 2002, “Pulsed photoacoustic techniques and glucose determination in human blood and tissue”, UNIVERSITY OF OULU, OULU FINLAN, ISBN 951-42-6690-0 (PDF), ISSN 1796-2226 (Online)

Zuzak. K, Francis. R, et al, 2008, “Novel hyperspectral imager aids surgeons SPIE Newsroom,” in SPIE Newsroom DOI: 10.1117/2.1200812.1394.

Zuzak. K, Schaeberle. M. D, et al, 2002, “Visible Reflectance Hyperspectral Imaging:Characterization of a Noninvasive, in Vivo System for Determining Tissue Perfusion,” Analytical Chemistry, Vol. 126 74, no. 9, Pages 2021-2028.

Zuzak. K, Schaeberle. M. D and Gladwin. M. T, 2001, “Noninvasive Determination of Spatially Resolved and Time-Resolved Tissue Perfusion in Humans during Nitric

Oxide Inhibition and Inhalation by Use of a Visible-Reflectance Hyperspectral Imaging Technique," Circulation, Vol. 104, Pages 2005-2910.

Zuzak. K, Schaeberl. M, et al, 2001. "Non-invasive Determination of Spatially Resolved and time-Resolved Tissue Perfusion in Humans during Nitric Oxide

Zuzak. K, et al, 2007, "Characterization of a Near-Infrared Laproscopic Hyperspectral Imaging System for Minimally Invasive Surgery," Anal. Chem, Vol 79, Pages 4709-4715.

Zuzak. K, et al, 2010, "The use of nasal skin temperature measurements in studying emotion in macaque monkeys ",Physiol Behav. Vol 102(3-4), Pages 347-55.

Zuzak. K, Schaeberle. M, et al, 2002, "Visible Reflectance Hyperspectral Imaging: Characterization of a Noninvasive, in vivo System for Determining Tissue Perfusion," Anal. Chem, Vol 74, Pages 2021-2028.

Zuzak. K, Gladwin. M, et al, 2003, "Imaging hemoglobin oxygen saturation in sickle cell disease patients using noninvasive visible reflectance hyperspectral techniques: effects of nitric oxide." Am J. Physiol: Heart Circulatory Physiol, Vol 285, Pages 1183-1189.